Design and Modeling of Pneumatic Mechanism for Improved Indirect Liquid Cooling of Shipboard Power Electronics

by

Christopher J. Sarao Jr.

B.S. Naval Architecture and Marine Engineering, United States Naval Academy, 2017

Submitted to the Department of Mechanical Engineering in partial fulfillment of the requirements for the degrees of

NAVAL ENGINEERS DEGREE

and

MASTER OF SCIENCE IN MECHANICAL ENGINEERING

at the

MASSACHUSETTS INSTITUTE OF TECHNOLOGY

May 2024

© 2024 Christopher J. Sarao Jr. All rights reserved.

The author hereby grants to MIT a nonexclusive, worldwide, irrevocable, royalty-free license to exercise any and all rights under copyright, including to reproduce, preserve, distribute and publicly display copies of the thesis, or release the thesis under an open-access license.

Authored by: Christopher J. Sarao Jr.

Department of Mechanical Engineering

May 10, 2024

Certified by: Julie Chalfant

Research Scientist, Thesis Supervisor

Certified by: Chryssostomos Chryssostomidis

Professor of Mechanical and Ocean Engineering, Thesis Supervisor

Accepted by: Nicolas Hadjiconstantinou

Professor of Mechanical Engineering

Chairman, Department Committee on Graduate Theses

Design and Modeling of Pneumatic Mechanism for Improved Indirect Liquid Cooling of Shipboard Power Electronics

by

Christopher J. Sarao Jr.

Submitted to the Department of Mechanical Engineering on May 10, 2024 in partial fulfillment of the requirements for the degrees of

NAVAL ENGINEERS DEGREE

and

MASTER OF SCIENCE IN MECHANICAL ENGINEERING

ABSTRACT

The U.S. Navy continues to explore the development of electric ships to meet the evolving challenges of maritime operations. This requires a significant evolution in naval ship design and technology which focuses on the advanced power distribution system to efficiently manage and distribute electrical power throughout the ship. The Electric Ship Research and Development (ESRDC), funded through the Office of Naval Research (ONR), focuses on the research and development of advanced technologies and concepts for electric ships. The Design Laboratory at the Massachusetts Institute of Technology (MIT) Sea Grant Program developed the concept of the Navy integrated Power and Energy Corridor (NiPEC) to serve as the power distribution system of a ship.

The NiPEC is comprised of modular units capable of operating independently or as part of a network to execute energy storage, conversion, protection, control, isolation, and transfer functions [Cooke et al., 2017]. The integrated Power Electronics Building Block (iPEBB) performs the power conversion process. Thermal management and securing of the iPEBB are critical to the installation of the new electrical distribution system on ships.

Padilla et al. [2021] conducted a preliminary analysis of the Power Electronics Building Block (PEBB) heat dissipation utilizing liquid-cooled cold plates across the dry interface of the PEBB shell's top and bottom surface. Further, Padilla [2023] explored the Thermal Interface Material (TIM) between the cold plate and the PEBB shell interface to determine an effective interface pressure that filled interstitial gaps at the interface to maximize the surface contact and heat transfer.

Using Tomlinson's [Tomlinson, 2022] first-pass securing mechanism design as a starting point, additional design iterations were conducted based on new research developments and the desire for increased power density of the iPEBB stack and a uniform interface pressure for maximized heat transfer. This thesis modeled a securing mechanism using a clamped based design that was suitable for ship-wide development which integrated with the proposed NiPEC cooling system architecture, increased the power density of the iPEBB stack, and maximized heat removal. This functional design meets the requirements of the imposed thermal, electrical, and mechanical constraints; however, the design does require an additional support system which may not be optimal. The airbag design feature for the securing mechanism required a pneumatic support system to be added into the NiPEC architecture.

One advantage of the airbag securing feature was the increased power density of 50% from 4 to 6 iPEBB per stack by minimizing the vertical space between each unit. A second advantage is the uniform pressure supplied at the interface for heat transfer. The implementation of the airbag for the securing mechanism in the clamp-based design proves to have a versatile capability to allow the interface pressure to be increased with minimal impact on the vertical space consumed. Increasing the interface pressure could have a significant impact on the rate of heat transfer, thus increasing the operational power of the iPEBB.

Additionally, a single iPEBB prototype was designed and constructed to validate the feasibility and performance of the proposed securing mechanism design. Furthermore, the proposed securing mechanism of the iPEBB and construction of the single iPEBB prototype will help researchers model the thermal behavior of the cooling system and the system architecture.

Thesis supervisor: Julie Chalfant

Title: Research Scientist

Thesis supervisor: Chryssostomos Chryssostomidis Title: Professor of Mechanical and Ocean Engineering

Acknowledgments

I am truly grateful for the opportunity to pursue my Master's Degree at the Massachusetts Institute of Technology (MIT) in the Naval Construction and Engineering program.

First, I wish to show my deepest gratitude to my thesis supervisors, Dr. Julie Chalfant and Professor Chryssostomos Chryssostomidis. Their guidance and mentorship have been invaluable as they provided me with the support and resources I needed to navigate through the difficult portions of the process. I would also like to extend a special thanks to the following individuals.

- Kelly Cooper and L.J. Peterson Provided ongoing research contributions and sponsorship from the U.S. ONR supported by, or in part by, the ONR under award number ONR N00014-21-1-2124.
- National Oceanic and Atmospheric Administration (NOAA) for funding the MIT Sea Grant College Program and Design Lab under grant number NA22OAR4170126.
- Trudi Walters and Maria Riefstahl Played an important role in placing purchase orders and keeping me informed as new shipments arrived.
- Mike Constrano, Todd Ervin, and Scott Pickett Played an integral role in providing technical support for the Tekscan (TEK) sensor software and hardware.

Finally, thank you to my family and friends for their unconditional support and encouragement not only during my time at MIT, but throughout my entire life. Most importantly, I would like to thank my wife Anastasia, daughter Esme, and son Tripp for their unwavering love, support, and commitment.

Contents

Ti	itle p	page	1
\mathbf{A}	bstra	act	3
A	cknov	wledgments	5
Li	st of	Figures	11
Li	st of	Tables	13
1	1.1 1.2 1.3 1.4 1.5	Background	17 17 17 18 19 20 21 22
2	2.1 2.2	d Plate and PEBB Structural Analysis Required Structural Analysis of the Cold Plate	25 25 25 26 28 29 30 30 32
	2.3	Required Structural Analysis of the PEBB	34 34 36 36 39 40
	4.4	OUTHINALY OF OUTUCEHIAL ANALYSIS	40

3	Uniform Pressure Distribution Rig						
	3.1	Design	43				
		3.1.1 Sensors	46				
		3.1.2 Airbag	47				
	3.2	Pressure Trials	47				
		3.2.1 Uniform Pressure Distribution Model Empirical Results	48				
		3.2.2 Accuracy of the Empirical Model	54				
	3.3	Temperature Trials	54				
		3.3.1 Empirical Model Results	55				
		3.3.2 Accuracy of the Empirical Model	56				
	3.4	Discussion	57				
4	Oth	ner System Component Evaluation	5 9				
	4.1	Gas Springs	59				
		4.1.1 Force Required	60				
		4.1.2 Design Layout	61				
	4.2	Flexible Hose	63				
		4.2.1 Flex Hose Design Layout	63				
		4.2.2 Flexible Hose Coupling Connections	65				
	4.3	Air Pressure System	66				
		4.3.1 STAR Low Pressure Air Compressor	67				
		4.3.2 Condenser-Filter Low Pressure Air Dehydrator and Electronics Dry	۵.				
		Air Membrane Dehydrator	67				
		4.3.3 Air Compressor Sizing	68				
		4.3.4 Air Pressure Diagram	69				
		4.3.5 Back-Up Air Supply	69				
5		erall Securing Mechanism for iPEBB and Cabinet Design	7 3				
	5.1	Full Scale Design	73				
	5.2	Prototype Design Approach	74				
	5.3	Single PEBB Prototype	76				
	5.4	Design Conclusions	79				
6	Fut	ure Work and Conclusions	81				
	6.1	Future Work	82				
		6.1.1 Condensation	82				
		6.1.2 PEBB Rail Locks	82				
		6.1.3 Airbag Physical Constraint	83				
	6.2	Conclusions	83				
Re	efere	nces	87				
\mathbf{A}	MA	TLAB Script for Deflection and Buckling Analysis	89				
В	Ros	ark's Formula for Stress and Strain MITcalc	99				

\mathbf{C}	SOLIDWORKS Simulation Results for Deflection and Buckling	105
D	MATLAB Script for Ideal Gas Law	107
\mathbf{E}	Air Flow Schematics	111
\mathbf{F}	Prototype Material List from TBUILD	115

List of Figures

1.1	Exponential increase in anticipated power demand [Markle, 2018]	18
1.2	Four-corridor NiPEC incorporated into destroyer-type vessel model [del Águila Fe	r-
	randis et al., 2019]	18
1.3	Nominal power corridor section for one compartment [Cooke et al., 2017]	19
1.4	Topdown and isometric views of a Navy iPEBB model [DiMarino, 2020]	20
1.5	Hinged-Type Securing Mechanism Design [Tomlinson, 2022]	21
1.6	Proposed model of iPEBB Stack Design with Hinged-Type Securing Mecha-	
	nism [Tomlinson, 2022]	22
2.1	Simply Supported Plate with Uniform Normal Loading [Jweeg et al., 2021] .	27
2.2	Cold Plate Deflection 3D Surface Plot - Exaggerated for Visualization	28
2.3	Cold Plate Deflection Simulation using SOLIDWORKS	29
2.4	Views of Modeled Brace Plates within the iPEBB Stack	30
2.5	Clamped Rectangular Plate [Ephraim et al., 2019]	31
2.6	Brace Plate Deflection 3D Surface Plot - Exaggerated for Visualization	32
2.7	Brace Plate Deflection Simulation with Four Fixed Edges using SOLIDWORKS	33
2.8	Brace Plate Deflection Simulation with Three Fixed Edges using SOLID-	
	WORKS - Exaggerated for Visualization	33
2.9	Views of Modeled iPEBB Shell	34
2.10	V I	35
	Navy iPEBB Multi-layer Substrate[DiMarino, 2022]	35
	Buckling Loading Analysis of iPEBB Sides [Gunjal et al., 2015]	38
	PEBB Shell Buckling Simulation using SOLIDWORKS- Short Side	39
	SOLIDWORKS Buckling Factor of Safety[SOLIDWORKS]	40
2.15	PEBB Shell Buckling Simulation using SOLIDWORKS - Long Side	40
3.1	CAD Model of Uniform Pressure Distribution Rig	44
3.2	Uniform Pressure Rig Exploded View of CAD Model	45
3.3	Uniform Pressure Experimental Rig	45
3.4	TekScan 5151 I-Scan Pressure Sensor[Tekscan]	46
3.5	Experimental Pressure Test Rig with Different TEK Sensor Locations	49
3.6	TEK Sensor between iPEBB shell and Cold Plate with (right) and without	
	(left) Pyrolytic Highly Oriented Graphite Sheet (PGS)	50
3.7	TEK Sensor between iPEBB shell and Aluminum Plate with (right) and with-	
	out (left) PGS	51

3.8 3.9	TEK Sensor between iPEBB shell and Airbag with (right) and without (left) PGS	52 53
3 10	Pressure and Temperature: Amontons's Law	55
	Plot of Cooled Water Temperature effect on Airbag Pressure	56
4.1 4.2	Gas Spring Technical Diagram [IQS]	60 62
4.3	Gas Strut PEBB Stack Arrangement Compressed - Front View (left) and Profile View (right)	62
4.4	Gas Strut PEBB Stack Arrangement Extended - Front View (left) and Profile View (right)	62
4.5 4.6	Reyes iPEBB stack design for first design iteration cold plate[Reyes, 2022]. Reyes [2022] Cold Plate Arranged as Counter-Flow Heat Exchanger [Reyes,	64
	2022]	65
4.7 4.8	Double Shut-Off Coupling [Boyd, 2019]	66 70
5.1 5.2	iPEBB Stack SolidWorks Design - Open State (left) and Closed State (right) Isometric View of Single PEBB Mockup	75 76
5.3	Single PEBB Mockup Design	77
5.4	iPEBB Prototype Electrical Connection	77
5.5	iPEBB Prototype Gas Spring V-lift	78
5.6	Single PEBB Prototype	78
B.1	Cold Plate Deflection Calculator [MITcalc]	99
B.2	Brace Plate Deflection Calculator [MITcalc]	100
B.3 B.4	Buckling Short Edge - Dimensions and Material Properties [MITcalc] Buckling Short Edge - Calculations [MITcalc]	$100 \\ 101$
B.5	Buckling Short Edge - Calculations [MITcalc]	$101 \\ 102$
B.6	Buckling Long Edge - Dimensions and Material Properties [MITcalc]	102
B.7		103
B.8	Buckling Long Edge - FOS Results [MITcalc]	104
C.1	Cold Plate Von Mises Stress	105
C.2	Brace Plate Von Mises Stress - Four Fixed Edges	106
C.3	Brace Plate Von Mises Stress - Three Fixed and One Short Free Edge	106
E.1	Condenser-Filter Dehydrator - Flow Schematic Diagram NSTM-551	111
E.2	Typical LP Air System Layout NSTM-551	112
E.3	Membrane Dehydrator - Flow Schematic Diagram NSTM-551	113

List of Tables

2.1	iPEBB Housing Material Properties - Delrin 570 Blend Del
2.2	iPEBB Top and Bottom Substrate Material Properties [606] [MatWeb] 36
2.3	Deflection Structural Analysis Summary
2.4	Buckling Structural Analysis Summary
3.1	Tekscan Sensor Properties[Tekscan]
3.2	WINBAG Properties[WINBAG]
3.3	Sensel Averaging
3.4	Airbag Sensor Cold Plate Interface
3.5	Airbag Sensor Aluminum Plate Interface
3.6	Airbag Sensor Interface
3.7	Ideal Gas Law Theoretical Pressure Percent Change
3.8	Pressure vs Temperature
4.1	80N Gas Spring Properties
4.2	Cold Plate Cooling Water Properties [Reyes, 2022]
4.3	Navy LP Air Compressor [NSTM-551]
4.4	Condenser-Filter Dehydrator [NSTM-551]

ATS Advanced Thermal Solutions

BFS Buckling Factor of Safety

CAD Computer Aided Design

COF Center of Force

ESD Electrostatic Discharge

ESRDC Electric Ship Research and Development

ETP Electrolytic Tough Pitch

iPEBB integrated Power Electronics Building Block

LED Light Emitting Diode

LPAC Low Pressure Air Compressor

LPAD Low Pressure Air Dehydrator

LRU Least Replaceable Unit

MIT Massachusetts Institute of Technology

NiPEC Navy integrated Power and Energy Corridor

NOAA National Oceanic and Atmospheric Administration

ODBC Organic Direct Bond Copper

ONR Office of Naval Research

 \mathbf{PGS} Pyrolytic Highly Oriented Graphite Sheet

PEBB Power Electronics Building Block

 \mathbf{PEPDS} Power Electronics Power Distribution System

PHE Plate Heat Exchanger

POM Polyoxymethylene

PTFE polytetrafluoroethylene

TEK Tekscan

TIM Thermal Interface Material

Chapter 1

Introduction

The focus of this thesis is a second pass design addressing the problem for securing an iPEBB with a uniform interface pressure on the top and bottom surface of the shell. This section provides the background information that is relevant to understanding the on-going development of the NiPEC and the association of this problem. In addition to outlining the constraints imposed on this design problem is a summary of the previous design. The final section of this chapter provides an overview for the remaining chapters of this thesis.

1.1 Background

Future Naval warships require an updated electrical distribution system to overcome the associated challenges of increased electrical generation and demand. Naval ship weapons, propulsion, sensors, and communication systems are becoming increasingly power-hungry onboard and require an optimal power distribution and management system across the ship that facilitates the integration of these systems. Figure 1.1 shows the exponential increase in anticipated power demand that current power systems cannot support.

The ESRDC was established in 2002 by the ONR to develop new technology for integrated power systems. A collaboration of research centers and institutes within the ESRDC are working together on the science and technology development for advanced electric ship concepts. To build off these concepts, the Power Electronics Power Distribution System (PEPDS) program aims to provide the Navy shipboard electrical systems with new power, energy, and control technologies.

1.2 Power Electronics Power Distribution System (PEPDS)

PEPDS utilizes advanced power electronics technologies to efficiently regulate, control, and distribute electrical power from the ship's power generation sources to various onboard systems. It is an integrated system ship that is responsible for managing and distributing power throughout the ship. The PEPDS concept is enabled by the following ONR developed technology; (1) high-power-density high efficiency power electronics, (2) Silicon-Carbide (SiC) power semiconductors, and (3) modeling and simulation design and analysis tools. Within

MORE POWER

STEP CHANGE INCREMENTAL DEVELOPMENT OF POWER GENERATION VS. INCREASE IN POWER REQUIREMENT OVER TIME

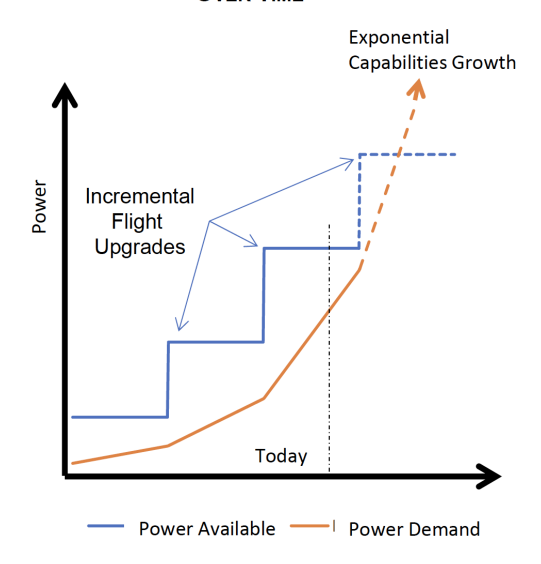


Figure 1.1: Exponential increase in anticipated power demand [Markle, 2018]

the PEPDS program, the MIT Sea Grant Design Laboratory is focusing on the NiPEC architecture which is one of the five main areas of research. The other four main areas of study are the Navy iPEBB, model is the specification, control, and system simulation. Figure 1.2 shows an initial four-corridor NiPEC incorporated into a destroyer-type vessel model which is further discussed below.

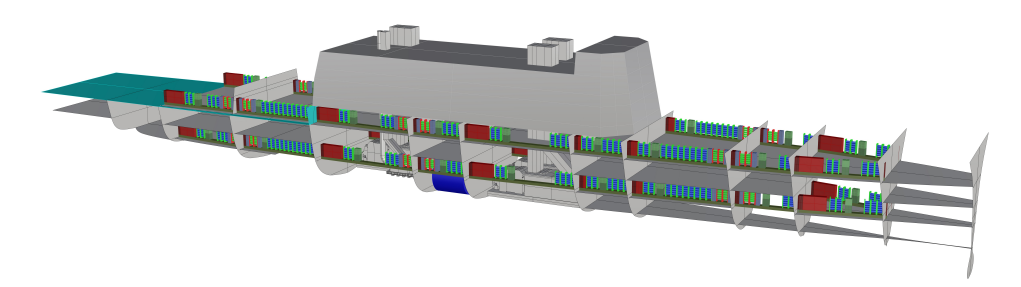


Figure 1.2: Four-corridor NiPEC incorporated into destroyer-type vessel model [del Águila Ferrandis et al., 2019].

1.2.1 Navy integrated Power and Energy Corridor (NiPEC)

The NiPEC incorporates in a single modular entity all the components of the electrical distribution system for the main bus power throughout the ship: main bus cables, conversion, protection, isolation, control, and energy storage [Cooke et al., 2017]. The modular power corridor requires reserved space in the ship design, as the repeated units are to be constructed and tested off-ship before being lifted into place for installation. Additionally, the NiPEC is

robustly designed so that if a single component were to fail the corridor remains fully capable for ship operations.

It is assumed that a ship's electrical distribution system would consist of at least corridors which run the length of the ship. Each watertight subdivision within a corridor would contain the proper number of iPEBBs to service loads within the compartment. The number of compartments will be dictated by the number of watertight subdivisions that a corridor passes through. The PEBB-based corridor provides the encompassing structure that combines iPEBBs to create appropriate converters, developing the interfaces required for smooth plug-in of the iPEBB [Petersen et al., 2022]. Figure 1.3 shows the notional NiPEC compartment module identifying the both the equipment and the associated dimensions.

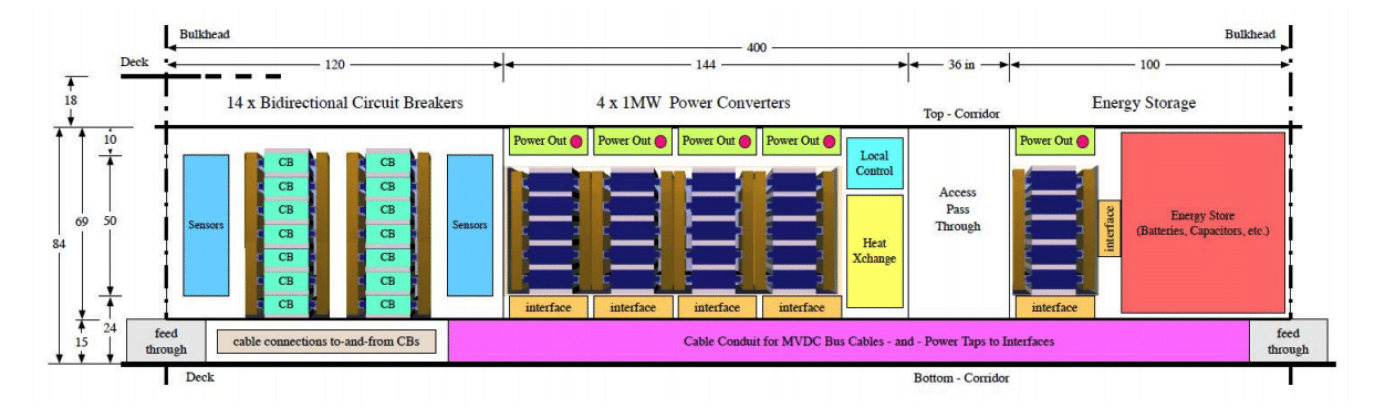


Figure 1.3: Nominal power corridor section for one compartment [Cooke et al., 2017].

1.2.2 Navy integrated Power Electronics Building Block (iPEBB)

Within the PEPDS architecture, the iPEBB is the most critical component, responsible for the electrical conversion process and management of power. The iPEBB is designed to be the the Least Replaceable Unit (LRU), thus instead of several bespoke large converters, there will be hundreds of identical units with the attendant logistical savings such as reduced cost, ease of replacement, installed spares, and reduced timing [Petersen et al., 2022]. Overall, the iPEBB ensures reliability and effectiveness of naval power systems in supporting a wide range of mission requirements.

The iPEBB is a standardized, modular converter unit that can be easily swapped by a sailor. The iPEBB consists of an enclosed shell that houses electrical components to convert power from one voltage and frequency to another. In this process, the electrical components generate heat that needs to be removed to avoid damage. A single iPEBB generates between 6000 and 11000W of waste heat which must be removed in order to maintain the temperature of the internal components of the iPEBB below 150°C [Padilla, 2021]. The heat removal is possible through conduction which supports the U.S. Navy's pursuit of a design for a dry interface liquid cooled system. Figure 1.4 displays the the current U.S. Navy model of the iPEBB electrical components and dimensions excluding any external components required for the cooling system. Each identical iPEBB is sized such that it can be carried through a ship's passageways by a sailor and can be easily installed by sliding into place and locking,

with no additional connection required, e.g. for cooling, power, data, or control [Petersen et al., 2022]. For this thesis it is assumed the dimensions of the iPEBB are $300mm \times 550mm \times 100mm$ and weighs 14kg. To note these dimension and weights can change in future iterations and are not finalized.

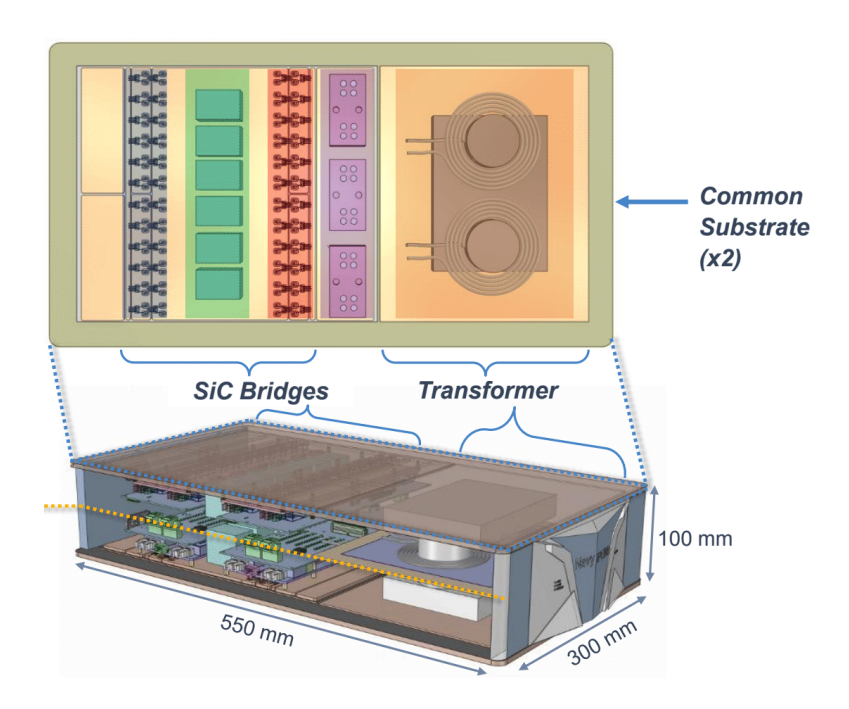


Figure 1.4: Topdown and isometric views of a Navy iPEBB model [DiMarino, 2020]

.

1.3 Problem Statement

PEPDS relies on the operation of the PEBB and the integration of the system components. One of the significant challenges involved in implementing the PEPDS is mechanically securing the PEBB from static and dynamic forces while managing the thermal load with associated constraints and maximizing the power density of the iPEBB stack. The PEBB anchoring design must secure the PEBB and transfer a uniform interface pressure through the top and bottom liquid cold plate to maximize heat transfer while not interfering with the limitations imposed by electrical and thermal constraints. Although the PEBB promises high-power efficiency in delivering its robust power conversion and storage functions, it still dissipates heat from electrical losses which pose thermal management challenges and which must be adeptly addressed [Yang et al., 2019].

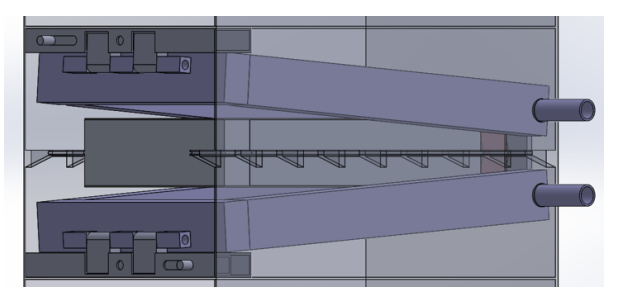
Removing the waste heat generated by the PEBB is key so that the power conversion device internal component temperature remains below $150^{\circ}C$ and does not become damaged. Conventional cooling methods using both air and water were explored, which eventually led to a design to transfer heat to the thermal management system via conduction. Conduction is an effective method for heat transfer, but poses the challenges of uniform surface area contact which can be affected by roughness and debris at the surface interface of the PEBB

shell and liquid cold plate. To maximize the surface contact and therefore the heat transfer a TIM was used. To optimize the heat transfer the following thermal management constraint was required: a uniform reference pressure of 13789.5 Pa be transferred through the liquid cold plate to the interface of the TIM and the PEBB shell. An additional thermal constraint was positioning the cooling water connections at the front of the PEBB cabinet to avoid close proximity with the electrical connections at the back.

The "sailor-carryable" PEBB units are limited to horizontal insertion and removal along a key/keyway system. This mechanical constraint assists with the electrical alignment connection at the back. The electrical constraints require the mating of the electrical plug at the back of the PEBB with the connection in the back of the cabinet. Added thermal constraints include keeping the cooling water connections away from any electrical connections and components. Within the thermal and electrical constraints there is a desire for modularity and power density of the iPEBB stack. These additional desires limit the space and size of the securing mechanism design and the integration of thermal and electrical connections within the iPEBB cabinet stack. Designing a solution that anchors the iPEBB while addressing the thermal management challenges and not imposing on the thermal and electrical constraints is a critical step in implementing PEPDS. For more information on the cooling and thermal management system, reference Chatterjee [2023], Padilla [2023], and Reyes [2022]. This thesis proposes a securing mechanism design for the iPEBB that withstands both static and dynamic forces of a ship environment and integrates with the thermal management solution.

1.4 Previous Research

Previous research has explored an alternative design for mechanically securing the iPEBB that integrated with an external liquid cooling approach utilizing a dry interface. Tomlinson [2022] conducted a preliminary design for a hinged-type mechanism that integrated with thermal management system. In this design, the hinge at the rear and elbow brackets in the front as shown in Figure 1.5 are the critical components. The hinges at the rear are where the cooling liquid enters and exits the cold plate. The elbow brackets are used to secure the PEBB when inserted and apply the reference pressure required. When the PEBB is removed the elbow brackets are used to hold the cold plate up.





(a) Open; Insertion/Removal

(b) Closed; Securing Force Applied

Figure 1.5: Hinged-Type Securing Mechanism Design Tomlinson, 2022.

While this design provided an excellent starting point in proposing a potential mechanical

securing force for the iPEBB thermal management problem, it likely cannot be feasibly scaled for shipwide employment. The disadvantages of the hinge design are: (1) there is no assistance for the heavy cold plate, (2) the hinge in back must be appropriately aligned to evenly distribute force on the iPEBB, and (3) the elbow brackets are the most significant risk of failure due to shearing when securing force is applied to the bolt [Tomlinson, 2022]. Additionally, the limitations of the hinge design include the power density of four iPEBB per stack as shown in Figure 1.6 due to the vertical space consumed as well as the disadvantage of an uneven applied securing force.

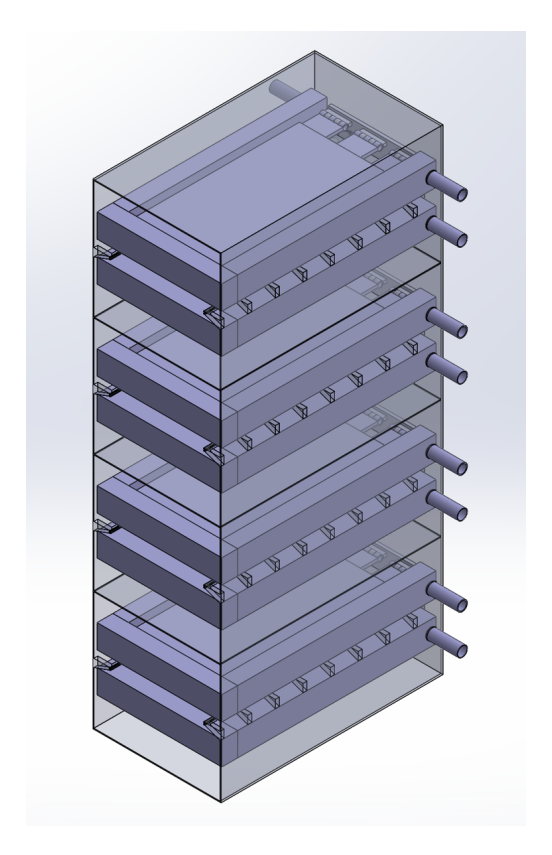


Figure 1.6: Proposed model of iPEBB Stack Design with Hinged-Type Securing Mechanism [Tomlinson, 2022]

1.5 Thesis Outline

The goal of this thesis was to research, design, evaluate, and model a PEBB securing mechanism and supporting system architecture suitable for shipwide deployment. This design must integrate with the ongoing NiPEC liquid cooling system and support systems.

In Chapter 2, theoretical calculations and simulations for structural integrity were performed on the PEBB and NiPEC cooling system support components. Using the first-pass securing mechanism calculations and design proposed by Tomlinson [2022] as an initial starting point, additional calculations and design iterations of the computer-modeled system were

performed based on relevant ongoing research provide by Virginia Tech on the PEBB shell material properties.

In an effort to validate the hypothesis of uniform pressure profiles using an airbag to transmit the force of the required interface pressure through the cold plate to the PEBB, experimental testing was conducted. Chapter 3 discusses the experiment performed using a uniform pressure distribution rig and TEK sensors. In conjunction with the uniform pressure experimental testing the TIM was used to validate the increase in surface contact at the interface of the PEBB shell for maximized heat transfer.

Chapter 4 documents the research on critical components for the integration of the PEBB securing mechanism design with the thermal management systems. Based on experimental results and design strategies, Chapter 5 recommends a modular stack consisting of six PEBB for integration with the shipwide cooling system. This securing mechanism design was tested for feasibility and performance with a single PEBB prototype. Chapter 6 provides conclusions of the work conducted in this research and recommendations for future work to pursue in the development of the shipwide NiPEC cooling system.

Chapter 2

Cold Plate and PEBB Structural Analysis

A structural integrity analysis is required on the cold plate, brace plate, and PEBB shell due to the assumed uniform force applied by the airbag for the thermal management and securing of the PEBB. It is import that the cold plate, brace plate, and PEBB shell not deform because the rate that heat transfers by conduction is directly proportional to the surface area contact at the interface. Any deformation in the surface area where the cold plate and PEBB shell interface would reduce the amount of heat transferred and could damage the electrical components inside the PEBB. In this section two cases will be analyzed. The first case is the deflection of the cold plate, brace plate, and top and bottom of the PEBB shell. The second case is the buckling of the PEBB shell housing consisting of two long and two short side plates.

2.1 Required Structural Analysis of the Cold Plate

As mentioned previously, the top and bottom of the PEBB shell interface with respective cold plates for thermal management using indirect liquid cooling. It is assumed that the airbag applies a uniform pressure to the cold plates which is then transmitted through the rigid body of the cold plate to the interface where the TIM PGS is located to assist in heat transfer by way of conduction. A deflection analysis of the cold plate is required because it is the location of the applied pressure from the airbag and where contact is made at the interface. For this analysis it is assumed that the cold plate is the limiting deflection and that the shell of the PEBB will not deform more than the cold plate.

2.1.1 Physical Characteristics of Cold Plate

For this analysis, the dimensions of the aluminum cold plate are assumed to be 550mm long by 350mm wide by 15mm thick. The ATS-TCP-1005[ATS] tubed cold plate specifications were used as a basis for calculating the total weight of the cold plate, because it is half the size of the one used in the analysis. Therefore all the weight properties provided by Advanced Thermal Solutions (ATS) for the referenced tubed cold plate were doubled. The

ATS-TCP-1005[ATS] base material is aluminum 6063 with 6 copper tube passes with a dry weight without fittings of 4.575kg and a tube fluid volume of about $200cm^3$. The total weight of the cold plate used in the deflection analysis was 9.55kg (94N) which accounts for the weight of the water in the tubes assuming a density of water of $1000kg/m^3$ at $10^{\circ}C$. The pressure applied by the inflated airbag to the cold plate was assumed to be a uniform load. The interface pressure used for deflection calculation was 2PSI (13790N/ m^2). The contact surface area of the cold plate is $0.165m^2$ and therefore a total applied force, F_A , is

$$F_A = (13790N/m^2)(0.161m^2) = 2275N (2.1)$$

2.1.2 Cold Plate - Deflection Analysis

The first step in this analysis is to verify that the cold plate classifies as a thin plate where the thickness, h, is assumed to be small compared to the other dimensions and loads are predominately perpendicular to the plane faces. Thin plate classification is based on the ratio of thickness (h) to the in-plane dimension (a). For thin plate classification the a/h ratio must be between 10 and 80. The in-plane dimension of the cold plate is 550mm and the thickness is 15mm, therefore the the a/h ratio is,

$$\frac{a}{h} = \frac{550mm}{15mm} = 36.6\tag{2.2}$$

which is within the thin plate classification range. A thin plate can further be subdivided by the ratio of maximum deflection, w, to plate thickness, h. A $w/h \le 0.2$ is classified as a stiff plate. A stiff plate is flexurally rigid and carries loads two dimensionally, mostly by internal bending and twisting moments and by transverse shear forces [Timoshenko et al., 1959]. If $w/h \ge 0.3$, then it is classified as a flexible plate where the lateral deflections is accompanied by stretching of the middle surface [Timoshenko et al., 1959].

Next, the deflection of the cold plate was calculated based on the assumption of a uniform pressure applied by the airbag. For the sake of simplicity, the cold plate is confined to a solid rectangular plate of aluminum 6063 which neglects the tubing. Navier's Method (double series solution) was used to analyze the deflection in the cold plate from the applied pressure. Roark's Formulas for Stress and Strain[Edge and LLC] was used to validate the theoretical results. Navier's Method makes the following assumptions [Timoshenko et al., 1959]:

- 1. The plate is initially flat.
- 2. The material, aluminum 6063, is elastic, homogeneous, and isotropic.
- 3. The deflection is small compared to the thickness of the plate.
- 4. Straight lines, initially normal to the middle plane remain normal to the middle plane during and after deformation.
- 5. Normal stress in the transverse direction is small compared with other stress components and can be disregarded.
- 6. The middle surface remains unstrained after bending.

Equation 2.3 below is the governing differential equation for the deflection of thin plate bending analysis based on Kirchoff's assumptions contained in those listed above. Lagrange introduced the governing equation 2.3 and Navier produced a solution for the deflection at any point in the form of an infinite Fourier series. ∇^4 is commonly referred to as the biharmoic operator.

$$\nabla^4 \omega = \frac{d^4 \omega}{dx^4} + 2 \frac{d^4 \omega}{dx^2 dy^2} + \frac{d^4 \omega}{dy^4} = \frac{p}{D}$$
 (2.3)

Equation 2.4 is the flexural rigidity, D, of the plate which plays the same role as the flexural rigidity EI in beam bending [Timoshenko et al., 1959]. Therefore D is:

$$D = \frac{Eh^3}{12(1-\nu^2)} \tag{2.4}$$

where E is the modulus of elasticity N/mm^2 of the aluminum 6063 cold plate, h is the thickness mm of the cold plate, and ν is the Poisson's Ratio.

Equation 2.5, $\omega(x,y)$ is the deflection surface and Equation 2.6, p(x,y) is the force distributed. Both ω and p are positive in the downward direction. In Equations 2.5 and 2.6, a and b are the side lengths of the plate and m and n are indexing variables.

$$\omega(x,y) = \sum_{m=1}^{\infty} \sum_{n=1}^{\infty} \omega_{mn} sin(\frac{mx\pi}{a}) sin(\frac{ny\pi}{b})$$
 (2.5)

$$p(x,y) = \sum_{m=1}^{\infty} \sum_{n=1}^{\infty} p_{mn} sin(\frac{mx\pi}{a}) sin(\frac{ny\pi}{b})$$
 (2.6)

Figure 2.1 shows a rectangular plate of sides a and b, simply supported on all edges and subjected to a uniform load p(x, y). The coordinates of the origin are placed in the lower left

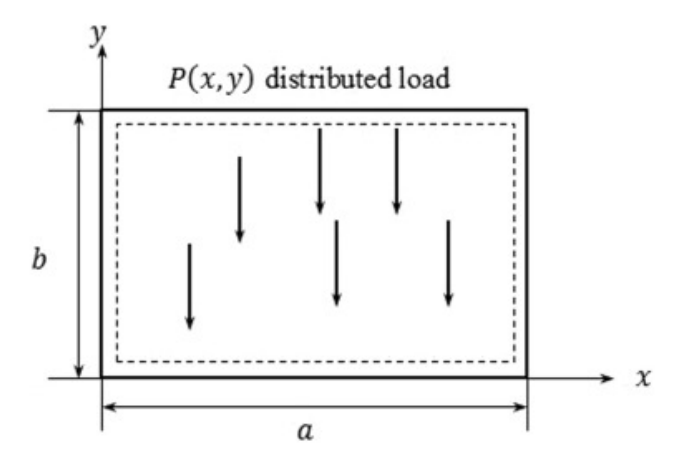


Figure 2.1: Simply Supported Plate with Uniform Normal Loading [Jweeg et al., 2021]

hand corner. The cold plate is assumed to be simply supported on all four edges, therefore

the boundary conditions are the following;

$$w = 0 \mid_{x=0}: \frac{d^2\omega}{dx^2} = 0 \mid_{x=0,a}: w = 0 \mid_{x=0}: \frac{d^2\omega}{dx^2} = 0 \mid_{x=0,b}$$
 (2.7)

Inserting the boundary conditions for a simply supported plate from equation 2.7 into equation 2.5 for the deflection surface, the double series sine expression for the deflection was yielded below:

$$\omega(x,y) = \frac{16p_o}{\pi^6 D} \sum_{m=1}^{\infty} \sum_{n=1}^{\infty} \frac{\sin(\frac{m\xi\pi}{a})\sin(\frac{m\eta\pi}{b})\sin(\frac{mu\pi}{2a})\sin(\frac{mv\pi}{2b})\sin(\frac{mx\pi}{a})\sin(\frac{ny\pi}{b})}{mn((\frac{m}{a})^2 + (\frac{n}{b})^2)^2}$$
(2.8)

From the Matlab script found in Appendix A, the maximum deflection was found when m=n=1 which showed the cold plate would deform $y_{N,max,CP}=0.089mm$. The small deflection analysis is valid and the $y_{N,max,CP}=0.089mm$ of deflection of the cold plate was acceptable. The deflection to thickness ratio was 0.0059 which classifies the cold plate as a stiff plate. Figure 2.2 is an exaggerated 3D surface plot to show the maximum deflection at the center of the cold plate with the deflection in mm found on the z-axis.

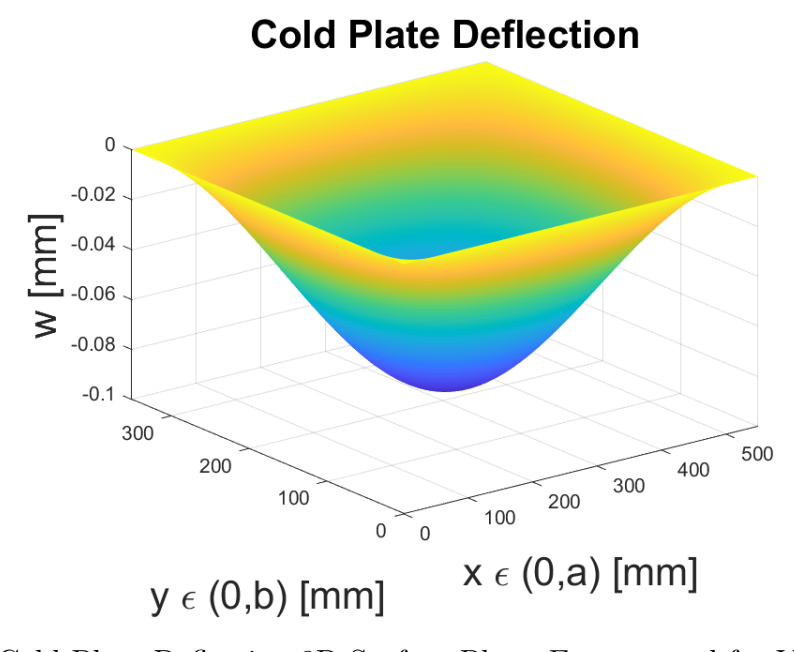


Figure 2.2: Cold Plate Deflection 3D Surface Plot - Exaggerated for Visualization.

Roark's Formula for Stress and Strain [Edge and LLC] was used to validate the theoretical calculations. From this analysis found in Appendix B, the deflection at the center was $y_{R,max,CP} = 0.05mm$ and stress was $\sigma_{R,max,CP} = 3.18N/mm^2$. This calculation supports the theoretical small deflection analysis calculated using the Matlab script, but is a more conservative deflection amount.

2.1.3 Cold Plate Modeling and Simulation

SolidWorks software tool was used to validate the theoretical calculations by modeling the geometry and simulating the applied load with the applicable boundary condition. The

SolidWorks software allows the user to see how the geometry of the model will deform based on the loading and boundary conditions applied as well as provide the numerical data. The first case that was modeled and simulated was the deflection analysis of the cold plate.

The rectangular cold plate was modeled with the dimensions of 550mm long by 350mmwide by 15mm thick. The material properties applied to the modeled cold plate were aluminum 6063. The cold plate was treated as a solid plate, excluding the tubing as was done in the theoretical calculations. The simply supported boundary conditions were applied along the four edges of the cold plate to model the restriction in movement of the cold plate. Then the uniform pressure load of $13790N/m^2$ was applied to the 550mm by 350mm face of the cold plate. Figure 2.3 shows the modeled cold plate with the green arrows along the edges showing the applied boundary condition and the red arrows showing the applied uniform load across the face. The legend is a heat map used to show the corresponding color to the deflection value $y_{S,max,CP}$ in mm displayed on the model. For the cold plate the maximum deflection was $y_{S,max,CP} = 0.082mm$ as annotated by the red in the center of the cold plate and the stress was $\sigma_{S,max,CP} = 3.53 N/mm^2$. The percent difference in the maximum deflection found using Navier's approximation for the theoretical calculations $(y_{N,max,CP} = 0.089mm)$ and the SolidWorks simulation $(y_{S,max,CP} = 0.082mm)$ was 8.2%. All of the deflection analysis results are consistent with one another and are within the acceptable values for a stiff plate. It is safe to assume the maximum deflection of the cold plate is $y_{N,max,CP} = 0.089mm$ based on Navier's theoretical calculations.

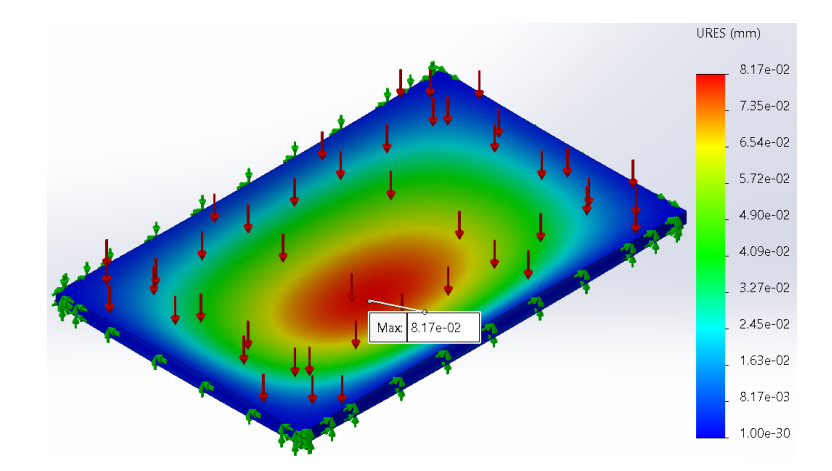


Figure 2.3: Cold Plate Deflection Simulation using SOLIDWORKS

2.2 Required Structural Analysis of the Brace Plate

The brace plate is a solid, uniform rectangular metal plate that partitions the iPEBBs vertically within the stack. The brace plates are required to resist the force applied by the inflated airbag and the weight of the cold plate without deformation. Figure 2.4 shows the proposed layout of the brace plates within the cabinet of the iPEBB stack. Based on this proposed iPEBB stack design a total of 6 iPEBBs are housed and 6 brace plates are required within the cabinet. The top face of the cabinet is assumed to be designed to the

same specifications of the brace plates to resist the force applied by the inflated airbag on the top iPEBB. The thin plate deflection analysis outlined in subsection 2.1.2 is applied to the aluminum brace plate.

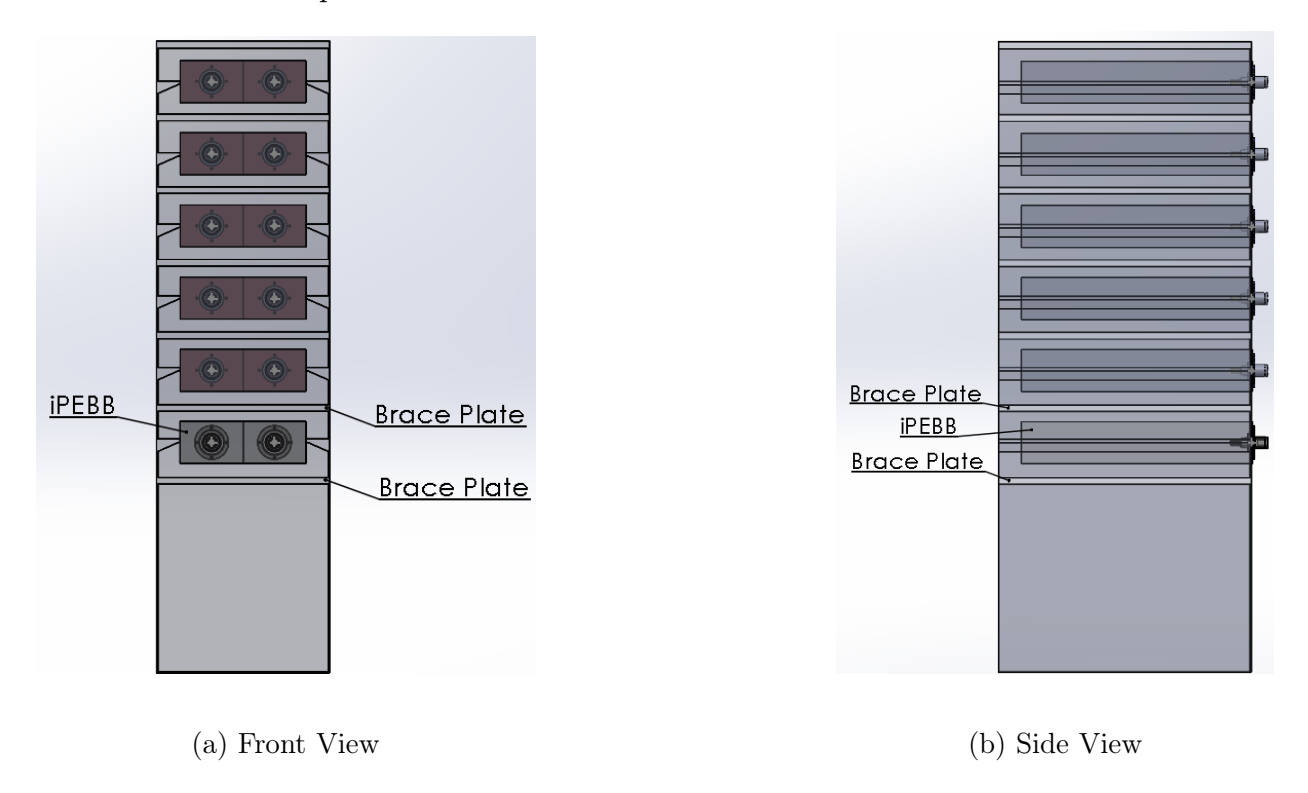


Figure 2.4: Views of Modeled Brace Plates within the iPEBB Stack

2.2.1 Physical Characteristics of the Brace Plate

The brace plate for this analysis is assumed to be a solid, uniform rectangular plate of 6063 aluminum. This is the same material used in the analysis of the cold plates which reduces the possibility of galvanic corrosion. The material properties of 6063 aluminum are ideal for corrosion resistance and weldability. The brace plate is assumed to be welded in the cabinet along three sides, with one short edge free to allow for the iPEBB stack's cabinet door. For this analysis, the dimensions of the aluminum brace plate are assumed to be 600mm long by 406.4mm wide by 25.4mm thick.

2.2.2 Brace Plate - Deflection

The brace plate meets the same classification requirements for a thin plate as outlined in the cold plate deflection analysis. To calculate the theoretical deflection of the brace plate the same governing differential equation 2.3 for the deflection of thin plates is used. Figure 2.5 shows a rectangular plate of sides a and b, clamped on all edges. The coordinates of the origin are placed in the upper left hand corner. For the brace plate deflection analysis all four edges of the plate are assumed clamped for simplicity of the calculation. Clamped boundary conditions are below:

$$w = 0 \mid_{x=0} : \frac{d\omega}{dx} = 0 \mid_{x=0,a} : w = 0 \mid_{x=0} : \frac{d\omega}{dx} = 0 \mid_{x=0,b}$$
 (2.9)

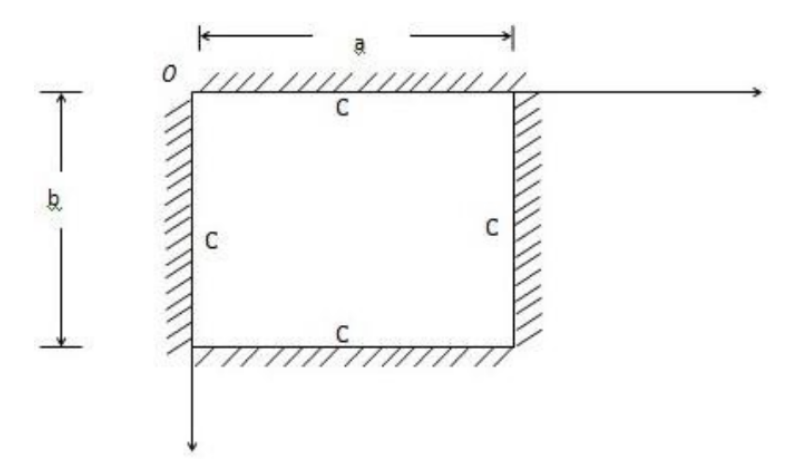


Figure 2.5: Clamped Rectangular Plate [Ephraim et al., 2019]

An exact solution for a clamped rectangular plate is given by [Taylor and Govindjee, 2004] using a double cosine series to satisfy the boundary conditions;

$$\omega(x,y) = \sum_{m=1}^{\infty} \sum_{n=1}^{\infty} (1 - \cos(\frac{2mx\pi}{a}))(1 - \cos(\frac{2ny\pi}{b}))\omega_{mn}$$
 (2.10)

The parameter ω_{mn} is determined using the Ritz method by using transformations to rewrite the functional in non-dimensional form;

$$\omega(x,y) = \sum_{m=1}^{\infty} \sum_{n=1}^{\infty} (1 - \cos(2mx\pi\xi))(1 - \cos(2ny\pi\xi))\omega_{mn}$$
 (2.11)

Inserting the boundary conditions from equation 2.9 into equation 2.11, the center deflection when the aspect ratio of the rectangular plate goes to infinity was yielded below:

$$\omega(x,y) = \frac{qb^4}{4\pi^4 D} \tag{2.12}$$

The maximum deflection was found when m=n=1 which showed the brace plate would deform $y_{max,BP}=0.03mm$. Figure 2.6 is an exaggerated 3D surface plot to show the maximum deflection at the center of the cold plate with the deflection in mm found on the z-axis. The small deflection analysis is valid and the maximum deflection of the brace plate was acceptable. The deflection to thickness ratio was $6.6e^{-4}$ which classifies the brace plate as a stiff plate. Roark's Formula for Stress and Strain [Edge and LLC] were used to validate the theoretical calculations. From this analysis found in Appendix B, the deflection at the center was $y_{R,max,BP}=0.05mm$ and stress was $\sigma_{R,max,BP}=5.47N/mm^2$. The brace plate deflection of 0.05mm supported the theoretical calculation and is a less conservative value to assume for the deflection.

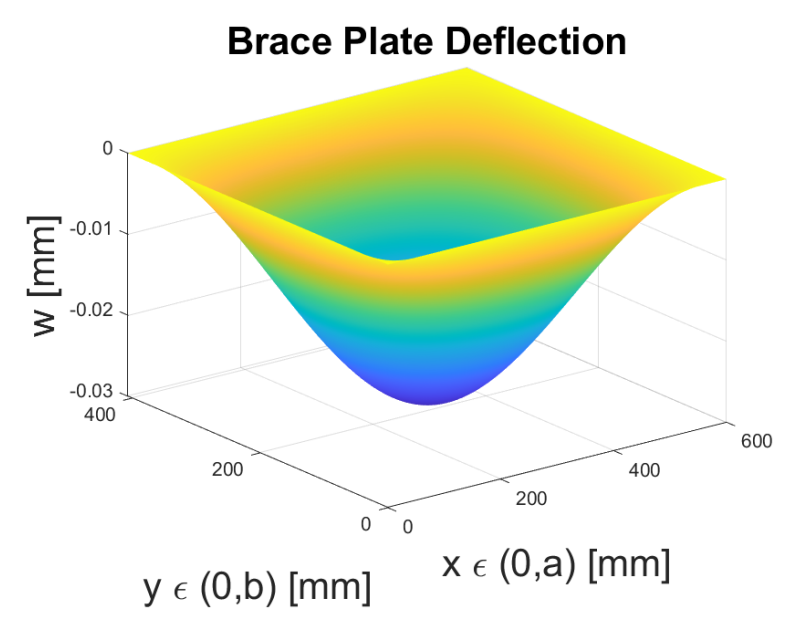


Figure 2.6: Brace Plate Deflection 3D Surface Plot - Exaggerated for Visualization

2.2.3 Brace Plate Modeling and Simulation

The second case that was modeled and simulated was the deflection analysis of the brace plate. The rectangular brace plate was modeled with the dimensions of 600mm long by 406.4mm wide 12.7mm thick. The material properties applied to the brace plate were aluminum 6063. Two cases of boundary conditions were evaluated for the brace plate, the first was with four edges fixed and the second was with three edges fixed and one short edge free. The uniform pressure load of $15795N/m^2$ was applied to the 600mm by 406.4mm face of the brace plate.

The first boundary condition case of four fixed edges was used to validate the theoretical deflection calculations using the double cosine series and Roark's formula. From the SolidWorks simulation the maximum deflection appears at the center of the plate based on the heat map legend as expected. The maximum deflection was $y_{S,max,BP} = 0.02mm$ and maximum stress was $\sigma_{S,max,BP} = 2.66N/mm^2$. Figure 2.7 shows the modeled brace plate with the four fixed edges. The more conservative approach is to base the max deflection and stress from Roark's formula which were acceptable values for the analysis of the brace plate.

The second boundary condition case of three fixed edges and one free short edge represents the actual layout of the brace plate anchored in the PEBB cabinet stack. Figure 2.8 shows the modeled brace plate with the three fixed edges and one free short edge. The heat map legend showed a maximum deflection of $y_{S,max,BP} = 0.03mm$ in the middle of the free edge and maximum stress of $\sigma_{S,max} = 3.51N/mm^2$. As expected the maximum deflection and stress values were more than the modeled brace plate with four fixed edges. All of the deflection analysis results are consistent with one another and are within the acceptable values for a stiff plate. It is safe to assume the maximum deflection of the brace plate is $y_{R,max,BP} = 0.05mm$ based on Roark's Formula for Stress and Strain[Edge and LLC]. Appendix C shows the maximum stress results of the SolidWorks simulation of the brace plate for both boundary condition cases.

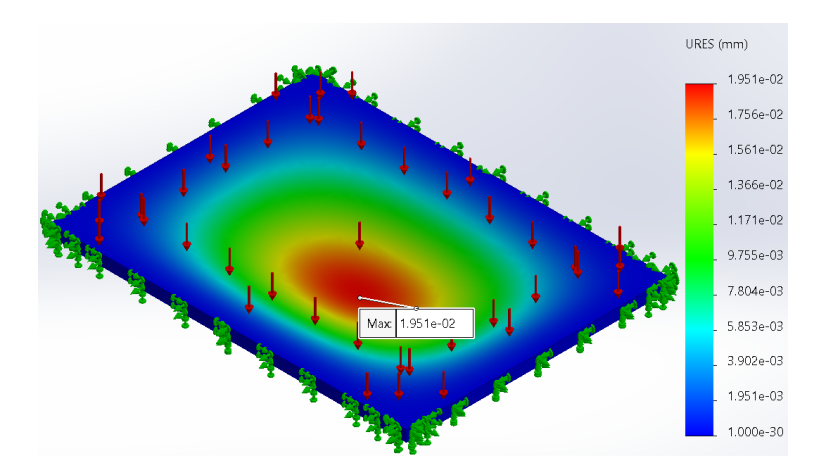


Figure 2.7: Brace Plate Deflection Simulation with Four Fixed Edges using SOLIDWORKS

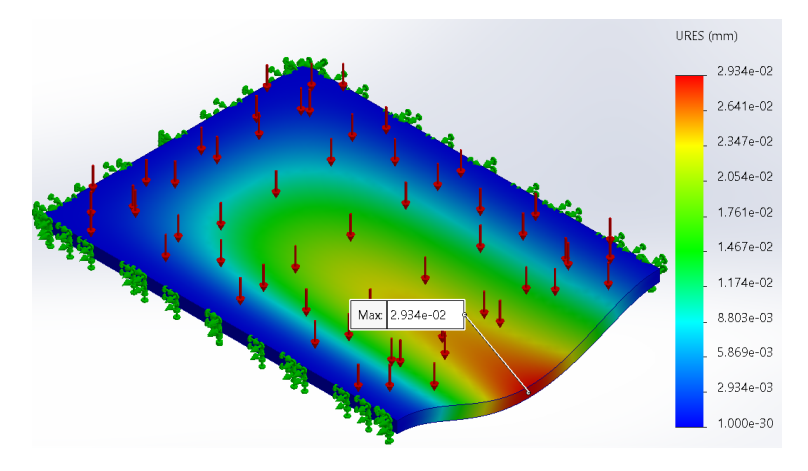


Figure 2.8: Brace Plate Deflection Simulation with Three Fixed Edges using SOLIDWORKS - Exaggerated for Visualization

2.3 Required Structural Analysis of the PEBB

The next step was a structural analysis of the PEBB shell to validate that it would not deform and the material would remain elastic under loading to maximize the heat transfer. The PEBB shell is specifically designed to be lightweight for transport yet sufficiently strong to protect the power conversion components secured inside while maximizing conduction. Therefore a deflection and buckling analysis was conducted with the total applied compressive forces of the airbags, weight of the cold plates, and dynamic loading based on the motions of the ship. For the structural analysis, the PEBB shell was treated as a hollow rectangular box and thin plate theory was applied to the top and bottom for deflection and buckling on the sides. Figure 1.4 shown in Section 1.2.2 displays the dimensions of the PEBB shell, measuring 550mm long by 300mm wide by 100mm high. Figure 2.9 is a representation of the PEBB model used in simulations to verify the theoretical structural analysis. The PEBB shell was not uniform material and thickness, the details of those properties specific to the structural analysis are further discussed below.

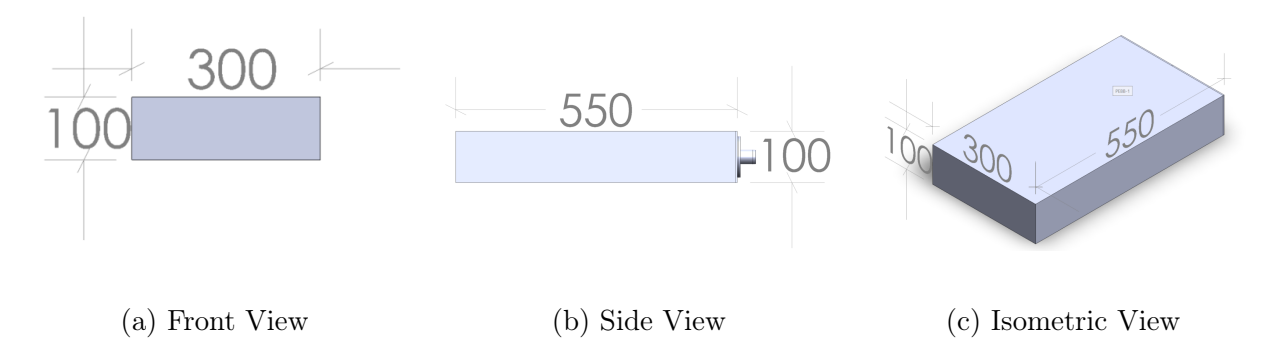


Figure 2.9: Views of Modeled iPEBB Shell

2.3.1 Physical Characteristics of iPEBB Shell

For this analysis the iPEBB shell was treated as an enclosed hollow rectangular box, with four side plates and a top and bottom plate. The four side plates of the shell are commonly referred to as the housing of the iPEBB and are made of an Delrin 570 blend. This material consists of 20% glass filled medium viscosity Polyoxymethylene (POM) copolymer which has a very high stiffness, low warpage, and good creep resistance at elevated temperatures [CAMPUS]. The material mechanical properties of the Delrin 570 blend are listed in Table 2.1 below. With the known material properties and dimensions of the iPEBB housing, the thickness of the housing was optimized to meet the required Buckling Factor of Safety (BFS) of 3. The resulting uniform thickness of the iPEBB housing was calculated to be 6mm. The total housing weight of the PEBB was 0.79kg.

For the iPEBB shell top and bottom plate, three different organic substrate stackups were preliminary analyzed to maximize the thermal conductivity and minimize weight. The first organic substrate investigated was a multi-layer Organic Direct Bond Copper (ODBC) substrate that consisted of copper and ODBC of varying thicknesses. The second organic

Table 2.1: iPEBB Housing Material Properties - Delrin 570 Blend [Del]

Material	Density	Tensile Strength	Tensile Modu-	Flexural	Flexural Modu-
		(yield)	lus of Elasticity	Strength	lus of Elasticity
Delrin 570	$1.56g/cm^{3}$	53.1MPa	$6.2e^3MPa$	10MPa	$5e^3MPa$
Blend					

substrate investigated was a multi-layer Risho substrate that consisted of copper and Risho of varying thicknesses. The third organic substrate was similar to the second with the minor difference in the bottom of the layer being aluminium rather than copper. Figure 2.10 shows the stackups of the organic substrates with associated thicknesses. The substrate selected

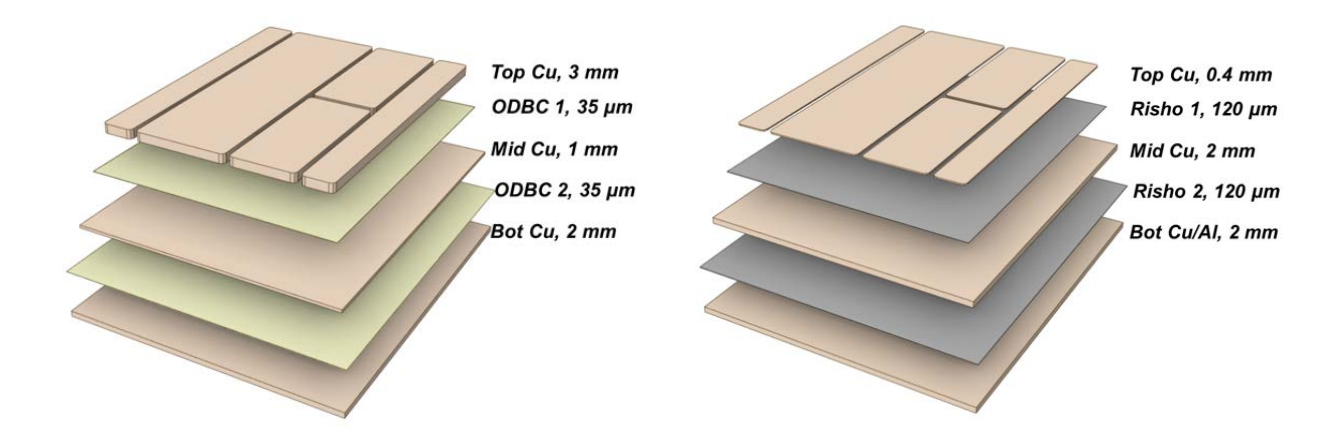


Figure 2.10: Multi-layer Substrates [DiMarino, 2022]

by Virginia Tech for the preliminary iPEBB design was a modified third organic substrate as shown in Figure 2.11 which had the best trade-off in thermal conductivity and weight. The outermost layer of the substrate was 1mm thick sheet of aluminum, followed by an organic dielectric of negligible thickness, and then a 1mm thick sheet of copper, followed by another negligibly thick organic dielectric before getting to the common substrate of 3mm copper. The 3mm common substrate is localized and does not extend the full area of the top and bottom PEBB shell, therefore was not accounted for in the deflection calculations of the top and bottom shell. The copper used in the substrate stackup is a copper alloy



Figure 2.11: Navy iPEBB Multi-layer Substrate[DiMarino, 2022]

composed of 99.6% copper and 0.4% oxygen with a mirror 8 finish that is commonly referred to as Electrolytic Tough Pitch (ETP). The type of aluminum was not specified so 6061 Aluminum was assumed for material based on the analysis from Tomlinson [2022]. The ETP and 6061 Aluminum substrate material properties are displayed in Table 2.2. The combined weight of the iPEBB top and bottom shell substrate is 1.91kg. The 14kg total electronic weight of the iPEBB already accounts for the weight of the substrate material used for the top and bottom shell plating.

Table 2.2: iPEBB Top and Bottom Substrate Material Properties [606] [MatWeb]

Material	Density	Tensile	Tensile Modu-	Flexural	Flexural Modu-
		Strength (ult)	lus of Elasticity	Strength	lus of Elasticity
ETP Cop-	$8.9g/cm^{3}$	220MPa	620.5MPa	N/A	$1.2e^5MPa$
per					
6061 Alu-	$2.7g/cm^3$	310MPa	N/A	299MPa	$6.9e^4MPa$
minum					

2.3.2 iPEBB Shell - Top and Bottom Face Deflection Analysis

As previously discussed in the deflection analysis of the cold plate, similar assumptions were carried forward for the multilayered top and bottom iPEBB shell:

- The cold plate and iPEBB shell top plate materials are isotropic
- Sliding between the multilayered materials was prevented
- The pressure applied by the airbag is uniform and transmitted through the cold plate to the iPEBB shell

The top plate of the iPEBB shell was selected as the face for analysis over the bottom because of the added force from the weight of cold plate (94N) on top of the shell. Furthermore it is assumed that the iPEBB shell will not deform more than the cold plate, because the uniform pressure is applied to the cold plate thus experiencing the most deflection. The overall deflection experienced is assumed to be less than 0.089mm theoretical calculation, because the additional thickness of the of the iPEBB shell will increase the overall flexural stiffness reducing the deformation from the uniform applied load.

2.3.3 iPebb Shell - Side Face Buckling Analysis

The next step in the analysis of the iPEBB shell was a buckling analysis of the housing, to confirm if the sides of the shell could withstand the compressing forces. The Equilibrium Method outlined in Timoshenko et al. [1959] was used to conduct the linear buckling analysis of plates. The Equilibrium Method makes the following assumptions:[Timoshenko et al., 1959]

- 1. Prior to loading, a plate is ideally flat and all the applied external loads act strictly in the middle plane of the plate.
- 2. States of stress are described by equations of the linear plane elasticity. Any changes in the plate dimensions are neglected prior to buckling.
- 3. All the loads applied to the plate are dead loads; that is, they are not change either in magnitude or in direction when the plate deforms.
- 4. The plate bending is described by Kirchoff's plate bending theory.

Equation 2.13 is the governing differential equation for linear buckling analysis of plates,

$$\frac{d^4\omega}{dx^4} + 2\frac{d^4\omega}{dx^2dy^2} + \frac{d^4\omega}{dy^4} = \frac{1}{D}\left(N_x \frac{d^2\omega}{dx^2} + 2N_{xy} \frac{d^2\omega}{dxdy} + N_y \frac{d^2\omega}{dy^2}\right)$$
(2.13)

where N_x , N_y , and N_{xy} are the in-plane stresses. The corresponding in-plane stress equation 2.14 identifies the internal forces acting in the middle surface of the plate based on the applied in-plane loading. For this analysis there are only compressive forces acting in y-direction along the long side of the plate (b) and the sides of the housing are simply supported, therefore N_x and N_{xy} are both zero.

$$N_y = -q_y : N_x = N_{xy} = 0 (2.14)$$

Figure 2.12 shows a plate and associated parameters with uniaxial compression along the y-direction. Where a is oriented in the y-direction and b is oriented in the x-direction, with $N_0 = N_y$. The governing differential stability equation for linear buckling of plates can be simplified to 2.15 after applying the boundary conditions for a simply supported plate from 2.7 and the in-plane stresses from 2.14.

$$D\nabla^2 \nabla^2 \omega + N_x \frac{d^2 \omega}{dx^2} = 0 \tag{2.15}$$

Next Equation 2.5 is inserted into Equation 2.15 which is further simplified to the following equation;

$$\sum_{m=1}^{\infty} \sum_{n=1}^{\infty} \left[D\pi^4 \left(\frac{m^2}{a^2} + \frac{n^2}{b^2} \right)^2 - q_y \pi^2 \frac{m^2}{a^2} \right] \omega_{mn} sin\left(\frac{mx\pi}{a} \right) sin\left(\frac{ny\pi}{b} \right) = 0$$
 (2.16)

One possible solution is the trivial solution when $\omega_{mn} = 0$. The trivial solution is neglected because it corresponds to an equilibrium in the unbuckled, flat state of the plate and is of no interest [Timoshenko et al., 1959]. Another possible solution is obtained by setting the quantity in the square brackets to zero, which is simplified and rearrange to find the edge load, q_y , show in the following Equation 2.17;

$$q_y = \frac{\pi^2 D}{b^2 h} (\frac{mb}{a} + \frac{n^2 a}{mb}) \tag{2.17}$$

The smallest value of q_y is the critical value, which is obtained when n=1 and m=1. The critical values for the housing side plates (Equation 2.18) and front and back plates (Equation 2.19) of the iPEBB are shown below.

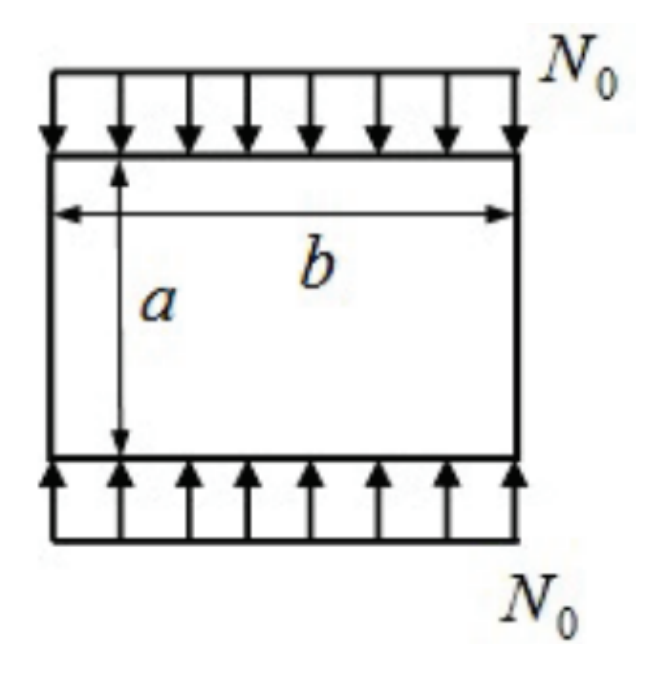


Figure 2.12: Buckling Loading Analysis of iPEBB Sides [Gunjal et al., 2015]

$$q_y = \frac{\pi^2 (100998N \cdot mm)}{(550mm)^2 (6mm)} \left(\frac{(1)(550mm)}{(100mm)} + \frac{(1)^2 (100mm)}{(1)(550mm)} \right) = 2.17 \frac{N}{mm^2}$$
 (2.18)

$$q_y = \frac{\pi^2 (100998N \cdot mm)}{(300mm)^2 (6mm)} \left(\frac{(1)(300mm)}{(100mm)} + \frac{(1)^2 (100mm)}{(1)(300mm)} \right) = 4.27 \frac{N}{mm^2}$$
 (2.19)

The next step was to determine the factor of safety against buckling by the calculating the total uniform applied load, $q_{y,applied}$, at the edge of the plate and compare that to the respective critical load. The total uniform applied load was determined by summing the total force applied to the PEBB shell's top plate. The total uniform applied load (2764.3N) accounted for the inflated airbag applied pressure (2275.3N), the dynamic force (395N), and the weight of the PGS and cold plate (94N). It was assumed that the edges of iPEBB shell would be loaded with a uniform distributed load, therefore the total uniform applied load was distributed across iPEBB shell edge area $(8500mm^2)$ of the top plate. The $q_{y,applied}$ load is

$$q_{y,applied} = \frac{2764.3N}{8500mm^2} = 0.33 \frac{N}{mm^2}$$
 (2.20)

which is less than the minimum buckling loads required for the side plates $(5.09 \frac{N}{mm})$ and front and back plates $(5.89 \frac{N}{mm})$. Therefore buckling of the iPEBB housing is not expected. The ratio of buckling loads to the applied loads for the BFS are shown below:

$$BFS_{side,plate} = \frac{2.17 \frac{N}{mm^2}}{0.33 \frac{N}{mm^2}} = 6.66 \tag{2.21}$$

$$BFS_{back,plate} = \frac{4.27 \frac{N}{mm^2}}{0.33 \frac{N}{mm^2}} = 13.14 \tag{2.22}$$

The MATLAB script that was used for the buckling analysis of the iPEBB housing plates is located in Appendix A. The Equilibrium method found that the sides of the iPEBB shell were safe from buckling under the compressive loading.

2.3.4 PEBB Side Plate Modeling and Simulation

The third case that was modeled and simulated was the buckling analysis was the short and long side plates of the iPEBB housing. The back plate of the iPEBB was modeled as rectangle with the dimensions of 300mm long by 100mm high by 6mm thick. The side plate of the iPEBB was modeled as a rectangle with the dimensions of 550mm long by 100mm high by 6mm thick. The material properties of Delrin 570 Blend were applied to the iPEBB shell plating model. For both iPEBB shell plates the boundary conditions for the short edges were assumed fixed and the long edges were free. The edge area loading of $0.33 \ N/mm^2$ was applied to the top and bottom edges of the plate models.

Figure 2.13 shows the modeled back plate of the iPEBB with the applied edge loading and associated deformation. The results from SolidWorks indicate that the iPEBB shell back and front plates are safe from buckling with a BFOS = 12.6.

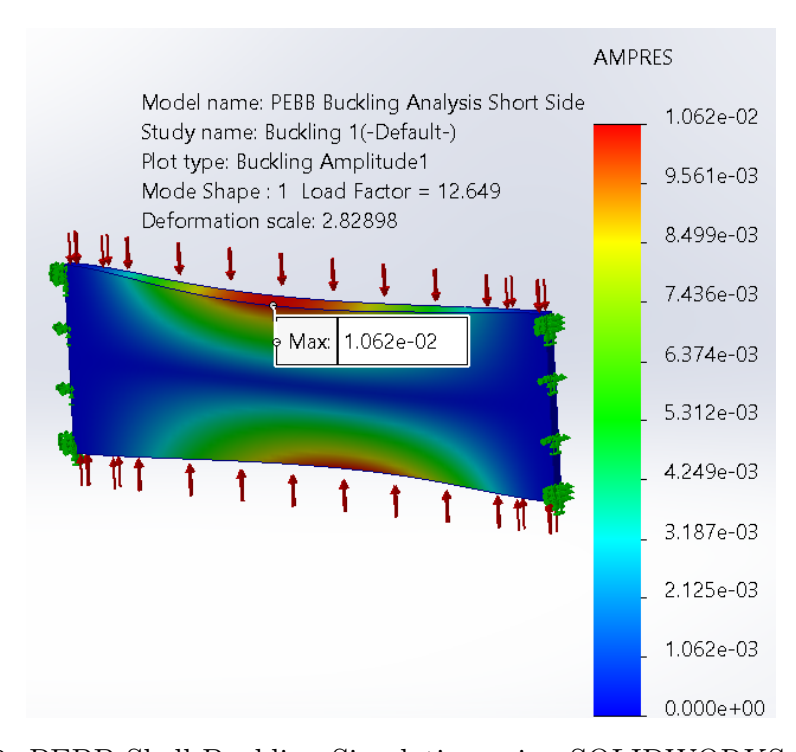


Figure 2.13: PEBB Shell Buckling Simulation using SOLIDWORKS- Short Side

Figure 2.15 shows the modeled side plate of the iPEBB with the applied edge loading and associated deformation. The results from SolidWorks indicate that the iPEBB shell side plates are safe from buckling with a BFOS = 3.2.

The ratio of the buckling loads to the applied loads is the factor of safety against buckling[SOLIDWORKS] . Figure 2.14 shows the interpretation of possible BFS values. The BFS output from SOLIDWORKs for the short and long sides of the iPEBB are greater than 1

BFS Value (factor of safety)	Buckling Status	Notes
1 < BFS	Buckling not predicted	The applied loads are less than the estimated critical loads. Buckling is not expected.
0 < BFS < 1	Buckling predicted	The applied loads exceed the estimated critical loads. Buckling is expected.
BFS = 1	Buckling predicted	The applied loads are exactly equal to the estimated critical loads. Buckling is expected.
BFS = -1	Buckling not predicted	The buckling occurs when the directions of the applied loads are all reversed. For example, if a bar is under tensile load, the BFS should be negative. The bar will never buckle.
-1 < BFS < 0	Buckling not predicted	Buckling is predicted if you reverse all loads.
BFS < -1	Buckling not predicted	Buckling is not expected even if you reverse all loads.

Figure 2.14: SOLIDWORKS Buckling Factor of Safety[SOLIDWORKS]

and therefore buckling is not predicted. This tells us that the applied loads are less than the estimated critical loads.

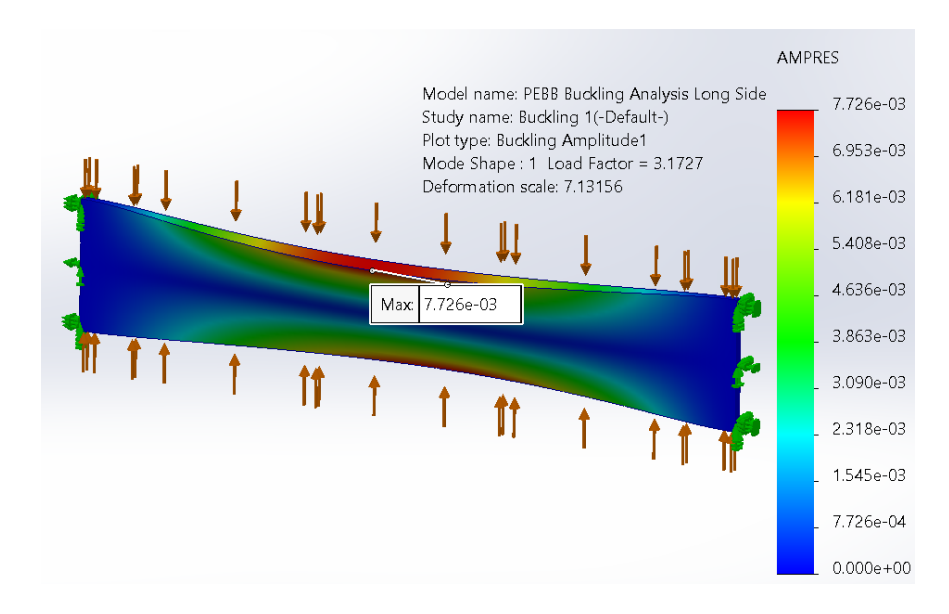


Figure 2.15: PEBB Shell Buckling Simulation using SOLIDWORKS - Long Side

2.4 Summary of Structural Analysis

Theoretical calculations and simulations presented in this chapter validated the structural integrity of the components associated with the proposed design. The deflection values of the brace plate, cold plate, and PEBB top and bottom shell are negligible and will not have an impact on the heat transfer. The PEBB housing will not buckle under the weight and applied pressure with a BFS of 3. Table 2.3 and 2.4 breakdown the conservative deflection and buckling analysis for the components withe corresponding method and boundary condition. Appendix B has the additional structural calculations performed.

Table 2.3: Deflection Structural Analysis Summary

	Material	Max Deflection (mm)	Boundary Condition	Method
Brace Plate	1060 Aluminum	0.03	3 Edges Fixed, 1	Simulation
			Short Edge Free	
Cold Plate	1060 Aluminum	0.09	4 Edges Simply Sup-	Matlab Script
			ported	

Table 2.4: Buckling Structural Analysis Summary

	Material	BFOS	Boundary Condition	Method
PEBB Shell Long Side	Delrin 570	3.2	2 Short Edges Fixed	SolidWorks
PEBB Shell Short Side	Delrin 570	12.6	2 Short Edges Fixed	SolidWorks

Chapter 3

Uniform Pressure Distribution Rig

Experimental testing was required to validate the assumption that the inflated airbag would provide a uniform pressure to the thermal interface between the cold plate and iPEBB shell. To validate this assumption the design and construction of a pressure test rig was required to test the mechanism. The pressure test rig was used to map the pressure profile generated by the securing force of the inflated airbag. The pressure profile should show that the pressure applied by the inflated airbag on the cold plate is a uniformly distributed pressure that is transferred through the rigid body to the heat transfer interface. It is important that the pressure test rig not deform or deflect under loading and that the same pressure be applied for repeatability of the experiments.

In this section two experiments are analysed. The first experiment tests the assumption that the inflated airbag can transfer a uniform pressure profile at the thermal interface. This experiment will also look at the impact of the PGS TIM filling interstitial gaps along with the smoothness tolerances on the faces of the plates. The PGS material is supposed to assist in the even distribution of heat removal by lowering the contact resistance when the cold plate and iPEBB are forced together. The PGS is meant to fill the interstitial gaps, reducing the loss of heat transfer from possible surface roughness or debris between the cold plate and iPEBB. The second experiment tests the effects of the cooled water circulating through the cold plate on the pressure of the inflated airbag. A change in the pressure of the airbag could have a significant impact on the heat transfer.

3.1 Design

The uniform pressure distribution rig was designed to experimentally map the uniform pressure distribution applied by the airbag from 0-10psi range. The rig was designed to measure and record a two-dimensional pressure profile with a reflection symmetry of the overall final design. The rig mapped the pressure profile of the load applied between the upper cold plate and the top of the iPEBB, represented by an aluminum plate. The midplane for the symmetry of the rig design is the lower aluminum plate and brace support. This pressure rig does not take into account manufacturing tolerances for the surface roughness on the faces of the aluminum plates and the cold plate. This issue became more apparent with the data from repeated experiments, more specifically from the sensitivity and location of the TEK sensor.

The uniform pressure distribution rig design, depicted in Figure 3.1, which displays the CAD model layout of the upper and lower brace supports with aluminum plates, the airbag, cold plate, PGS, and the TEK sensor. An exploded view with the labeled components is shown in Figure 3.2, and the full experimental rig is shown in Figure 3.3.



Figure 3.1: CAD Model of Uniform Pressure Distribution Rig

Two sets of steel support cross bars were used on the outside of the aluminum brace plates to absorb the bending deformation as the airbag inflated applying pressure to the rig. The steel support cross bars, measuring 304.8mm x 12.7mm x 12.7mm each, minimized the deflection in the aluminum brace plates. A total of ten steel braces are used, five on each aluminum brace plate. The orientation of the five steel bars consists of three bars running parallel to one another with equal spacing across the aluminum brace plate. The additional two steel bars run orthogonal and on top of the three steel bars.

The bottom and top aluminum brace plates measured 152.4mm x 152.4mm x 12.7mm and were fixed to the T-slot aluminium extrusion linear rail foundation, shown in Figure 3.3. The bottom brace plate replicated boundary conditions of the iPEBB top shell plate. The TEK I-scan pressure sensor was placed on top of the bottom brace plate to map the pressure profile at the thermal interface with the PGS interface material. The PGS material was located on top of the TEK I-scan pressure sensor to fill interstitial gaps and maximize surface contact between the replicated iPEBB plate and cold plate. The cold plate showed more surface defects than the aluminum plate which justified the location of the PGS material on top of the sensor.

The cold plate used was the ATS-TCP-1021 which had 6 total tube passes made of stainless steel with a 12.7mm inner diameter piping. The dimensions of the ATS cold plate measured $152mm \times 119mm \times 15mm$ with a total of 229mm of piping for cooled water. The cold plate used for conductive thermal regulation with circulating cooled water was stacked on top of the PGS material.

A 12.7mm vertical gap was left between the top of the cold plate and the top aluminum brace plate, which was fixed to the rig. The airbag used to apply a constant uniform pressure was placed in the gap on top of the cold plate. The deflated airbag thickness occupied 2mm of the 12.7mm gap extending to the upper aluminum brace plate. When inflated, the airbag fills the gap and applies pressure to the full system. To maximize the surface area contact for the pressure profile data collection the airbag was inflated to 8psi for the experiments.

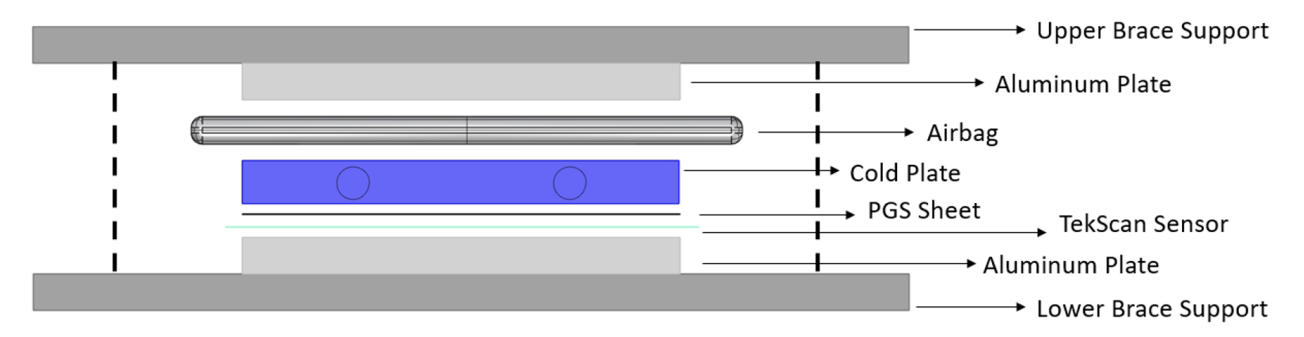


Figure 3.2: Uniform Pressure Rig Exploded View of CAD Model

The results obtained from this experimental rig setup were subject to controllable and uncontrollable factors that may have impacted the data. Controllable factors include the pressure applied by the inflated airbag on the system, the temperature of the cool water circulating through the cold plate, and the flow rate of the circulating cooled water. The uncontrollable factors include the ambient air temperature and the manufacturing tolerances of the surfaces used in the pressure rig, specifically the faces of the cold plate and the top and bottom aluminum plates. When analyzing the results from the uniform pressure rig, these factors must be considered and addressed. To validate the experimental results, theoretical calculations and analytical models are used for comparison.



Figure 3.3: Uniform Pressure Experimental Rig

3.1.1 Sensors

The TEK I-scan 5151 pressure sensor mat displayed in Figure 3.4 was used in the mapping of the uniform pressure distribution profile. This pressure mat has an array of 44 by 44 sensor elements, which is each approximately $1mm \times 1mm$.

Table 3.1 displays the properties of the TEK sensor used for data recordings in the pressure rig to include the associated pressure ranges and uncertainties. The sensor was calibrated prior to use by TEK, however with repeated use of the sensor, it is expected that elements of the sensor experience drift over time.

Table 3.1: Tekscan Sensor Properties Tekscan

Sensor	Manufacturer	Range	Uncertainty	Quantity
I-scan 5151 Pressure Mat	Tekscan	0-150 <i>PSI</i>	3-9 %	1



Figure 3.4: TekScan 5151 I-Scan Pressure Sensor[Tekscan]

To reduce the error in the pressure recording experienced by drift in the sensor elements, equilibration and zeroing functions were explored. Equilibration is a function used to correct the raw sensor output for unevenness across sensing elements, whereas the zeroing function of the sensor removes the preload. Performing both these functions in conjunction offsets the other. The zeroing function did provide a practical benefit, because the small preload of the deflated airbag was negligible. But removing the unevenness across the sensing elements was beneficial; therefore the equilibration function was applied to the TEK sensor in accordance with the manual prior to use. Equilibration requires perfect uniform physical loading of the sensor.

3.1.2 Airbag

The airbag in the pressure rig applied the pressure to the cold plates required for the PGS material to maximize the heat transfer through conduction. The airbag design offers a unique added benefit of a thin profile that applies an external uniform distribution of sufficient pressure across the face of the cold plate. That uniform pressure distribution is then transmitted through the rigid body of the cold plate to the iPEBB shell, allowing for the transfer of heat from the iPEBB to occur using indirect liquid cooling.

The durable fiber-reinforced material of the WINBAG[WINBAG] airbag used in the experimental rig allowed for repeatable experiments requiring inflation, deflation, and different interface pressures. Table 3.2 displays the properties of the two different sizes of the WINBAG airbags that were used during the experiments.

The airbag was connected to a pressure calibrated hand pump with an accuracy of $\pm 1.5\%$ for the experimental testing. The Baker Instruments Baker pressure calibrated hand pump was used to inflate the airbag to the desired pressure, secure the air, and deflate the airbag. This specific hand pump provided an analog gauge display that measured pressure ranges from 0 to 18 PSIG.

Table 3.2: WINBAG Properties[WINBAG]

Manufacturer	Part Number	Area Dimensions	Gap Span	Load Capacity
WINBAG MAX	E15730MAX	330.3 by 254 mm	2 to 70 mm	$250 \ kg$
WINBAG	15730	177.8 by 177.8 mm	2 to 50 mm	$135 \ kg$

3.2 Pressure Trials

For the metrics of repeatability, pressure mapping profiles were recorded with the same external uniform pressure of 8psi applied by the airbag over the interface of interest with all of the other experimental settings held constant. To compare the pressure profiles, the TEK sensor was staged in different levels of the uniform pressure distribution rig with and without the PGS thermal interface in place. The pressure data from these experiments were compared using the fixed area averaging of the sensor elements. These sensor elements are commonly referred to as sensels. The TEK I-Scan 5151 pressure mat is an array of 44 by 44 sensor elements, for 1936 total sensels[Tekscan].

Two analyze the data, two averaging methods were explored to most accurately account for the sensel loading and contact area. The first averaging method reviewed, displayed each sensor elements pressure value modified to reflect the value of its neighbor which overestimated the loading and contact area. The second method, the fixed area averaging method, did not result in an increased total loading and contact area because the sensels that had zero load remained unloaded. The intended effect of fixed area averaging was to increase the accuracy of the sensor data due to the sensels left unloaded because of defects and surface roughness in the plate faces and sensitivity of the TEK sensor. An example of fixed area

averaging for the average pressure value of X in the group of nine cells in Table 3.3 is given by the following equation,

$$X_{avg} = \frac{\frac{A+C+F+H}{2} + B + D + E + G + X + X}{8}$$
 (3.1)

Table 3.3: Sensel Averaging

A	В	С
D	X	Е
F	G	Н

A Center of Force (COF) feature was used to show how the force applied by the pressurized airbag is balanced on the sensor as indicated by the gray and white icon. The COF coordinates were calculated using the following two equations,

$$X_{cof} = \frac{\left(\sum_{i=0}^{Cols-1} (i \sum_{j=0}^{Rows-1} [F_{ij}])\right)}{\left(\sum_{i=0}^{Cols-1} (i \sum_{j=0}^{Rows-1} [F_{ij}])\right)}$$
(3.2)

$$Y_{cof} = \frac{\left(\sum_{i=0}^{Rows-1} (i \sum_{j=0}^{Cols-1} [F_{ij}])\right)}{\left(\sum_{i=0}^{Rows-1} (i \sum_{j=0}^{Cols-1} [F_{ij}])\right)}$$
(3.3)

where F is the force at each sensel. The COF feature was used to track the force.

The experimental testing was used to validate the theory that the force applied by the airbag would provide a uniform pressure distribution that could be transmitted through the cold plate to the thermal interface.

An additional benefit the airbag would provide was the minimum vertical distance consumed to apply to required pressure for the heat transfer to take place. Reducing the vertical clearance would allow the power density of the PEBB stack to increase 50% from 4 to 6 PEBB per stack. With the volume of the airbag confined, a greater interface pressure could be applied to maximize the heat transfer and not increase the vertical clearance required.

3.2.1 Uniform Pressure Distribution Model Empirical Results

As detailed above, the TEK sensors were staged in three different levels of the pressure rig to record the pressure profile with and without the PGS thermal interface. The three different sensor locations are described below.

- 1. TEK sensor between the aluminum plate (iPEBB shell) and cold plate. (Figure 3.2)
- 2. TEK sensor between the aluminum plate (iPEBB shell) and another aluminum plate with the cold plate stacked on top. (Figure 3.5)
- 3. TEK sensor between the aluminum plate (iPEBB shell) and the airbag. (Figure 3.5)

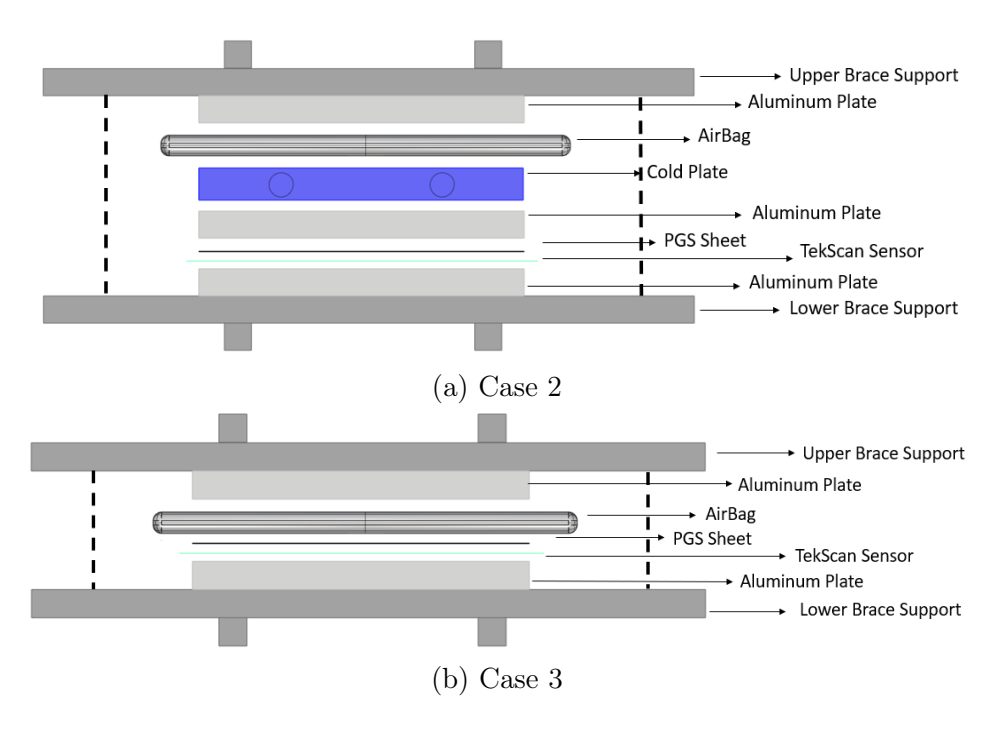


Figure 3.5: Experimental Pressure Test Rig with Different TEK Sensor Locations

The pressure profiles showed that the external pressure applied by the airbag was transmitted uniformly through the cold plate to the iPEBB shell. The interface uniform pressure applied by the airbag was 8psi. Each test was run twice: once with and once without PGS in the interface. In Figures 3.6, 3.7, and 3.9, the pressure map profiles without PGS are located on the left and the profiles with PGS are located on the right in the side by side view. The legend between the two side-by-side pressure profile maps displays the color-to-pressure correlation. It can be seen from the comparison of the pressure map that those with PGS have a smoother profile depicting a more uniform pressure distribution across the thermal interface. The PGS material fills the interstitial gaps due to surface roughness which is demonstrated by the increased contact area recorded by the pressure map profiles with PGS material. By filling the interstitial gaps with PGS the loss of heat transfer is reduced from the surface roughness or debris between the cold plate and iPEBB.

The black areas in the pressure map profiles are the unloaded sensels of the TEK sensor, which are due to interstitial gaps not filled by the thermal interface material or the sensitivity of the sensor. Throughout the experimental pressure mapping, unloaded sensels were seen in the corners of the pressure mapping profiles and higher pressure recordings were seen at the edges of the border of the pressure mapping profiles. The unloaded sensels at the corners of the sensor were due to bulging of the airbag during inflation which reduced its surface contact. The higher pressure recordings at the borders were because the area of TEK sensor was larger than the area of the bottom aluminum plate (iPEBB shell); therefore, as the airbag applied pressure, the sensor was pinched by the edge of the aluminum plate, causing anomalous high readings.

Table 3.4: Airbag Sensor Cold Plate Interface

	Area	Pressure
Expected Values	$36in^2$	8psi
Without PGS	$20.17in^2$	6.68psi
With PGS	$33.09in^2$	7.92psi
Percent Difference	48.5%	17%
Percent Change	64% increase	19% increase

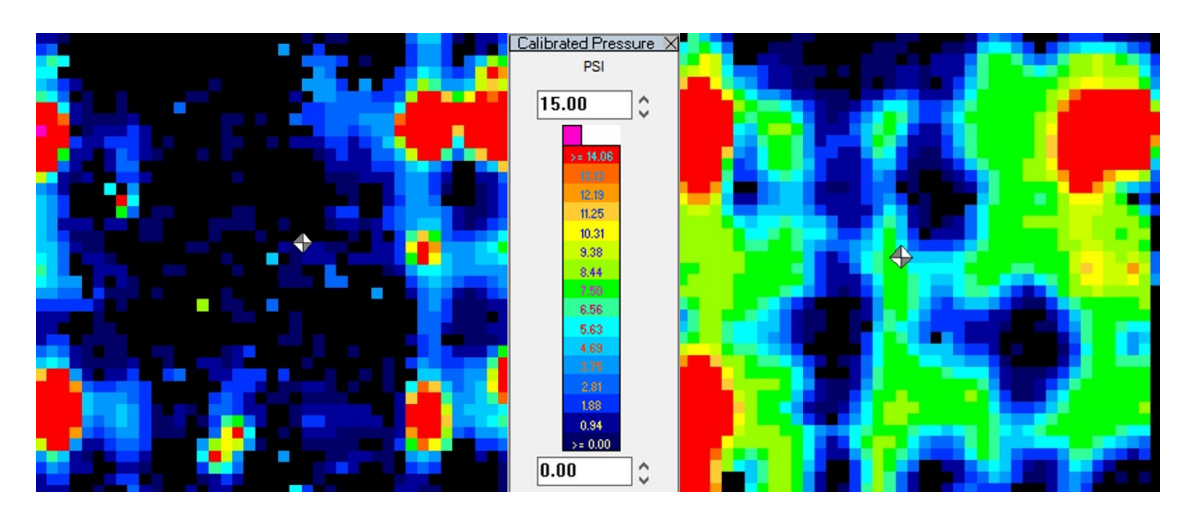


Figure 3.6: TEK Sensor between iPEBB shell and Cold Plate with (right) and without (left) PGS

Figure 3.6 is the first staged TEK sensor location between the aluminum plate (PEBB shell) and the cold plate. In this experiment the pressure was applied directly by the airbag to the cold plate and transmitted to the TEK sensor interface at the PEBB shell. From this side by side comparison with and without the PGS material, the pressure plot with the PGS material has a smoother, more uniform pressure profile than without the thermal interface material. The pressure map profile without the PGS material is blotchy and uneven as seen by the amount of black which shows the unloaded sensels. Table 3.4 compares the area and pressure data recorded by the TEK sensor for the profiles with and without the PGS material. From the comparison of the pressure profile maps with and without the PGS material there is a substantial difference in the area and average pressure. The PGS material fills the interstitial gaps left by the defects in the cold plate and the TEK sensor captures a more accurate loaded area and even pressure profile. With the PGS material the percent difference in area captured was 48.5% larger than without the TIM. With the PGS TIM the average pressure recorded by the sensor was 7.92psi which was more accurate to the gauge pressure of 8psi applied by the airbag. The percent change in pressure increased by 19% with the PGS material than without it.

Table 3.5: Airbag Sensor Aluminum Plate Interface

	Area	Pressure
Expected Values	$36in^2$	8psi
Without PGS	$28.50in^2$	7.58psi
With PGS	$34.64in^2$	7.87psi
Percent Difference	20%	4%
Percent Change	22% increase	4% increase

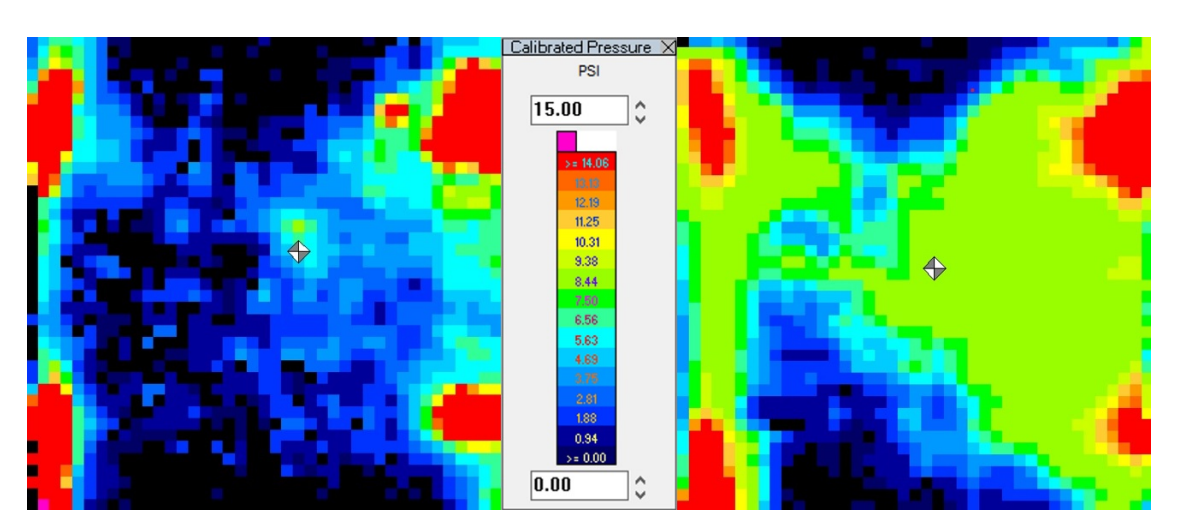


Figure 3.7: TEK Sensor between iPEBB shell and Aluminum Plate with (right) and without (left) PGS

The next experiment recorded the pressure profiles with the TEK sensor in the second staged location between the aluminum plate (PEBB shell) and another aluminum plate with the cold plate stacked on top. In this pressure rig setup the pressure was transmitted through the cold plate and aluminum plate to the TEK sensor interface by the pressurized airbag. This experiment was repeated with a different intermediate plate face was used to document how the tolerances in the flatness and smoothness of the faces in the plates affected the pressure profile. Figure 3.8 compares the tolerances in the face of the aluminum plate and the cold plate. The aluminum plate face had a mirror-like finish that was polished and free of grain lines, whereas the cold plate face was abrasive and warped.



Figure 3.8: Cold Plate and Aluminum Plate Face Surfaces

Figure 3.7 is the side-by-side comparison of the pressure profiles just for the second TEK sensor location with and without the PGS material. The pressure plot with the PGS material has a smoother, more uniform pressure profile. Table 3.5 compares the area and pressure data recorded by the TEK sensor for the profiles with and without the PGS material. With the PGS material we see the same trend of an increase in both area and average pressure as the thermal interface material fills the interstitial gaps left by defects or debris on the face of the aluminum plate. To note, the PGS material has a positive impact on the contact area and recorded pressure. The percent difference and change shows a smaller increase than the first experiment, but that is due to the change in the smoothness of the plates. The PGS material had less interstitial gaps to fill with the aluminum plate compared to the cold plate face.

When comparing the results of the first experiment to the second without PGS a significant difference in pressure and contact area were noted. The difference between these experiments was the addition of the aluminum plate to compare the tolerance in the smoothness and flatness of the plate faces. In the first staged rig without the PGS the area recorded was $20.17in^2$, whereas with the second staged aluminum plate the area captured increased to $28.50in^2$. The percent difference in the areas was 34%, which shows the how tolerance in the plate face with respect to surface smoothness and flatness affects the average pressure and how it is distributed. With the PGS material applied in the first staged experiment compared to the second there was negligible difference in the area and average pressure as the thermal interface material filled the interstitial gaps left behind. The percent difference of the area and pressure have drastically reduced when the results of the second experiment are compared to the first experiment due to the tolerance in the face of the aluminum plate. Because the face of the aluminum plate was smoother and even, there were less defects which allowed the pressure to be more uniformly distributed across a larger area. Therefore the

tolerance in the finish of the plate face is critical. The plate face of the cold plate for the final design should be free of defects and completely flat to allow for a uniform pressure distribution to the entire area of the iPEBB shell to maximize the heat transfer.

Table 3.6: Airbag Sensor Interface

	Area	Pressure
Expected Values	$36in^2$	8psi
Without PGS	$27.21in^2$	8.20psi
With PGS	$27.28in^2$	8.24psi
Percent Difference	0.26%	0.49%
Percent Change	0.26% increase	0.49% increase

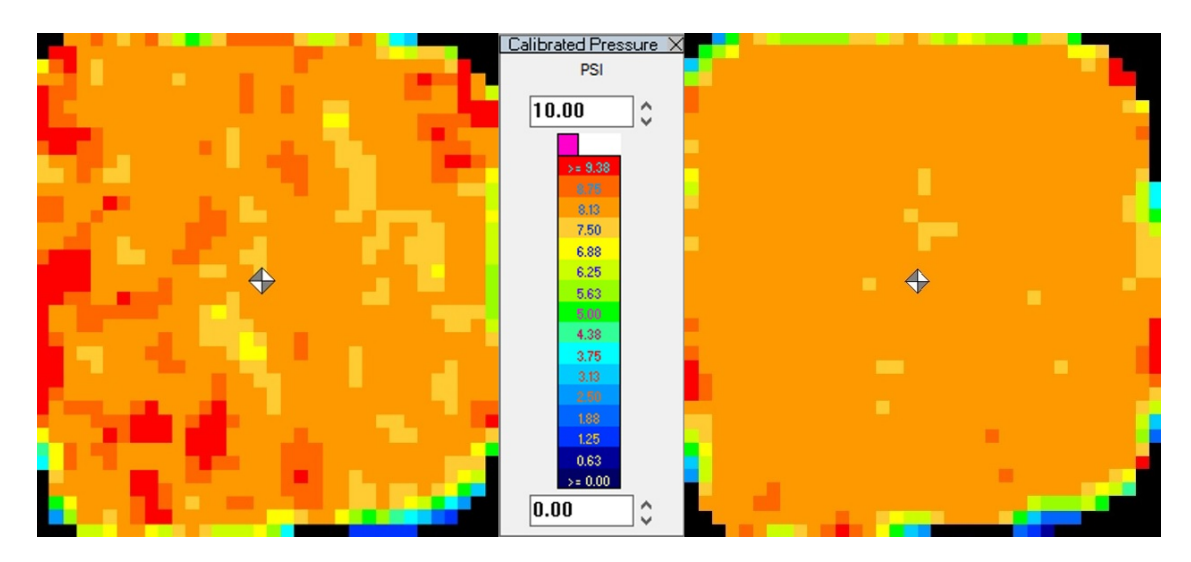


Figure 3.9: TEK Sensor between iPEBB shell and Airbag with (right) and without (left) PGS

Figure 3.9 is the third staged TEK sensor location between the aluminum plate and the airbag. The pressure from the airbag was not transmitted through another solid medium such as the cold plate or another aluminum plate to the TEK sensor interface. In this staged experiment the pressure was applied directly from the airbag to the sensor which would provide an ideal pressure map profile with negligible surface tolerance impact.

From this side by side comparison with and without the PGS material, the pressure plot with the PGS material has a smoother, more uniform pressure profile. Table 3.6 compares the area and pressure data recorded by the TEK sensor for the profiles with and without the PGS material. The percent difference in area and pressure with and without the PGS material were negligible because there were minimal interstitial gaps left by scratches or defects in the intermediate plate faces that needed to be filled by the TIM. The percent change showed the same trend with a slight increase in area and pressure with the PGS material. To note, one difference between this experiment and the previous two was that the vertical clearance gap for the airbag to fill when expanded was not adjusted with the

removal of the cold plate and aluminum plate. Therefore the $27in^2$ contact area of the airbag is substantially less than maximum sensor area of $36in^2$ due to bulging. To maximize the pressure contact area, the airbag should extend slightly beyond the cold plate area to account for bulging and the vertical clearance should as small as possible while allowing for the iPEBBs extraction.

3.2.2 Accuracy of the Empirical Model

As previously outlined in sections 3.1.1 and 3.1.2 the TEK pressure sensors and the airbag calibrated hand pump had associated ranges of uncertainty and accuracy. The uncertainty in measurements using the TEK pressure sensor was 3-9% of the average pressure recorded on the interface of interest [Tekscan]. The associated range of accuracy of the Baker Instrument calibrated hand pump was +/-1.5% [Baker]. Repeatability of the uniform pressure distribution rig was conducted to determine the trend and accuracy of the empirical model. More specifically, the empirical model of the uniform pressure distribution rig required that the airbag be pressurized to the same interface pressure of 8psi for each trial.

The pressure data from these experiments were compared and validated the airbag design for a securing force of the thermal management system modules. The securing force applied a uniform pressure distribution that was transmitted through the cold plate to the thermal interface. The manufacturing tolerances for the smoothness on the faces of the aluminum plates and the cold plate were an issue. With repeatability of the experiments and the repositioning of the TEK sensor at different locations within the rig, the data further supported the issue of surface roughness at the plate faces. Therefore the surface of the iPEBB shall be as smooth and flat as possible for maximizing the heat transfer by way of conduction. The pressure rig produced repeatable uniform pressure distributions between the cold plate and iPEBB shell interface thus validating the uniform pressure distribution securing force.

3.3 Temperature Trials

The ideal gas law was used to help understand how the pressure in the airbag would be affected as the temperature of the air in the inflated airbag decreased due to the contact with the cooled cold plate. The atmospheric air used for the experiment has similar behaviors to an ideal gas therefore can be reasonably approximated as ideal. Four governing assumptions were made for an ideal gas:

- 1. The gas particles have negligible volume.
- 2. The gas particles are equally sized and do not have intermolecular forces with other gas particles.
- 3. The gas particles move randomly in agreement with Newton's Law of Motion.
- 4. The gas particles have perfect elastic collisions with no energy loss.

The ideal gas law principle is given by the following equation,

$$PV = nRT (3.4)$$

where P is the pressure (Pa), V is the volume (m^3) , n is the number of moles of gas, T is the temperature $(^{\circ}C)$, and R is the ideal gas constant. The assumption of an isochoric process was made for the cooling of the air in the airbag which is an inelastic container and that the volume of air remained constant. Therefore the change in the temperature of the air would directly affect the pressure of the airbag. Once heat was removed by the interaction of the airbag with the cooled cold plate the pressure of the airbag would decrease with the decreasing temperature. The ambient air temperature in the room was measured and found to be $13.9(^{\circ}C)$ which was the assumed air temperature inside the airbag. The water circulating through the cold plate was cooled to $5.5(^{\circ}C)$ which was required for the heat transfer of the iPEBB by means of conduction. The theoretical results according to Amonton's Law of pressure and temperature being directly proportional for two different airbag volumes are shown in Figure 3.10.

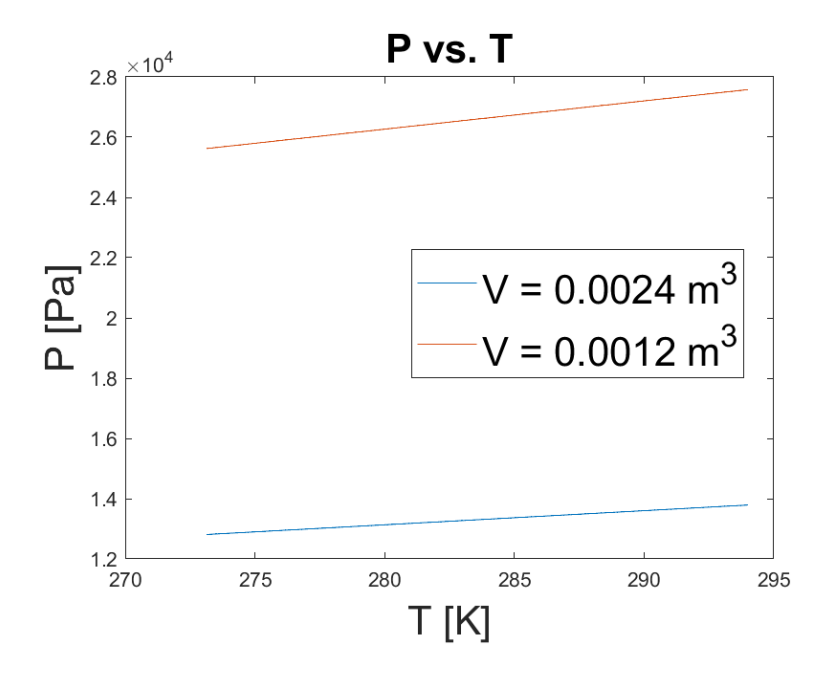


Figure 3.10: Pressure and Temperature: Amontons's Law

Table 3.7 breaks down the theoretical percent change when the airbag comes in contact with the cold plate and the temperature of the ambient air cools down. From the theoretical calculation it was concluded that the pressure of the airbag should decrease by 2.77% when the airbag temperature decreases from $13.9^{\circ}C$ to $5.5^{\circ}C$.

3.3.1 Empirical Model Results

The pressure of the airbag was held constant, while the temperature of the cooled water circulating through the cold plate was incrementally decreased. The temperature values were recorded using the chiller and the airbag pressure values were recorded with the gauge and TEK sensor. The temperature of the distilled water in the chiller was at ambient air temperature prior to cooling. The chiller was used to incrementally decrease the temperature of the water by $1^{\circ}C$. At every temperature change of $1^{\circ}C$ the temperature was held constant

Table 3.7: Ideal Gas Law Theoretical Pressure Percent Change

			Ambient Temperature	Cooled Water Temperature
Temperature	T	$(^{\circ}C)$	13.9	5.5
Pressure	P	Pa	55158.06	53632.82
Volume	V	m^3	95.63	95.63
Number of Mols	n	mol	0.04	0.04
Gas Constant	R	$\frac{J}{mol*k}$	8.31	8.31
Pressure Percent Change				2.77%

for 3 minutes to allow the gauge and pressure sensor to stabilize for accurate data recordings. This process of recording the pressure at each interval continued until the cooled water temperature of $5.5^{\circ}C$ was established and held constant. Figure 3.11 is a graph showing the trend of the recorded gauge pressure at every $1^{\circ}C$ step. Table 3.8 displays the values of the gauge pressure recorded at every measured temperature. The percent difference in the pressure of the airbag based on the pressure gauge data was 2.5%. The percent difference from the experimental data supports the theoretical percent difference calculated. The pressure values from the TEK sensor increased as the temperature decreased, contradicting theory and the simultaneous gauge pressure recordings. The TEK pressure sensor data was excluded from the analysis, but theories as to why the sensor recorded increased pressures are discussed.

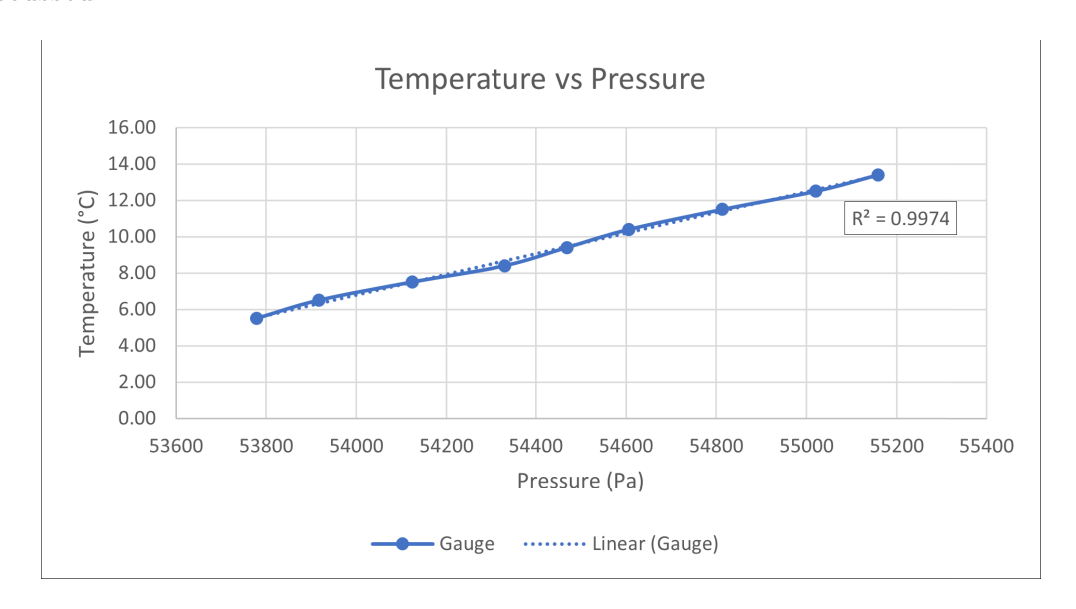


Figure 3.11: Plot of Cooled Water Temperature effect on Airbag Pressure

3.3.2 Accuracy of the Empirical Model

Two theories were considered for the contradicting results from the TEK sensor pressure values compared to the pressure gauge readings. When under constant load, TEK sensors

Table 3.8: Pressure vs Temperature

Temperature	Gauge Pressure
$^{\circ}C$	Pa
13.40	55158.06
12.50	55020.16
10.40	54813.21
9.40	54606.48
8.40	54468.58
7.50	54123.84
6.50	53917.00
5.50	53779.11

will exhibit drift over time which follows a log time scale. Typically the drift can be on the order of 3-5% per the logarithmic scale of time, but this can vary based on the mechanics of the loading. The best way to compensate for the drift is to leave the sensor constantly loaded over a period of time and plot the force output, take the inverse of that curve, and then apply that correction to the final test data. TEK sensors will also report higher pressure values with a stiffer material interface compared to a soft material interface under the same physical loading conditions. It is possible the airbag material became stiffer as the temperature decreased. This could have affected the pressure profile and data recorded.

Overall, the experimental gauge readings were consistent with the theoretical values using the Ideal Gas Law. The plot of the experimental data supports a linear, directly proportional relationship between the pressure and temperature. The experimental pressure in the airbag dropped by 2.5% compared to the theoretical pressure change of 2.77%. This pressure change could have a significant impact on the transfer of heat and should be further evaluated. The condensation noted during the experiment on the cold plate and airbag is concerning with the electrical connections and components and should be further evaluated. Given the accuracy of the TEK sensor, the data collected was used to validate the evenness of the pressure profile at the thermal interface and not the absolute value of the pressure being applied.

3.4 Discussion

Overall the hypothesis of the inflated airbag transferring a uniform pressure to the thermal interface was supported by experimental results. This proven design minimizes the vertical clearance between iPEBB and thermal management system modules in the iPEBB stack due to the thin profile of the airbag. By decreasing the vertical distance between the thermal management system modules the power density of the iPEBB stack increased by 50%. This increase in power density changes the iPEBB stack initial design from 4 to 6 iPEBB. To maximize the thermal transfer by way of conduction an average pressure across the thermal interface surface is more important than localized pressure at any point. A high degree of tolerance and smoothness at the faces of the iPEBB shell and the cold plate could increase the thermal transfer in addition to the uniform spreading of the pressure provided by the

PGS.

The pressure in the airbags will drop as they make contact with the chilled cold plates. Recommendations to minimize the drop in pressure are to precool the air supplied to the airbag, over-inflate the airbags, or have an automatic pressure indicator and inflation. The temperature of the supplied air to the airbags could be precooled to the cooling water temperature of $5.5^{\circ}C$. The airbags could be marginally overinflated above the interface pressure to account for the pressure loss when cooled water begins circulating through the cold plate. Pressure indicator and alarms could be implemented that would automatically inflate the airbag to required interface pressure. It is recommend that future work look at the effect of the pressure drop on the efficiency of the transfer of waste heat.

As the cooled water circulated through the cold plate, condensation appeared on the cold plate and airbag. This is because the capability of air to hold moisture decreases and relative humidity of air increases. It is not ideal to have condensation inside the iPEBB stacks which are providing electrical power to the ship grid. Therefore it is recommended to minimize the amount of condensation that could form.

Chapter 4

Other System Component Evaluation

The assumed iPEBB cabinet stack design of 6 vertical PEBB each with a respective set of cold plates and airbags requires components that ensure adequate cooling of the iPEBB architecture within the NiPEC compartment. Air compressor, airbags, hoses, pipes, fittings, and control instruments are major components to be assessed in assuring adequate cooling. Gas springs were selected to support lifting the upper cold plate when the airbags are deflated to allow for the smooth insertion and extraction of the iPEBB. A NiPEC air pressure system was evaluated to supply and maintain the required pressure in the airbag for uniform loading of the cold plates. Design standards and assumptions for the air pressure system were based on NSTM-551, which provides the requirements for compressed air plants and systems. The hosing and fitting connections from the cooling water system piping to the cold plates were evaluated to allow the cold plate to traverse vertically for insertion and extraction of the iPEBB while eliminating the potential for leaks at the connections. Design standards and assumptions for the hosing were based on MIL-H-24136 and MIL-F-24787, which provides the requirements for flexible hose assemblies and fittings.

4.1 Gas Springs

Gas springs were selected as the final design variant required to lift the top cold plate when the airbag is deflated to extract the PEBB for replacement. The advantages of gas springs are that they are compact devices with the ability to generate force in tight spaces and they are low maintenance. Other mechanical and electrical lifting devices consider were compression springs, rack and pinion gears, and electrical linear actuators. Gas springs were not required for the lower cold plate because as the lower airbag deflated the cold plate would gradually descend under its own weight and the effects of gravity.

Gas springs have the same basic principles as a mechanical spring, as a device that stores energy by compressing inert nitrogen gas. "It is the difference between the nitrogen gas pressure acting on the internal face of the rod, and the atmospheric pressure acting on the external end of the rod that causes it to extend. As the rod is pushed into the tube the available volume is reduced, gas is compressed and the internal pressure increases, this compression creates the spring like behaviour. An orifice in the piston that is attached to the rod allows the flow of gas across the piston and controls the extension speed" [CAMLOC].

Figure 4.1 is a technical diagram that shows the components of the gas spring.

The Working of a Gas Spring

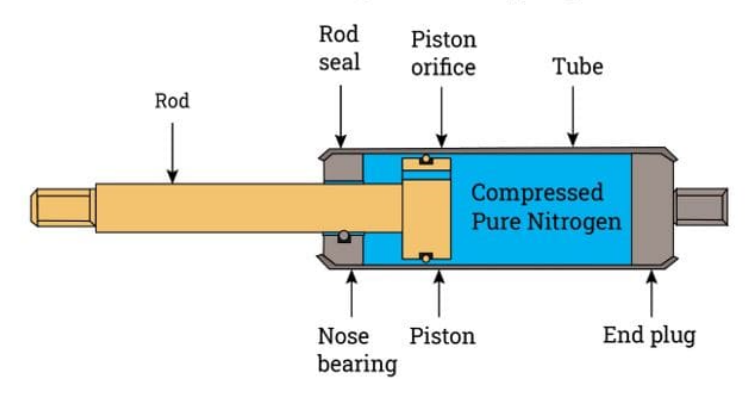


Figure 4.1: Gas Spring Technical Diagram [IQS]

After selecting the gas springs as the lifting device, the force rating had to be calculated to lift the weight of the cold plate a vertical distance of 12.7 mm. The vertical distance of 12.7 mm is the clearance required for the PEBB to be extracted for replacement from the top and bottom cold plates. Calculating the force rating of the gas spring involved several factors, such as the weight to be lifted, quantity, and arrangement of the gas springs. The arrangement of the gas springs determined the angles, effective length between the mounting points, and the extended distance required for the vertical clearance of 12.7 mm. Three different arrangements were evaluated using four gas springs with two mounted on each PEBB rail to the sides of the upper cold plate. The initial gas spring arrangement considered was a scissor or X-lift orientation. This lift arrangement was not selected because it required the gas springs to be transversely offset from another for mounting and offered challenges for sailors to access for replacement and maintenance. The second design arrangement considered of the four gas springs had the two gas springs on the PEBB rail longitudinally offset and mounted at the same angle making them parallel, but this design could cause the cold plate to be jammed or lodged in the cabinet. The final and selected design arrangement was a V-lift orientation that evenly lifted the upper cold plate without being jammed or lodged.

4.1.1 Force Required

Advanced Thermal Solutions, Inc, provided the dry weight for the aluminum 6063 cold plate with copper tubing excluding fittings. The dry weight for the cold plate with dimensions of $610mm \times 356mm \times 15mm$ was 9.15kg[Solutions]. The chilled water weight was calculated from the volume of the total loop passing in the cold plate. The weight of the cooled water in the cold plate was 0.4kg. The total weight of the cold plate including the weight of the cooled water in the loops was 9.55kg. The total force required to lift the cold plate was given by the following equation,

$$F = W * g \tag{4.1}$$

where F is the force required to lift the cold plate (N), W is the total weight of the cold plate (kg), and g is gravitational acceleration constant (m/s^2) . From this equation the total force required to lift the cold plate was 93.69N. The total force required to lift the cold plate was equally distributed amongst the four gas springs, therefore the force requirement for each gas spring was 23.42N. Since the gas springs are mounted at an angle, the force is exerted in horizontal and vertical components. The PEBB rails are fixed and the cold plate is simply supported it can only translate in the vertical direction, therefore we are only concerned with the vertical force.

$$F_{compressed} = F * sin(\theta_1) \tag{4.2}$$

$$F_{extended} = F * sin(\theta_2) \tag{4.3}$$

 $F_{compressed}$ is the vertical force exerted by the gas spring when the airbag is inflated and θ_1 is the angle measured between the PEBB rail and the gas spring. $F_{extended}$ is the vertical force exerted by the gas spring when the airbag is inflated and θ_2 is the angle measured between the PEBB rail and the gas spring.

The vertical force required to lift the cold plate at an angle of 18.86° based on a gas spring force rating of 80N was 25.86N. The vertical force of 25.86N exerted by the gas spring is greater than the force required to lift the cold plate 23.42N. When the airbag is deflated, the extended gas spring has an angle of 23.87° relative to the PEBB rail. Therefor the airbag pressure when inflating must overcome a vertical force of 32.37N per gas spring before it stats to compress.

4.1.2 Design Layout

The final gas spring design layout selected was a V-shaped lift requiring a total of four gas springs per upper cold plate. Two gas springs are on either side of a PEBB spaced longitudinally along the length. The final gas spring measurements and orientation are based on an 80N total force and are displayed in Figure 4.2 and Table 4.1.

Table 4.1: 80N Gas Spring Properties

	Compressed	Extended
Length	125.86mm	137.63mm
Angle	18.86°	23.87°
Force	25.86N	32.37N

The gas springs are mounted to the top of the PEBB rails and to the bottom edge of the upper cold plate. The length of the upper cold plate is 550mm and the location of the mounted gas strut on this surface is 175mm in from the cold plate edges in the profile view. The total distance between the two gas springs longitudinally on the cold plate surface is 300mm. At the PEBB rail the gas springs are fixed 250mm in from the edge in the profile view with a 50mm distance between the mounting locations. A detailed final design of the gas springs and the respective locations in the PEBB cabinet both extended and compressed are shown in Figures 4.4 and 4.3.

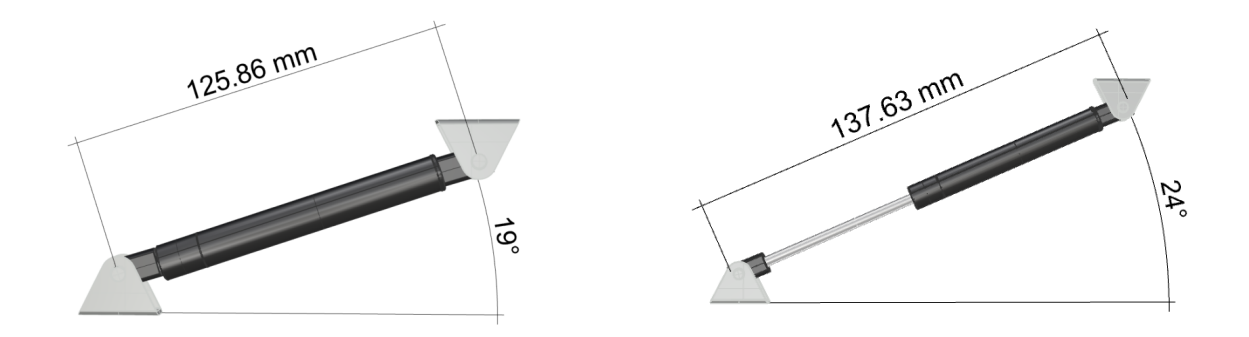


Figure 4.2: Upper Cold Plate Gas Spring Dimensions - Compressed (left) and Extended (right)

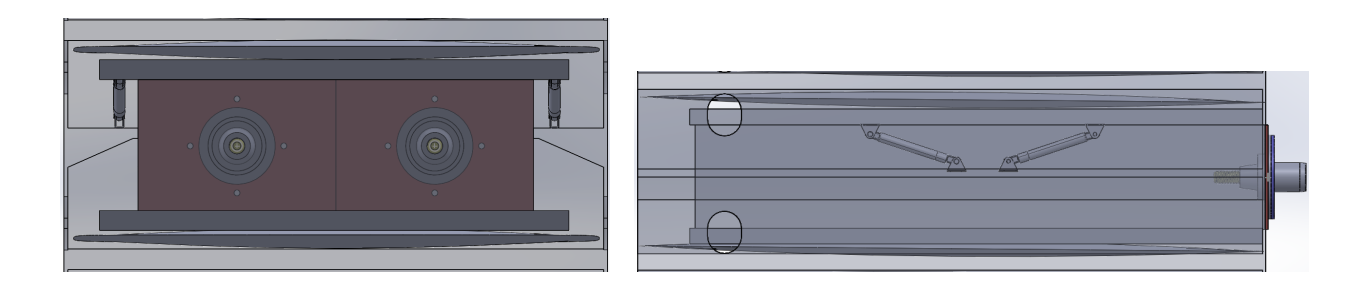


Figure 4.3: Gas Strut PEBB Stack Arrangement Compressed - Front View (left) and Profile View (right)

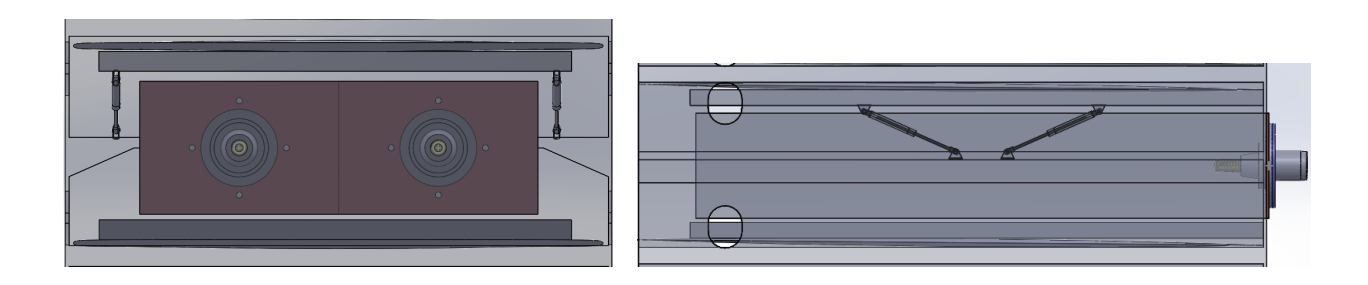


Figure 4.4: Gas Strut PEBB Stack Arrangement Extended - Front View (left) and Profile View (right)

4.2 Flexible Hose

To implement the design decision of vertical motion of the cold plates in the proposed securing mechanism, flexible hoses are required to integrate the cooling system. The flexible hose segments would direct water from the cooling system piping to the PEBB stack. An initial analysis of the use of flexible hoses as part of the cooling water system was conducted by Reyes [2022] referencing NSTM-505. From this initial analysis it was determined that rubber hoses reinforced by synthetic fibers were the optimal flexible hose material. The rubber hoses reinforced with synthetic fibers were compatible with the demineralized water and minimized the possibility of electrical conductance as well as galvanic corrosion and were less prone to kinking during installation [Reyes, 2022]. Reyes [2022] found that rubber hoses reinforced with synthetic fibers were more advantageous than polytetrafluoroethylene (PTFE) hoses for this specific cooling system integration when analyzing the types of flexible hoses. The U.S. Navy recommends the use of PTFE hoses on new construction ships when using flexible hoses, because of the life cycle maintenance and cost associated. For integration of the proposed securing mechanism design, the recommendation of rubber hoses reinforced with synthetic fibers was carried forward.

There are limitations to the use of flexible hoses which include the permitted configurations, minimum hose lengths, temperature ratings, and life-cycle specifications that must be taken into account. Cooling circuits have the following permitted acceptable flexible hose configurations:

- Single hose assembly one straight hose with fittings at each end.
- U or 180-degree return bend hose assembly two straight hose lengths connected by a 180-degree elbow fitting.
- 90-degree dog leg hose assembly two straight hose lengths connected by a 90-degree elbow fitting.

Based on the proposed cooling system integration, it is recommended that the flexible hoses be single hose assemblies. Although flexible hoses are in accordance with the naval technical directives and standards, specific NAVSEA approval is required for single hose assemblies, as they are not recommended for installation on new construction ships due to sound attenuating characteristics [NSTM-505]. The length of flexible hose assemblies are limited to 228.6mm between fittings for hose sizes between -4 (0.25in) and -64 (4in). The service life of rubber hoses are limited to 12 years, which has an added burden on the spare parts required onboard as well as more frequent inspection periodicity as compared to metal or polymer hoses. The flexible hoses would require lagging to be installed to limit condensation, further complicating required inspections.

4.2.1 Flex Hose Design Layout

Expanding on the analysis for the type of flexible hose, an initial layout for the implementation is based on previous design recommendations. Referring to Figure 4.5, the rubber hose segment would branch off the inlet/outlet piping and connect to the cold plate. Coupling

fitting connections would be located at each end of the rubber hose as well as at the branch of the pipe and cold plate connection.

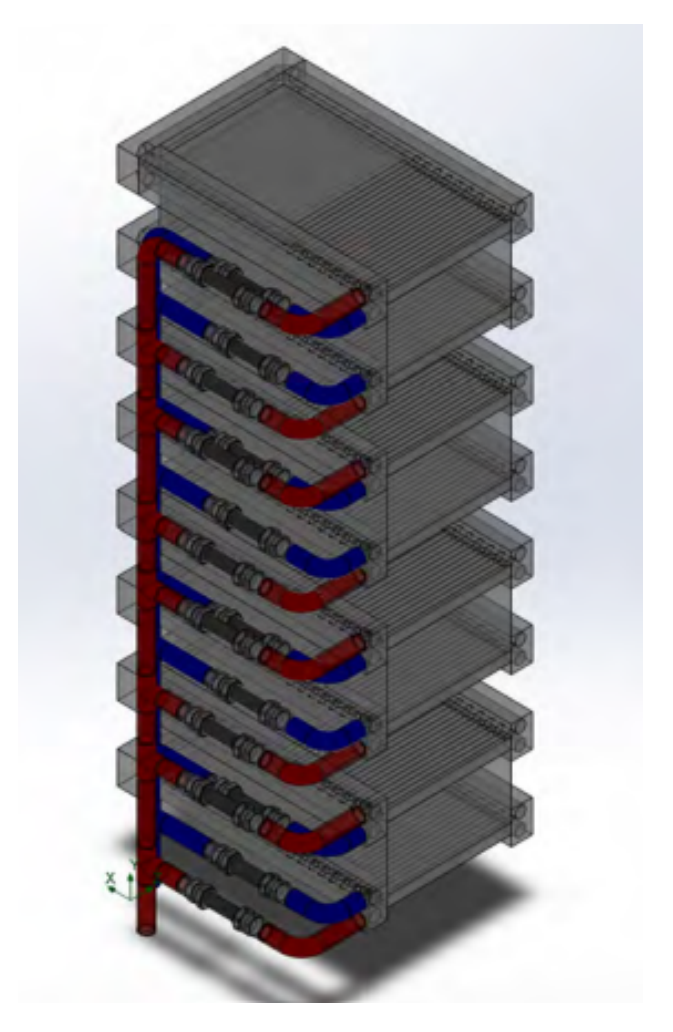


Figure 4.5: Reyes iPEBB stack design for first design iteration cold plate[Reyes, 2022]

This initial layout references Reyes [2022] final design recommendations for the counterflow cold plate and integration with the cooling system. Figure 4.6 shows the proposed cold plate arranged as a counter-flow heat exchanger with an inlet for the demineralized water and outlet for the waste water heat on the opposite side.

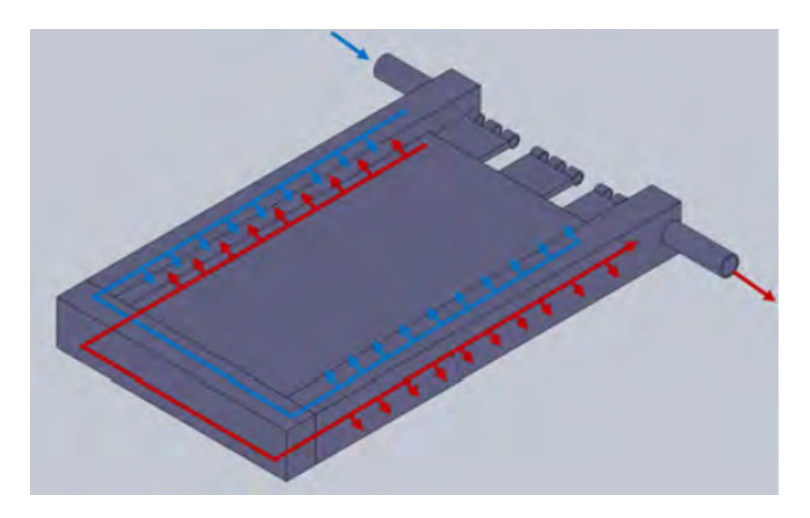


Figure 4.6: Reyes [2022] Cold Plate Arranged as Counter-Flow Heat Exchanger [Reyes, 2022]

The PEBB stack design carried forward the recommendation of keeping the cooling system piping external to the cabinet. The inlet cooling piping would remain external to one side of the cabinet and the outlet waste water piping would remain external to the opposite side. The recommended single straight rubber hose would extend from the external piping to the cold plate coupling connection which would extend through access hole in the cabinet. An identical rubber hose assembly would connect from the cold plate outlet to the return pipe. Two rubber hoses would be required for each PEBB for a total of 12 rubber hoses per PEBB stack. To implement the vertical motion design of the securing mechanism would require thousands of rubber hoses and couplings to support the NiPEC cooling system. This would have a burden on the shelf life, service life, logistics, and maintenance requirements as well as the cooling systems footprint [Reyes, 2022] which must be accounted in this design implementation of flexible hoses. The coupling fitting connection intention is for the rubber hose ends to have the jacks and the plug connections be fixed to the pipping and the cold plate. The coupling connections for the rubber flexible hose are expanded on below.

4.2.2 Flexible Hose Coupling Connections

The rubber hose has jack connections at either end and the plugs of the couplings are threaded inline to the pipe and at the elbow of the cold plate. To select the optimized coupling fitting the following constraints were considered: temperature, pressure, media, shutoff options, and flow. Table 4.2 shows the cooling system operating environment for the coupling fittings.

Two-way shut-off quick-disconnect couplings also known as double shut-off couplings were selected for the liquid-cooled connection to prevent leaks and maintain the cooling system integrity. The quick disconnect coupling is ideal for the disconnection of the rubber hose for maintenance without leakage or air getting into the system. The quick disconnect plugs allows the rubber hose and couplings to be isolated for maintenance or repair without discarding the entire assembly. The two-way shut-off coupling has a check valve on both the male and female halves eliminating the spillage of residual water left in either the cold plate or the flexible hose when the hose is disconnected. Figure 4.7 displays the internal

Table 4.2: Cold Plate Cooling Water Properties [Reves, 2022]

Fluid Media	Demineralized Water
Mass Flow Rate	0.5245kg/s
Inlet Pressure	$100lbf/in^2$
Pressure Drop	$0.2159 lbf/in^2$
Temperature	$42^{\circ}C$

components of the double shut-off coupling.

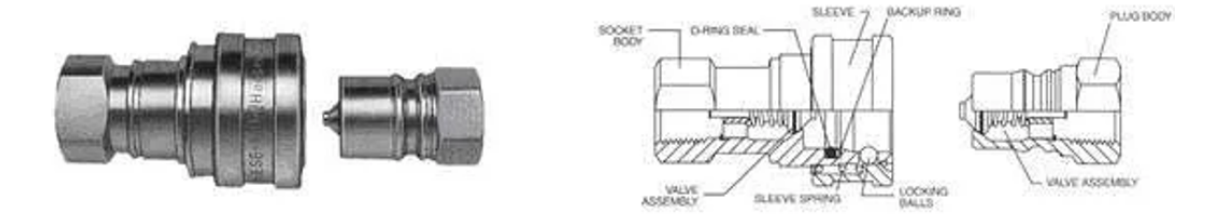


Figure 4.7: Double Shut-Off Coupling [Boyd, 2019]

MIL-HDBK-251 recommends the use of non-conductive coupling for connecting the cooling system to the cold plate. Using a non-conductive material for the coupling reduces the risk of electrical potential being transmitted from the iPEBB to the cooling system. Further analysis is recommend for using an engineered polymer to replace the metal couplings given the low pressure environment. Polymer couplings are acceptable in low-pressure fluid handling environments typically operating in less than 125psi. The pressure of the demineralized water at the inlet of the cold plate is assumed to be 100psi which does not exceed the operating limits for polymer couplings.

4.3 Air Pressure System

The NiPEC serves as the vessel's vital power distribution system. The corridor compromises several modular compartments capable of operating independently or as part of a network to execute energy storage, conversion, protection, control, isolation, and transfer functions [Cooke et al., 2017]. The pressurized airbag is a critical component to mechanically securing the iPEBB and providing a uniform interface pressure to the cold plate for maximized heat transfer. Based on the airbags' critical role in the the system architecture it was determined that the air supply system be independent and redundant. Therefore the air supply system would not integrate directly with other shipboard Low Pressure Air Compressor (LPAC) systems, but would rather be designated as vital air. The designation of vital air make the system continuously available for mission capability and survivability. Given the vital electrical nature of PEPDS it was determined that the compressed air supplied to the airbags be electronics dry air which is free of particulate matter and has a very low moisture content, used to isolate equipment from contamination [NSTM-551]. Design standards and assump-

tions for the air pressure system were based on NSTM-551 [NSTM-551], which provides the requirements for compressed air plants and systems. The proposed NiPEC shipwide cooling system referenced is the final six-cooling zone design proposed by [Chatterjee, 2023]. It was encouraged to implement existing ship architecture with known reliable components with the NiPEC cooling system design. Based on the design decisions and assumptions discussed above it was determine that the STAR LPAC supply the compressed air. Shipboard Low Pressure Air Dehydrator (LPAD) were further analysed to supply the required pressure, cleanliness, and flow rates of air to the airbags.

4.3.1 STAR Low Pressure Air Compressor

LPACs are oil-free compressors that deliver compressed air at discharge pressure from 80 to 150psig [NSTM-551]. Rotary compressors were a Navy-sponsored development program that were an improvement over the reciprocating compressors. The rotary compressor is 40% less weight and consumes 40% less volume in addition to be more reliable and quieter compared to the reciprocating compressor. Table 4.3 shows specifications for two referenced LPACs installed onboard Navy surface ships.

Table 4.3: Navy LP Air Compressor [NSTM-551]

Model Number	Nominal Capacity	Discharge Pressure	Service
NAXI 100-3	100scfm	125psig	Surface Ships
STAR 200	200scfm	125psig	Surface Ships

The STAR 200 and NAXI 100-3 are both rotary, water flooded, single screw LPACs commonly found onboard surface ships for supplying vital/non-vital air [NSTM-551]. The STAR 200 LPAC has a dedicated Condenser-Filter dehydrator installed downstream whereas the NAXI 100-3 has a Type I LPAD. Currently condenser-filters are phasing out Type I LPADs because of the simpler, more reliable design. The STAR 200 was selected over the NAXI 100-3 because of the condenser-filter dehydrator and higher SCFM, even though it has a slightly higher dewpoint than the Type I dehydrator. The benefits of the condenser-filter dehydrator is further discussed below along with an installed membrane to further decrease the dewpoint level in the supplied air system.

4.3.2 Condenser-Filter Low Pressure Air Dehydrator and Electronics Dry Air Membrane Dehydrator

Condenser-Filter LPADs use a chill-water heat exchanger to cool the air and condense the moisture. The benefits of this simpler design are (1) reduced maintenance due to fewer moving parts, (2) cooling medium is chilled water vice refrigerant for Type I, and (3) lower electrical load [NSTM-551]. Table 4.4 displays the Condenser-Filter Dehydrator specifications.

Given the critical electrical nature of PEPDS it is recommend that the air supply architecture have a dedicated dry air main. Supply to this main is from the vital main by way

Table 4.4: Condenser-Filter Dehydrator [NSTM-551]

Influent Air Conditions	
Temperature	maximum 125° F
Pressure	80 to 155 <i>psig</i>
Moisture Content	Saturated at 80 psig
Cooling Water Inlet	
Flow	4~GPM
Temperature	up to 51° F
Pressure	10 to 155 <i>psig</i>
Influent Air Conditions	
Pressure	no less than 5 psig from inlet pressure
Dewpoint	within 4° F from cooling water inlet temperature

of membrane dehydrators installed in parallel so that one serves as a 100% redundancy for the other [NSTM-551]. This is accomplished by replacing the Type II dehydrator with a membrane dehydrators. Therefore supplying clean, oil-free, dry air with a maximum dewpoint of $-40^{\circ}F$ when measured at 80psig. Moisture is removed from the incoming wet air by passing through an array of semi-permeable membranes, where the clean, dry air is trapped in tubes. Although the membrane dehydrator is a more reliable and simple design, it does pose the risk of higher air losses than the condenser-filter. The benefits to this design are (1) reduced maintenance due to fewer moving parts, (2) no cooling medium is required, (30 dewpoint acquired is often far better than ship requirements, and (4) low/no electrical load [NSTM-551]. The flow schematics for the condenser-filter dehydrator and the membrane dehydrator are located in Appendix E.

4.3.3 Air Compressor Sizing

In order to appropriately size the NiPEC air pressure system two key parameters were required: (1) the total airbag volume per compartment, and (2) the flow rate of air. Based on the proposed NiPEC shipwide six-cooling zone architecture there are a total of 42 compartments and 600 PEBB. To calculate the total airbag volume per compartment, the volume of one airbag had to be calculated based on the assumed dimensions that maximized contact area with the cold plate when inflated and allowed for an adequate vertical clearance when deflated. The calculated compressed air volume per airbag was $4.6e^{-3}m^{3}$ based on the dimensions provided in Equation 4.4.

$$V_{airbag} = 570mm \times 320mm \times 25.4mm = 4.6e^6mm^3 \tag{4.4}$$

Based on the proposed power dense stack design of 6 iPEBB, a total air volume required for the initial pressurization is $5.6e^{-2}m^3$. That calculated volume per stack is based on a total of 12 airbags, 2 per iPEBB. Four iPEBB stacks make up one compartment which is equivalent to 48 airbags for a total volume of $2.2e^{-1}m^3$. Adhering to the envisioned six-cooling zone design, the STAR 200 LPAC could pressurize the estimated 600 PEBBs in approximately

30 seconds. The total volume of air required to fill the 1200 airbags is $2.76m^3$ and the STAR 200 LPAC is rated for 5.66cmm. For redundancy it is proposed that two STAR 200 LPACs be dedicated to supplying and maintaining air to the airbags. The two LPACs could be centralized within the 6 cooling skid locations along with the heat exchangers. By integrating the air pressure system with the NiPEC shipwide liquid cooling system, the piping from the air compressor to the airbags would follow the same piping layout for the cooling water to the cold plates.

4.3.4 Air Pressure Diagram

In addition to the condenser-filter dehydrator and the membrane dehydrator flow schematic diagrams located in Appendix E, an initial air flow schematic design to the PEBB stack is shown below in Figure 4.8.

This air flow schematic has a primary and secondary loop for regulating the outlet pressure. The secondary loop remains closed and is reserved for redundancy in the system for both casualty and maintenance. Within the loops are a pressure gauge on either side of a pressure reducing regulator. The pressure-reducing regulator controls the outlet pressure that is supplied by the compressor. The regulator controls the downstream interface pressure of 2psi to the airbags. The gauges on either side show compressor supplied pressure and regulated pressure. The air flows from the pressure reducing regulator to the air manifold with 6 ports which supplies air to the 12 airbags. At each manifold port there is motorized actuator ball valve with a bleeder and pressure indicator alarm system.

When triggered to inflate the airbag the motorized actuator ball valve will open allowing air to flow to the airbag and close once the pressure indicator records the interface pressure of 2psi. The pressure indicator will continually monitor the pressure of the 2 airbags per PEBB and regulate the pressure as needed. An alarm system is set within the pressure indicator if the pressure exceeds the set limits.

From each manifold port, two pneumatic whips branch off to their respective airbags. The pneumatic whips are flexible which enables freedom of movement between the components. The whips are equipped with quick disconnect couplings at either end and will extend from the manifold port outside the cabinet through the access hole to the airbag. The piping for the air is to remain external to the cabinet, similar to the cooling water piping as shown in 4.5. Additionally, the airbag coupling connections are located near the front of the cabinet along with the cooling water connections to adhere to the sailor-center objective for simplicity for maintenance and repairs. Overall, this is an initial air flow schematic to the the PEBB stack which requires additional iterations to include accounting for the loses for the sizing and length of piping and fittings as well as the material compatibility. The maintenance requirements and associated parts with the air system should be further evaluated.

4.3.5 Back-Up Air Supply

An emergency scenario was evaluated for a back-up air supply in the case the ship losses power due to battle damage or collision and the LPACs were non-operational. The back-up air supply shall supply the required interface pressure to the airbags using reserve K-bottle gas cylinders. The reserve K-bottle gas cylinders would be equipped with a regulator circuit

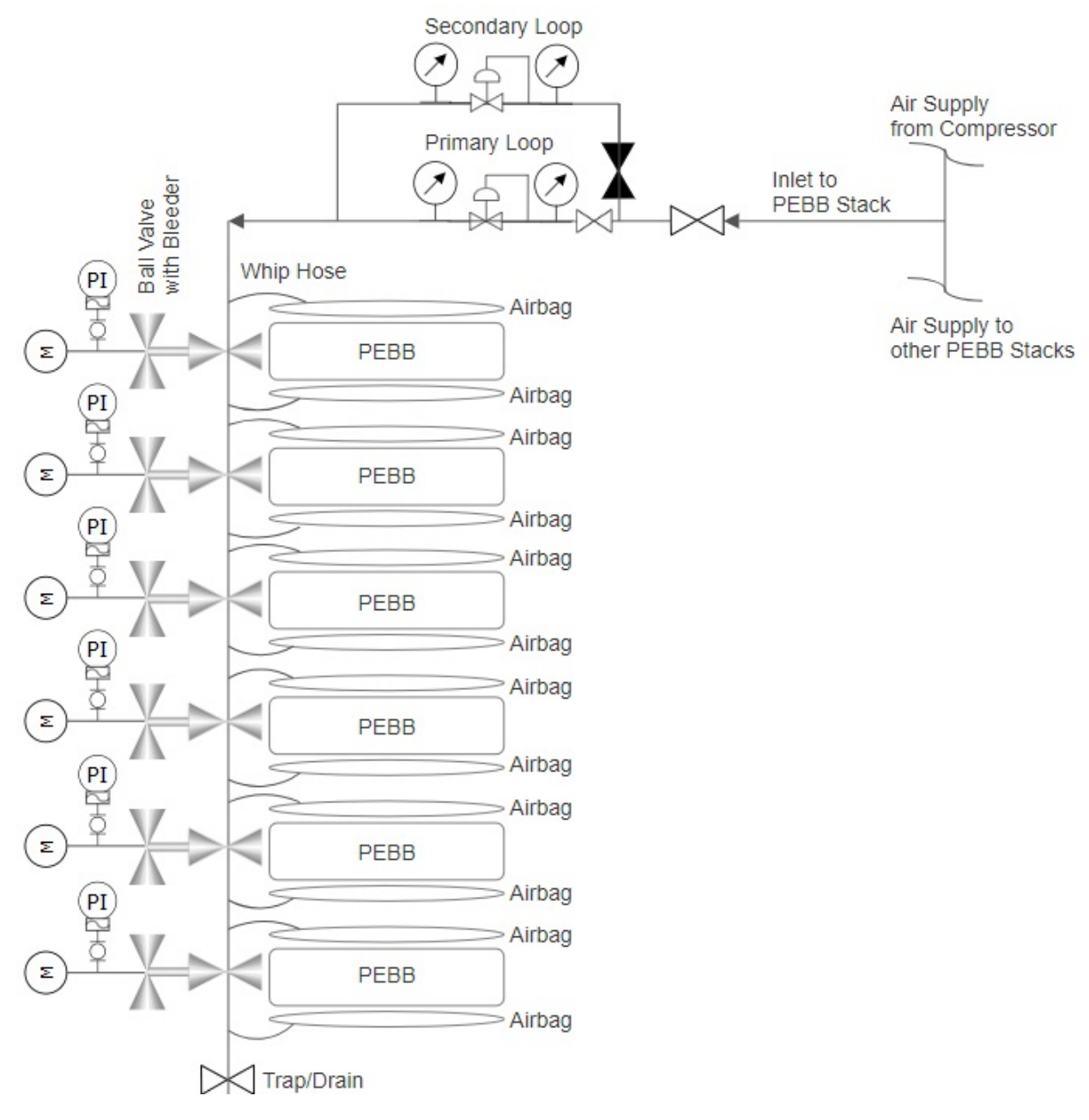


Figure 4.8: PEBB Stack Air Flow Schematic Diagram

to activate the K-bottle in the case of loss of power, automatically inflating the airbags to the required reference power. Additionally, the K-bottles would be an immediate one time use until they are recharged. The K-bottles would be stored in the compartment of the PEBB stacks or an adjacent compartment. This is an initial casualty response concept for restoring emergency power that could integrate with the NiPEC architecture. Further analysis is required for the sizing of the K-bottles, storage location, connections, and maintenance for this back-up air supply system.

Chapter 5

Overall Securing Mechanism for iPEBB and Cabinet Design

Taking all the research presented above into account, a full scale mockup of a 6 PEBB stack was designed using the Computer Aided Design (CAD) software SolidWorks. This design tool was able to validate the standoff clearances with the stack as well as show the supporting system connection locations. Following the CAD model of the full scale mockup, a prototype was constructed for a single PEBB to validate the functionality of the securing mechanism. In general, the prototype was used to assess the overall feasibility and performance of the design. This section discusses the design decisions associated with the construction of the prototype which lead from the proposed 6 PEBB stack model to a single PEBB mockup.

5.1 Full Scale Design

The full scale cabinet design considers the constraints and requirements of the PEBB assembly securing mechanism and the associated systems. The PEBB stack cabinet is designed to be 1524mm tall with a width of 406mm and depth of 600mm to accommodate 6 PEBB assemblies and supporting connections. The iPEBB, cold plates, and airbags are evenly spaced in the cabinet which occupy a total of 158mm vertically between the brace plates. The lowest PEBB slides in on linear rails 550mm above the bottom of the cabinet, with the subsequent PEBBs evenly spaced 171mm apart vertically. This was a sailor-centric shipboard design decision for simplicity for insertion and extraction of the PEBB. The vertical void of 447mm from the bottom of the cabinet to the first aluminum brace plate is occupied with a Plate Heat Exchanger (PHE). The 6 aluminum brace plates partition the 6 PEBBs within the stack and provide the critical fixed support for the pressurized airbag. The brace plates are designed to the width and depth of the cabinet with a thickness of 12.7mm and spaced evenly every 173mm vertically. Future design decisions may choose to incorporate a honeycomb or perforated structural plate to replace the solid aluminum brace plates used in this design analysis. The added benefits of a honeycomb structured brace plate could facilitate air flow in the cabinet and decrease the weight of the stack. The PEBB linear rails are used for aligning the electrical connections at the back of the PEBB with the electrical mating at the rear of the cabinet. The electrical connections are evenly spaced vertically 171mm apart and the side by side connections are laterally separated 150mm. The linear rails are supported by triangular beams that extend the depth of the cabinet which was incorporated in the previous design iteration for increased structural integrity and air flow. Access holes were cut in the side shell of the cabinet to allow for cooling water and pneumatic system access. The access holes were cut near the front of the cabinet and evenly spaced vertically along the sides of the cabinet. The access holes are elliptical in shape which allow for both the cooling water and pneumatic system connections as well as the vertical motion of the cold plate. The dimensions of the access holes has a major axis of 101.6mm and minor axis of 76.2mm. The pneumatic air supply piping is located outside the cabinet distributing the air through a manifold to the airbag by way of a compressed air whip hoses. The whip pneumatic hoses extend from the manifold through the access hole to the airbag and have quick disconnect couplings. Placement of the inlet and outlet piping of the cooling water is external to the cabinet along with the flexible hose extension to the cold plate to increase the chances of detection of a cooling water leak and limit the potential risk of damage to the electrical components. The cold plate inlet and outlet tubing would extend from inside the cabinet through the access to a two-way shut-off coupling connecting to the flexible hose. Additionally, placing both the cooling water and pneumatic system coupling connections near the front of the cabinet adheres to the sailor-centric objective for simplicity with regards to maintenance and repairs. The gas springs are fixed to the upper cold plate and the linear rail as outlined in the design layout in Section 4.1.2. Further, detailed cabinet design features and requirements shall conform with MIL-DTL-2026E107 and MIL-DTL-108. An idealized model for an iPEBB stack cabinet is shown in Figure 5.1 displaying the open and closed states below.

5.2 Prototype Design Approach

The initial approach for the prototype construction started with the design objective to validate the functionality of securing mechanism with a single PEBB. The plan was to make a prototype that was portable and used commercial off the shelf available products for the construction. A mockup of the prototype was designed using TBUILD Design Software [TBUILD] and had an approximate length to width ratio of 1/3 the full scale cold plate and PEBB. With a single PEBB focus, the mockup and prototype were modeled and constructed to the height of the bottom PEBB. This design decision was made to assess the impact on the sailor for insertion and extraction of the PEBB. Figure 5.2 shows the mockup designed using the TBUILD Software.



Figure 5.1: iPEBB Stack SolidWorks Design - Open State (left) and Closed State (right)

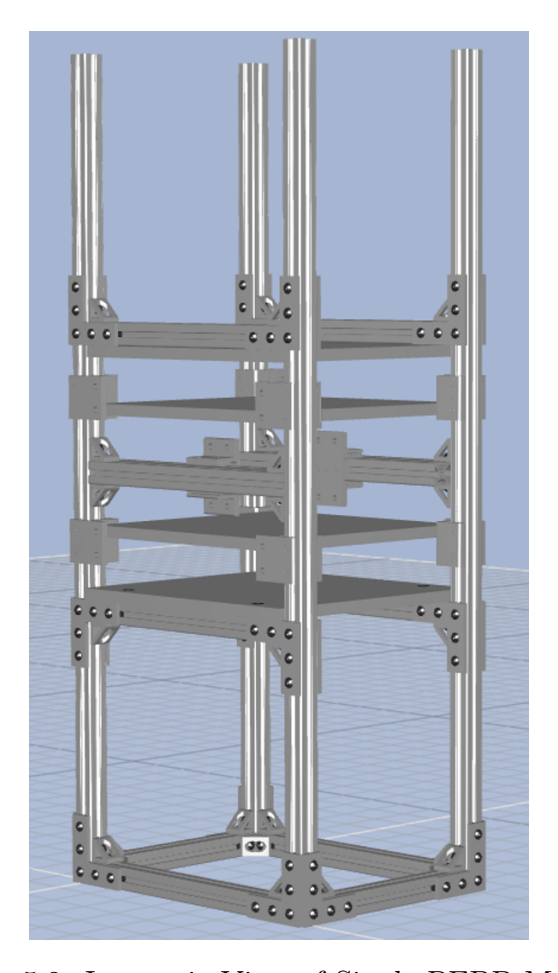


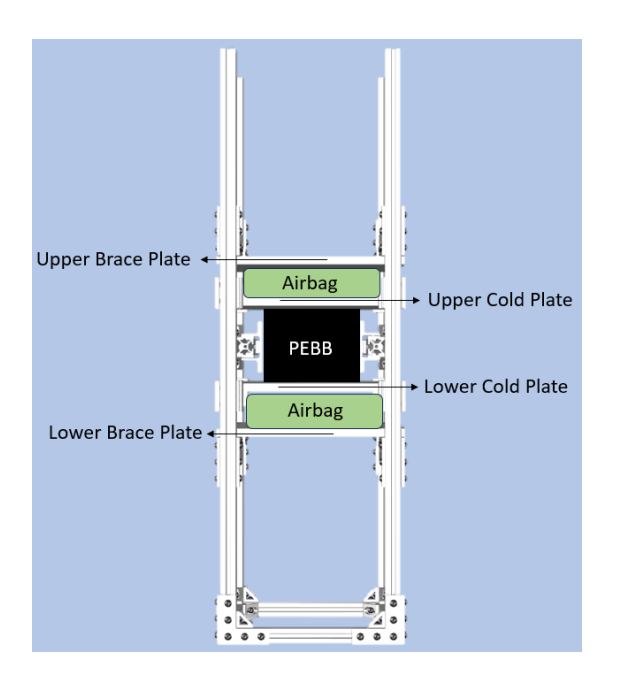
Figure 5.2: Isometric View of Single PEBB Mockup

Figure 5.3 shows a front and side view of the proposed prototype based on the securing mechanism design with labels identifying the locations of the airbags, brace plates, cold plates, and PEBB.

5.3 Single PEBB Prototype

The material build list used for the construction of this prototype is located in Appendix F. The TBUILD Design Software provided a list of materials for the aluminum T-Slot extrusion frame based on the design. Actual liquid cooled cold plates were used in the construction of the prototype. The cold plates were fastened to linear motion sleeve bearings at the four corners of the T-Slot frame which allowed for the vertical translation. The cold plates were positioned so the cooling water connections were located at the front of the PEBB. This simulated design decision was proposed to keep the cooling water connections away from any electrical connections and components.

To simulate the electrical connection when the PEBB is inserted to the rear of the cabinet on the rails, banana connections, a Light Emitting Diode (LED) bulb, and battery pack for power source were installed to complete the circuit. The external power source consisted of a battery pack of 8 AA batteries in series which was wired to insulated banana plugs. The



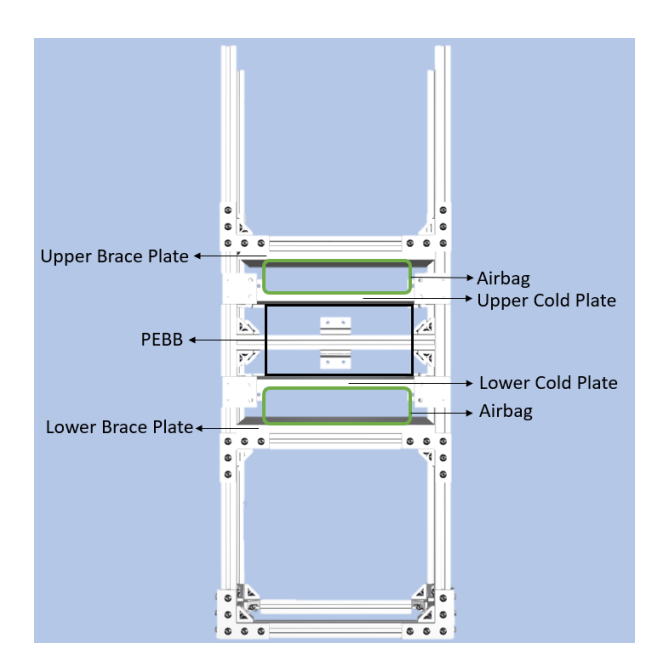


Figure 5.3: Single PEBB Mockup Design

banana plugs was fastened to the back of the T-Slot extrusion using an aluminum bar as a brace. The shrouded, insulated banana jacks was fastened to the back plate of the aluminum PEBB shell. A 12V LED bulb was attached to the banana jack inside the PEBB shell. The front plate of the PEBB shell was removed to see the illuminating LED bulb when the PEBB was inserted on the rails to the rear of the cabinet where the electrical connections are mated. This simulated the design decision for the electrical jack location at the back of the PEBB and the electrical plug located inside the cabinet of the PEBB stack. Figure 5.4 shows the electrical connection constructed for the prototype. This design decision reduced the risk of damage to the electrical plug had it been installed at the back of the PEBB rather than the cabinet.



Figure 5.4: iPEBB Prototype Electrical Connection

The V-lift design using four gas springs to lift the upper cold plate when the airbag was deflated was implemented in the construction of the prototype for validation. The top of the gas springs were mounted to the four corners of the upper cold plate at the exterior of the linear motion sleeve bearings. The bottom of the gas springs were mounted to the PEBB rail. When the airbag was inflated the gas springs were compressed, which allowed the cold plate to rest evenly on the surface of the PEBB. When the airbag was deflated the gas springs extended, lifting the cold plate vertically. Figure 5.5 shows the implementation of the gas springs in the prototype. Through the construction of the prototype, the application of the gas springs and the V-shape lift design functionality were validated.



Figure 5.5: iPEBB Prototype Gas Spring V-lift

Figure 5.6 shows the constructed securing mechanism prototype of a single PEBB in the clamped and open state. Overall, the prototype validated the feasibility and performance of the securing mechanism design. Furthermore, the single PEBB prototype could be further implemented in experimental testing to evaluate the system architecture moving forward.





Figure 5.6: Single PEBB Prototype

5.4 Design Conclusions

The design proposed in this thesis achieved the goals of mechanically securing the PEBB from static and dynamic forces while managing the thermal load with associated constraints and maximizing the power density. These design goals were validated by constructing a prototype of a single PEBB module. This design required an additional system level interface for pneumatic air supply for the airbags. Both the cooling water and pneumatic system piping is placed external to the cabinet allowing for the liquids and gases to flow through hoses to the cold plate and airbag. This increased the chances of detection of a cooling water leak and limited the potential risk of damage to the electrical components.

The use of an airbag for the securing mechanism anchored the PEBB and transferred a uniform pressure to the thermal interface to maximize the heat transfer. Additionally, the airbag maintains a thin profile that minimizes the vertical clearance of the PEBB and thermal management system module. By minimizing the vertical clearance per module this increased the power conversion units from four PEBB per stack to six PEBB per stack. This had an increase of 50% in power density per stack.

Chapter 6

Future Work and Conclusions

Building off of previous research, this thesis proposed a second pass design for a securing mechanism of the PEBB that integrated with the cooling system. This section summarizes the results from the previous chapters and provides a brief look at future work. First in Chapter 2, a structural integrity analysis was performed on the cold plate, brace plate, and PEBB shell to determine the ability to resist the applied interface load of 2psi (13790) N/m^2) based on the required thermal constraint. The materials selected for the design of the cold plate, brace plate, and the PEBB were based on their corrosion resistance, thermal conductivity, and strength-to-weight ratio properties. Analysis was performed using theoretical calculations and verified with simulations of models. In summary, the deflection of the brace plate, cold plate, and PEBB shell were calculated to be 0.03mm, 0.09mm, and 0.09mm which were determined to be negligible. The deflection calculation took into account the dynamic loading applied by the ship's motion. The calculated buckling factor of safety of the PEBB shell side plates was 3.1 which determined that the applied loads are less than the estimated critical loads therefore buckling is not expected. From this analysis it was determined that the associated materials with the applicable thicknesses and boundary conditions of these parts met the designed factor of safety for the applied load.

In Chapter 3, the design and testing of an experimental pressure testing rig used an airbag as a securing force to validate uniform pressure profiles and the effect of the cooled water on the pressurized airbag. From the results of several experiments, an empirical model was developed that demonstrated the uniform pressure profiles when using the airbag to transmit force through the cold plate to the thermal interface. Additionally, the experiments validated the PGS performance for filling interstitial gaps which increased the surface contact and average interface pressure. Using the chiller to circulate cooled water through the cold plate the interface pressure in the airbag dropped by 2.5%. The effect on the PEBB heat transfer due to the drop in pressure of the airbag would need to be further evaluated.

In Chapter 4, the additional system connections required for this mechanical securing design to integrate with the cooling system were researched and analyzed. The additional systems looked at were: (1) sizing and placement of the gas springs for the upper cold plate, (2) sizing of the LPAC system to supply the airbags, and (3) the flexible hose connections for the cooled water connections to the cold plates. This research is important as it allows for future designers and researchers in the ESRDC to have a template for future iterations of the iPEBB design. Additionally, it is important to understand how design decisions influence or

are influenced by other systems specific to the NiPEC.

Finally, in Chapter 5, a prototype of the proposed securing mechanism was constructed focusing on single iPEBB within the cabinet rack. In general, the prototype was used to assess the overall feasibility and performance of the design. The prototype was constructed to the height of the bottom PEBB in the cabinet stack to assess if this height was easily accessible for Sailors. Overall, the prototype validated the functionality of the design and provided a starting point for future development and improvements.

6.1 Future Work

This is a second pass design for a securing mechanism of the PEBB that provides uniform pressure distribution and integrates with the cooling system of the NiPEC. Three significant topics were discovered in the process of this design which require further study, (1) condensation, (2) PEBB rail locks, and (3) the airbag physical constraint. These topics are not all-inclusive, but were identified as a significant challenge to the component and system architecture.

6.1.1 Condensation

It was evident from the experimental testing using the chiller to circulate cooled water that atmospheric condensation would be an issue in the design. Condensation was observed to appear on the exposed cold plate surfaces. This creates an environment that fosters corrosion and poses the possible issue of electrical damage. One of the design decisions was to install the cooled water connections to the cold plate at the front of the cabinet. The purpose of this design decision was to minimize possibility of electrical damage with the PEBB electrical connection at the back of the cabinet that could be caused by downstream leakage at the cold plate coupling connection. Potential solutions to mitigate the condensation build up along the piping would be the use insulation such as pipe lagging to reduce the temperature difference between the cooling water and the ambient air. Additionally, using either a dehumidifier and/or desiccant bags to reduce the moisture vapor content will control the humidity by lowering the dew point. Using compressed, cool, dry filtered air to circulate through the PEBB is a viable option that should be further explored to control the temperature and humidity of the cabinet and mitigate Electrostatic Discharge (ESD).

6.1.2 PEBB Rail Locks

The initial idea of this proposed design was that the pressure applied to the top and bottom of the PEBB would secure the PEBB in place once the airbags were inflated to the interface pressure. This design change removed the retaining brackets incorporated in the previous design for locking the PEBB into place once inserted on the rails ensuring the electrical connection was made. However, to ensure the PEBB electrical connection is made and does not move once inserted on the rails a locking system should be incorporated. Additionally, this locking system protects the PEBB from damage in the case an airbag loses pressure and cannot retain the iPEBB or the ship experiences excessive force ejecting the PEBB. A

locking system would ensure safety and redundancy in securing the PEBB in the longitudinal direction along the rails. Ideally, the PEBB lock and release action should be located at the front of the cabinet to avoid crossing an electrical plane during extraction. The previous design iteration used a horizontal key design on the long sides of the PEBB shell which minimized the added weight and eliminated the use of hardware that would need to be removed or potentially lost. A detailed redesign of the PEBB rail system should be further evaluated for both the structural integrity and implementation of locking system. Potential solutions could be spring loaded pins, a quick release push pin, or ratchet bar that extends in front of the PEBB.

6.1.3 Airbag Physical Constraint

If the uniform pressure securing mechanism is retained, future design analysis should focus on constraining the airbag in the lateral and longitudinal direction. The airbags ability to expand and contract in the vertical direction when inflated and deflated cannot be impeded. The constraint imposed on the airbag should not impact the uniform pressure profile when the airbag is inflated and have minimal alterations to the cabinet and securing mechanism design. Possible solution paths to constraining the airbag include the following; (1) securing one face of the bladder membrane of the airbag to the brace plate and (2) an elastic mesh/netting in the lateral and longitudinal boundaries. After further research, prototyping of the airbag constraint is the next logical step to be validated with the prototype.

6.2 Conclusions

In conclusion, this thesis demonstrated a validated design for a securing mechanism that applies a uniform pressure profile at the thermal management interface of the iPEBB while increasing the overall power density of the iPEBB rack by 50%. Theoretical calculations and simulations presented in this thesis validated the structural integrity of the components associated with the proposed design. Experimental testing substantiated the uniform pressure profile using an airbag as the securing mechanism to transmit force to the thermal interface in addition to the effect of the PGS interface material filling interstitial gaps and maximizing surface contact. Research was conducted to evaluate additional system connections that would be required for this design. The groundwork of a iPEBB prototype was designed and constructed, validating the feasibility and performance of the securing mechanism design, laying-out the necessary steps required to create a full scale prototype.

The advantages of this design minimized the vertical space consumed between each PEBB, which increased the power density of the stack from 4 to 6 PEBB's per cabinet. In addition, this design was Sailor friendly and eliminated the use of hardware required to apply the securing force, which had the disadvantages of getting lost or using incorrect specifications. Further, this design solved the non-uniform loading of the interface pressure at the PEBB interface. The disadvantages of using an airbag as the securing force for the PEBB is the increased maintenance and complexity of additional systems and connections. The airbag requires compressed air to pressurize and maintain pressure in the airbags thus adds to the complexity of the system architecture of the NiPEC. Additionally, altering the

previous hinged design to clamped required the cold plates restricted to vertical motion. This design alteration removed the use of the hinges for inlet and outlet for the cooled water connections which influenced the design decision of flexible hoses with two-way shut off couplings.

Future development of the NiPEC cooling system and PEBB design are an on-going collaborative research with goals for a more robust power distribution system for next generation all electric warships. In addition to the areas of future work noted above, there are a number of areas for further study given the complexity of the thermal management of the iPEBB. Moreover, the research, calculation, simulations, and models explored in this thesis can guide and further on-going NiPEC and PEPDS research. This securing mechanism design can continue to be evaluated and modified leading to a better performing, power dense iteration. The single PEBB prototype designed and constructed herein could be further implemented in experimental testing to evaluate the system architecture.

References

- Aluminum 6061 t-6. URL https://www.matweb.com/search/DataSheet.aspx?MatGUID=b8d536e0b9b54bd7b69e4124d8f1d20a.
- Delrin 570 natural. URL https://www.ensingerplastics.com/en-us/shapes/products/delrin-570.
- ATS. ATS-TCP-1005. URL https://www.qats.com/Products/Liquid-Cooling/Tubed-Cold-Plates/ATS-TCP-1005.
- Baker. Baker B1800 Squeeze Bulb Pressure Calibrator, 0 to 18 psig. URL https://www.globaltestsupply.com/product/baker-b1800-squeeze-bulb-pressure-calibrator?gad_source=1&gclid=Cj0KCQjw5cOwBhCiARIsAJ5njub_ay6cs9qmBHjr07WveGZ9KESHZei9lnsk1zMCM5lZI8lioSND0csaAvDwEALw_wcB.
- Boyd. Couplers, Hose Clamps and Fitting Selection, July 2019. URL https://www.boydcorp.com/blog/couplers-hose-clamps-and-fitting-selection.html.
- CAMLOC. How do gas struts work? URL https://camloc.com/us/help-centre/how-gas-struts-work/how-do-gas-struts-work/.
- CAMPUS. CAMPUSplastics | datasheet Delrin R 570 NC000. URL https://www.campusplastics.com/campus/en/datasheet/Delrin $\textcircled{C}2\%AE+570+NC000/DuPont+Engineering+Polymers/52/5f0bca94}$.
- Avi Chatterjee. Design and modeling of shipwide navy integrated power and energy corridor cooling system. Master's thesis, Massachusetts Institute of Technology, 2023.
- C Cooke, C Chryssostomidis, and J Chalfant. Modular integrated power corridor. In 2017 IEEE Electric Ship Technologies Symposium (ESTS), pages 91–95. IEEE, 2017.
- José del Águila Ferrandis, Julie Chalfant, Chathan M Cooke, and Chryssostomos Chryssostomidis. Design of a power corridor distribution network. In 2019 IEEE Electric Ship Technologies Symposium (ESTS), pages 284–292. IEEE, 2019.
- Christina DiMarino. Navy integrated power electronics building block (iPEBB). In Office of Naval Research iPEBB Program Review, November 2020.
- Christina DiMarino. Navy integrated power electronics building block (ipebb). ONR Power Electronics Power Distribution System (PEPDS) Risk Reduction Program Review, October 2022.

- Engineers Edge and Engineers Edge LLC. Flat Rectangular Plate with All Edges Simply Supported Equations and Calculator. URL https://www.engineersedge.com/calculators/flat_rectangular_plate_with_all_edges_simply_supported_15090.htm.
- M. E. Ephraim, T. Ode, and C. A. Ohia. Dynamic response of rectangular orthtropic plates based on characteristic orthogonal polynomials and reyleigh-ritz model. *International Journal of Civil and Structural Engineering Research*, 2019.
- Sachin M. Gunjal, Rajesh B. Jahare, Atteshamuddin S. Sayyad, and Mana D. Ghodle. Buckling analysis of thick plates using refined trigonometric shear and deformation theory. *Journal of Materials and Engineering Structures*, 2015.
- IQS. Gas Springs: Types, Design, Benefits, and Applications. URL https://www.iqsdirectory.com/articles/gas-spring.html.
- Muhsin J Jweeg, Muhannad Al-Waily, and Kadhim K. Resan. *Energy Methods and Finite Element Techniques*. Elsevier Science, 2021. URL https://www-sciencedirect-com.libproxy.mit.edu/book/9780323886666/energy-methods-and-finite-element-techniques.
- S Markle. IPES harnessing total ship energy & power. Sea-Air-Space Exposition, 2018.
- MatWeb. Electrolytic Tough Pitch (ETP) Copper, UNS C11000, OSO50 Temper flat products, rod, tube, shapes. URL https://www.matweb.com/search/datasheet_print.aspx?matguid=41a3ab3af15a4ca7b8d558b974d8eb51.
- MITcalc. MITcalc Mechanical, Industrial and Technical Calculations. URL https://www.mitcalc.com/index.htm.
- NSTM-505. Naval ships' technical manual chapter 505 piping systems. Department of Navy Technical Manual, January 2008. Revision 4.
- NSTM-551. Naval ships' technical manual chapter 551 compressed air plants and systems. Department of Navy Technical Manual, April 2010. Revision 5.
- Joush Padilla. Cooling power electronic building blocks aboard navy ships. Bachelor's thesis, Massachusetts Institute of Technology, 2021.
- Joush Padilla. Characterizing the thermal behavior of pyrolytic graphite sheets (pgs) at low interface pressures. Master's thesis, Massachusetts Institute of Technology, 2023.
- Joushua Padilla, Julie Chalfant, Chryssostomos Chryssostomidis, and Chathan Cooke. Preliminary investigation into liquid-cooled PEBBs. In 2021 IEEE Electric Ship Technologies Symposium (ESTS), August 2021.
- Lynn Petersen, Christian Schegan, Terry S Ericsen, Dushan Boroyevich, Rolando Burgos, Narain G Hingorani, Mischa Steurer, Julie Chalfant, Herbert Ginn, Christina DiMarino, Gian Carlo Montanari, Fang Z Peng, Chryssostomos Chryssostomidis, Chathan Cooke, and Igor Cvetkovic. Power electronic power distribution systems (pepds) plan. ESRDC Website, www.esrdc.com, 2022.

- Ivan Reyes. Design and modeling of the navy integrated power and energy corridor cooling system. Master's thesis, Massachusetts Institute of Technology, 2022.
- SOLIDWORKS. Buckling Factor of Safety 2021 SOLIDWORKS Help. URL https://help.solidworks.com/2021/english/SolidWorks/cworks/c_Buckling_Load_Factor.htm.
- Advanced Thermal Solutions. Cold Plates | Advanced Thermal Solutions. URL https://www.qats.com/cms/category/cold-plates/.
- Robert L. Taylor and Sanjay Govindjee. Solution of clamped rectangular plate problems. Communications in Numerical Methods in Engineering, 20(10):757–765, October 2004. ISSN 1069-8299, 1099-0887. doi:10.1002/cnm.652. URL https://onlinelibrary.wiley.com/doi/10.1002/cnm.652.
- TBUILD. MockUp | TBUILD. URL https://tbuild.io/projects/5497.
- Tekscan. Pressure Mapping Sensor 5151 | Tekscan. URL https://www.tekscan.com/products-solutions/pressure-mapping-sensors/5151.
- Stephen Timoshenko, Sergius Woinowsky-Krieger, et al. *Theory of plates and shells*, volume 2. McGraw-hill New York, 1959.
- Chris Tomlinson. Design of securing mechanism for power converter in navy integrated power and energy corridor. Master's thesis, Massachusetts Institute of Technology, 2022.
- WINBAG. Home. URL https://winbagusa.com/.
- S Yang, JS Chalfant, JC Ordonez, JA Khan, C Li, I Cvetkovic, JVC Vargas, MB Chagas, Y Xu, RP Burgos, et al. Shipboard PEBB cooling strategies. In 2019 IEEE Electric Ship Technologies Symposium (ESTS), pages 24–31. IEEE, 2019.

Appendix A

MATLAB Script for Deflection and Buckling Analysis

```
%% Cold Plate Deflection
clear
clc
close all
fs = 20; % font size
%% Sources:
st [1] Thin Plates and Shells: Theory, Analysis and Applications by Krauthammer and m{arkappa}
% [2] Properties of Cold Plate
%% Assumptions:
% Sides: Simply Supported
% Cold Plate Material: Aluminum 6063
% Units: mm
% Kirchoff's assumptions are valid:
% - Material is elastic, homogeneous, and isotropic
% - Plate is initially flat
% - Small deflection (w/h < 10)
% - Vertical shear strains are negligible and normal strain be omitted
% - Stress normal to the midplane is negligible
% - Middle surface is unstrained after bending
% Thin plate (a/h = 10-80)
%% Constants
              % Plate length in x-axis direction (mm)
   = 550;
    = 550;
              % Length of applied pressure area in x-axis direction (mm)
             % Distance from origin to center of pressure area in x-axis direction ✓
   = 275;
(mm)
              % Plate length in y-axis direction (mm)
   = 350;
              % Length of applied pressure area in the y-axis direction (mm)
    = 300;
              % Distance from origin to center of pressure area in y-axis direction ✓
   = 175;
              % Maximum deflection
   = 1;
              % Maximum deflection
   = 1;
n
   = 15;
          % Thickness (mm)
h
   = 68947.5; % Modulus of Elasticity (N/mm2)
Ε
   = 0.33; % Poisson Ratio
       = E*(h^3)/(12*(1-(v^2))); % Flexural Rigidity of Plate [N-mm]
\Box
      = 2;
                                    % Pressure applied to plate [psi]
psi
conv
      = 0.00689476;
                                    % Converting psi to N/mm2
      = psi*conv;
                                    % Pressure applied to plate [N/mm2]
р
area
       = 192500;
                                    % Top and Bottom of PEBB (550x350) [mm2]
F g = p*area; % Force applied by airbag (N)
```

```
F dyn = 394; % Dynamic Loading Worst Case (N)
qx = (F g + F dyn)/area; % Total Uniform Load per
                                                   [N/mm2]
%% Deflection
   = 1000;
Ν
   = linspace(0,a,N);
Х
   = linspace(0,b,N);
У
                   % makes NxN zero matrix
   = zeros(N,N);
for i = 1: length(x)
    for j = 1:length(y)
               w(i,j) = \sin(m*pi*s/a)*\sin(n*pi*r/b).*...
                        \sin(m*pi*u/(2*a))*\sin(n*pi*c/(2*b)).*...
                        sin(m*pi.*(x(i)./a))*sin(n*pi.*(y(j)./b))/...
                         ((m*n)*(((m/a)^2 + (n/b)^2)^2));
    end
end
w = w .* (-16*qx/(pi()^6 * D));
%% Plotting
figure()
surf(x,y,w,'LineStyle','none')
title('Plate Deflection','FontSize',fs)
xlabel('x \epsilon (0,a) [mm]', 'FontSize',fs)
ylabel('y \epsilon (0,b) [mm]', 'FontSize',fs)
zlabel('w [mm]','FontSize',fs)
xlim([0 a])
ylim([0 b])
%% Results
% Acceptable Deflection?
        = max(abs(w),[],'all');
wmax
% Small Deflection (w/h <10)
defl = wmax/h;
disp(['The maximum deflection is: ',num2str(wmax),' mm']);
if defl < 10
    disp("Small Deflection Assumption is valid");
    disp(['The deflection to thickness ratio is: ',num2str(defl),'.']);
else
    disp("Small Deflection Assumption is not met");
```

end

```
%% Brace Plate Deflection
clear
clc
close all
fs = 20; % font size
%% Sources:
st [1] Thin Plates and Shells: Theory, Analysis and Applications by Krauthammer and m{arkappa}
% [2] Properties of Aluminum Brace Plate
%% Assumptions:
% Sides: Simply Supported
% Cold Plate Material: Aluminum 6063
% Units: mm
% Kirchoff's assumptions are valid:
% - Material is elastic, homogeneous, and isotropic
% - Plate is initially flat
% - Small deflection (w/h < 10)
% - Vertical shear strains are negligible and normal strain be omitted
% - Stress normal to the midplane is negligible
% - Middle surface is unstrained after bending
% Thin plate (a/h = 10-80)
%% Constants
              % Plate length in x-axis direction (mm)
   = 600;
    = 550;
              % Length of applied pressure area in x-axis direction (mm)
             % Distance from origin to center of pressure area in x-axis direction ✓
   = 300;
(mm)
                 % Plate length in y-axis direction (mm)
   = 406.4;
                % Lenght of applied pressure area in the y-axis direction (mm)
    = 300;
                % Distance from origin to center of pressure area in y-axis direction ✓
   = 203.2;
(mm)
   = 1;
               % Maximum deflection
               % Maximum deflection
   = 1;
n
   = 25.4;
              % Thickness (mm)
h
   = 68947.5; % Modulus of Elasticity (N/mm2)
Ε
   = 0.33;
            % Poisson Ratio
       = E*(h^3)/(12*(1-(v^2))); % Flexural Rigidity of Plate [N-mm]
\Box
      = 2;
                                    % Pressure applied to plate [psi]
psi
conv
      = 0.00689476;
                                    % Converting psi to N/mm2
      = psi*conv;
                                    % Pressure applied to plate [N/mm2]
р
area
       = 243840;
                                    % Top and Bottom of PEBB (600 x 406.4) [mm2]
F w = 94; % Weight of cold plate and thermal pad (N)
```

```
F g = p*area; % Force applied by airbag (N)
               % Dynamic Loading Worst Case (N)
F \, dyn = 395;
qx = (F g + F w + F dyn)/area; % Total Uniform Load per [N/mm2]
%% Deflection
    = 1000;
N
  = linspace(0,a,N);
Х
    = linspace(0,b,N);
У
   = zeros(N,N);
                       % makes NxN zero matrix
for i = 1: length(x)
    for j = 1:length(y)
               w(i,j) = \sin(m*pi*s/a)*\sin(n*pi*r/b).*...
                        \sin(m*pi*u/(2*a))*\sin(n*pi*c/(2*b)).*...
                        sin(m*pi.*x(i)./a)*sin(n*pi.*y(j)./b)/...
                         ((m*n)*(((m/a)^2 + (n/b)^2)^2);
    end
end
w = w .* (-16*qx/(pi^6 * D));
%% Plotting
figure()
surf(x,y,w,'LineStyle','none')
title('Plate Deflection', 'FontSize', fs)
xlabel('x \epsilon (0,a) [mm]', 'FontSize',fs)
ylabel('y \epsilon (0,b) [mm]', 'FontSize',fs)
zlabel('w [mm]', 'FontSize', fs)
xlim([0 a])
ylim([0 b])
%% Results
% Acceptable Deflection?
        = max(abs(w),[],'all');
wmax
% Small Deflection (w/h <10)
defl = wmax/h;
disp(['The maximum deflection is: ',num2str(wmax),' mm']);
if defl < 10
    disp("Small Deflection Assumption is valid");
    disp(['The deflection to thickness ratio is: ',num2str(defl),'.']);
else
```

```
{\tt disp}\,({\tt "Small} Deflection Assumption is not met"); end
```

```
clc %Clear all test from Command Window
clear %Clear all variables from the work space
%% Sources:
st [1] Thin Plates and Shells: Theory, Analysis and Applications by Krauthammer and oldsymbolarksim
% [2] Properties of Delrin 570 Blend
% [3] Properties of Cold Plate
%% Assumptions:
% Sides: Simply Supported
% PEBB Side Material: Delrin 570 Blend
% Units: mm
% Thin plate (a/h = 10-80)
% Linear Buckling
% - Plate is initially flat and loads applied at midplane
% - No change in plate dimensions prior to buckling
% - All loads applied are dead loads (not dynamic)
% - Kirchoff's plate bending assumptions are true
% Equilibrium Method
% Edge loaded uniformly
%% Constants
a = 100; % Plate height (mm)
b = 550;
          % Plate width (mm)
c = 300; % Plate width (mm)
m = 1; % Smallest critical load
n = 1; % Smallest critical load
kb = (((m*b)/a) + (n^2*a/(m*b))); % Side Plate Buckling parameters
kc = (((m*c)/a) + (n^2*a/(m*c))); % Front and Back Plates Buckling
h = 6;
       % Thickness (mm)
E = 5000; % Modulus of Elasticity (N/mm2)
          % Poisson Ratio
D = E*(h^3)/(12*(1-(v^2))); % Flexural Rigidity of Plate (N-mm)
p = 0.0137895; % Pressure applied to top and bottom (2 psi in N/mm2)
area = 165000; % Top and Bottom of PEBB (550 \times 300) (mm2)
F w = 94; % Weight of cold plate and thermal pad (N)
F q = p*area; % Force applied by the airbag (N)
F dyn = 395; % Dynamic Loading Worst Case (N)
qx = (F g + F w + F dyn)/((2*(h*b))+(2*(h*c))); % Assumes uniform loading to entire \checkmark
edge of top plate (N/mm2)
Ny = 0; % Only loaded vertically
Nxy = 0; % Only loaded vertically
%% Buckling
qxminb = kb*(pi^2)*D/(b^2*h); % Eqn 8.19 [1]
FOS b = qxminb/qx; % Factor of Safety of Side Plate Buckling
qxminc = kc*(pi^2)*D/(c^2*h); % Eqn 8.19 [1]
FOS c = qxminc/qx; % Factor of Safety of Front and Back Plate Buckling
```

```
%% Results
% Side Plate Results
if qxminb > qx
    disp("Applied load will not cause buckling in the side plates");
    fprintf('The Buckling Factor of Safety is %3.2f\n',FOS_b);
else
    disp("Applied load will cause buckling in the side plates");
end
% Front and Back Plate Results
if qxminc > qx
    disp("Applied load will not cause buckling in the front and back plates");
    fprintf('The Buckling Factor of Safety is %3.2f\n',FOS_c);
else
    disp("Applied load will cause buckling in the front and back plates");
end
```

Appendix B

Roark's Formula for Stress and Strain MITcalc

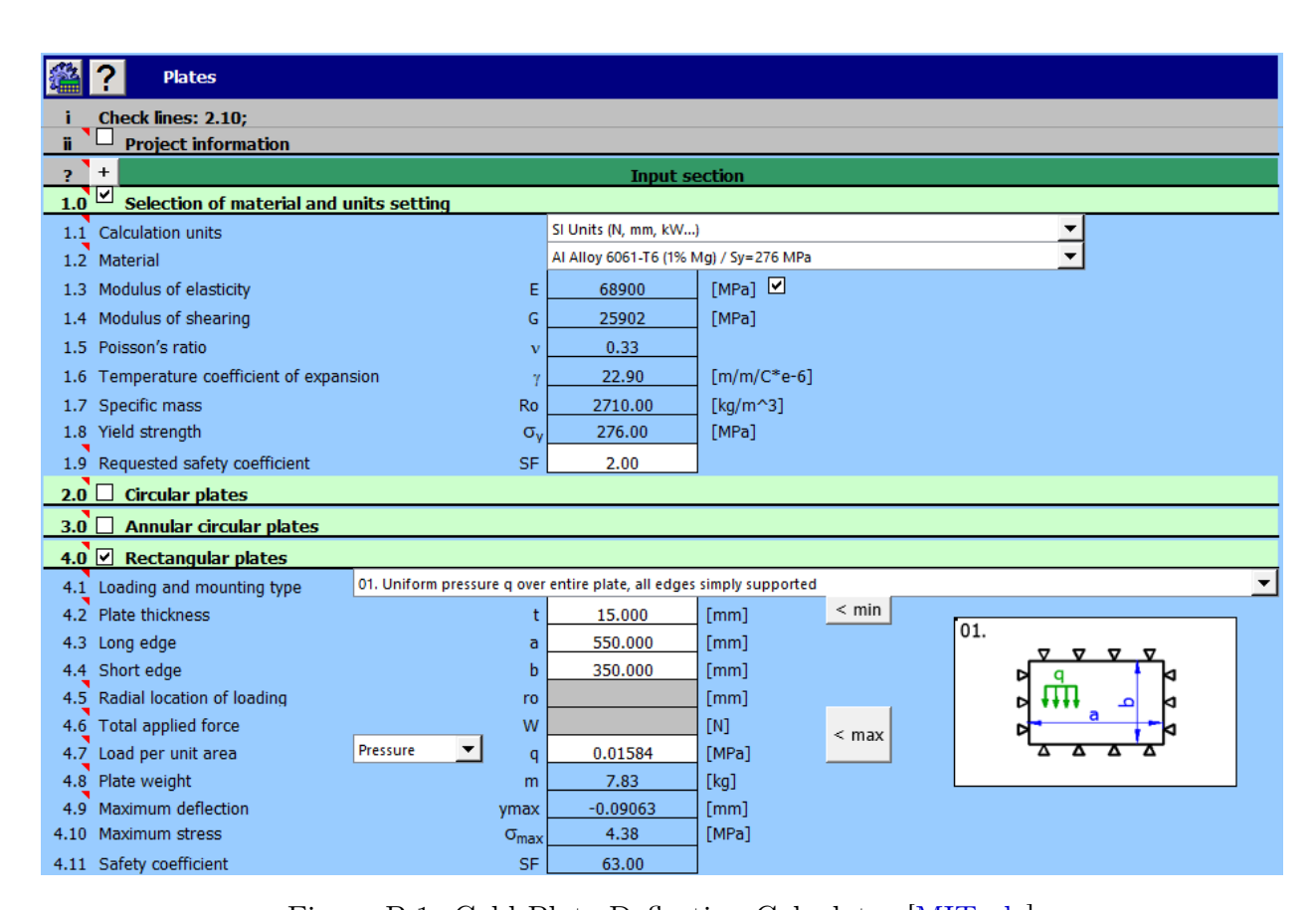


Figure B.1: Cold Plate Deflection Calculator [MITcalc]

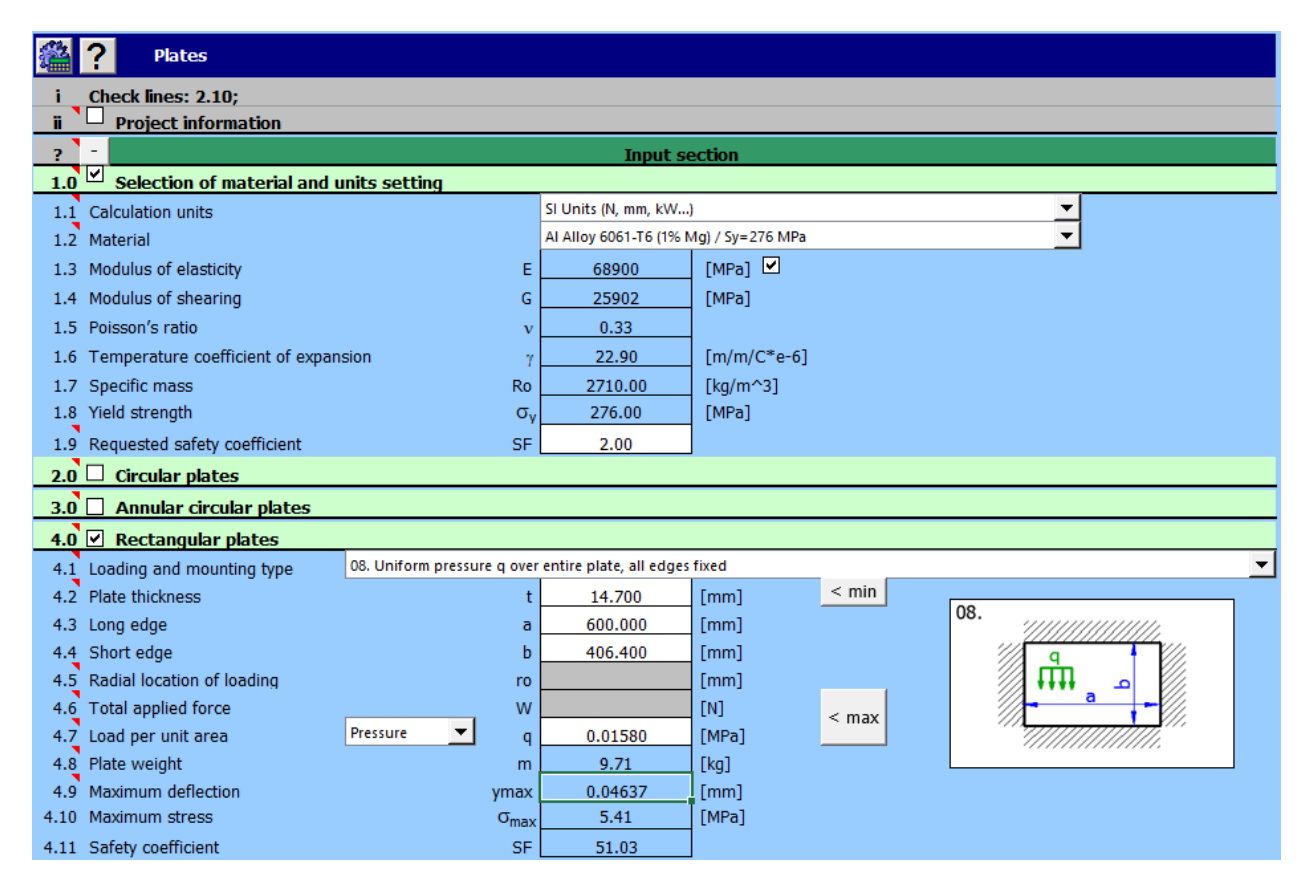


Figure B.2: Brace Plate Deflection Calculator [MITcalc]

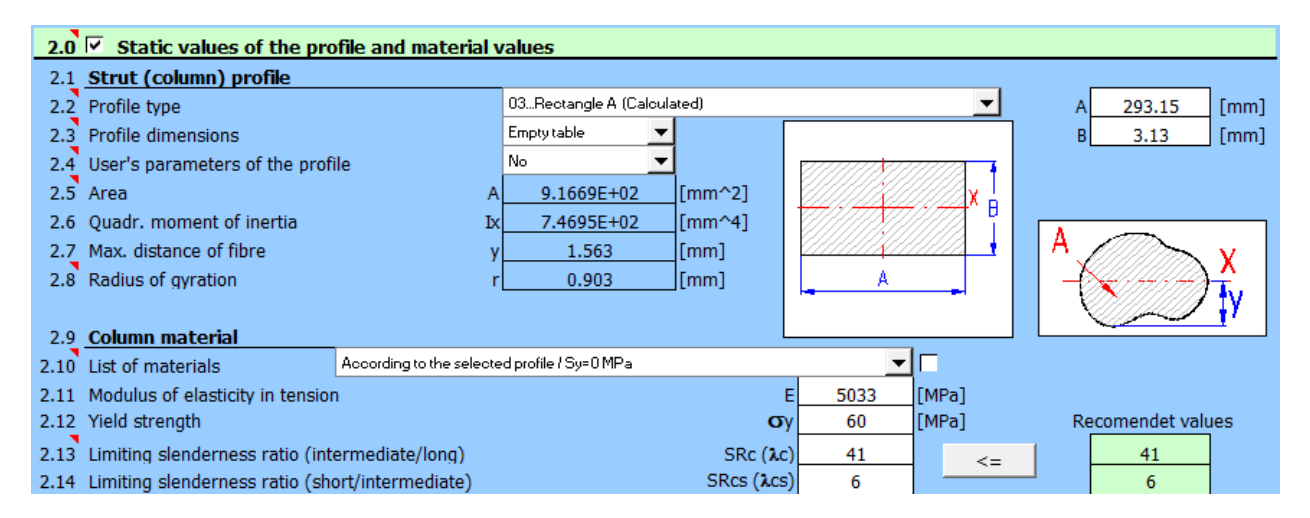


Figure B.3: Buckling Short Edge - Dimensions and Material Properties [MITcalc]

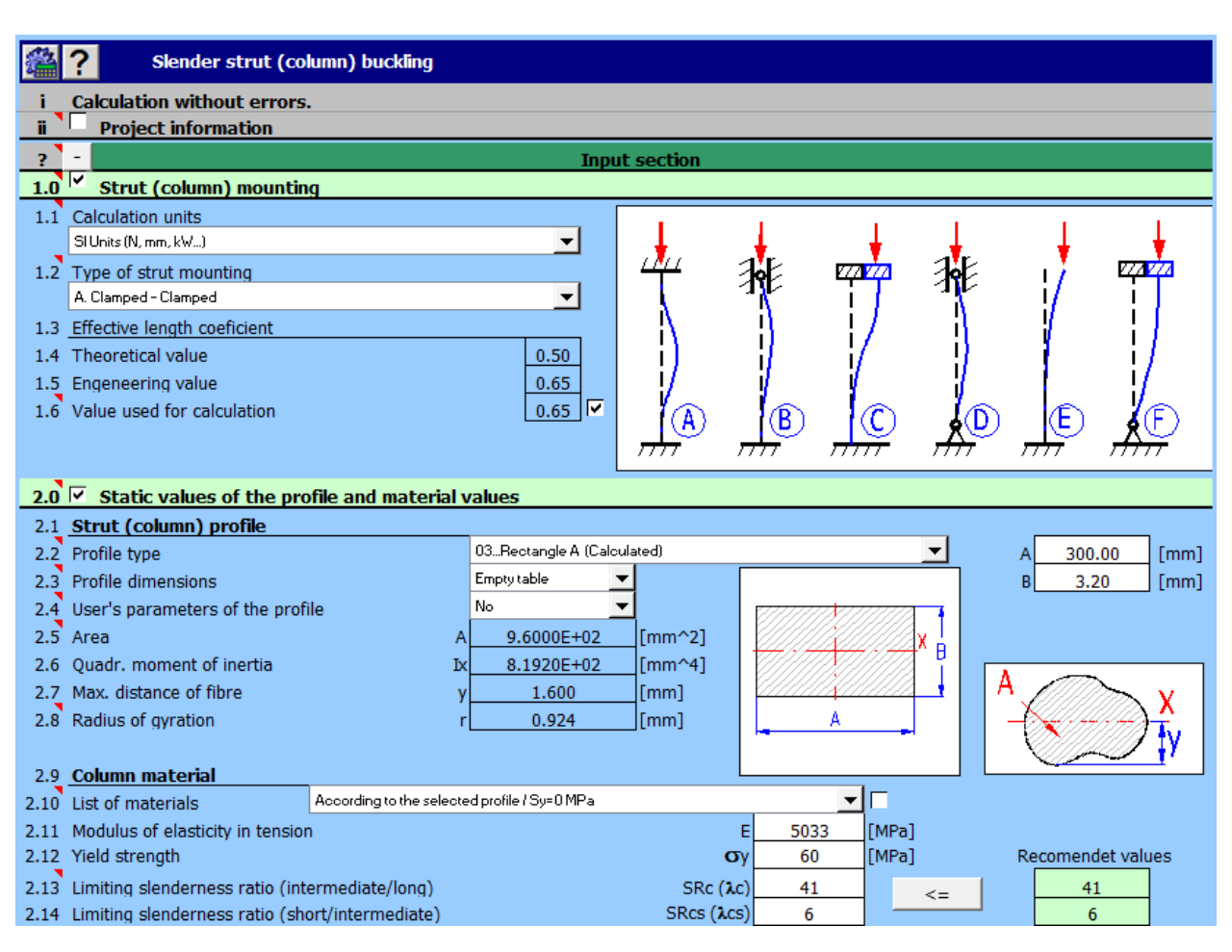


Figure B.4: Buckling Short Edge - Calculations [MITcalc]

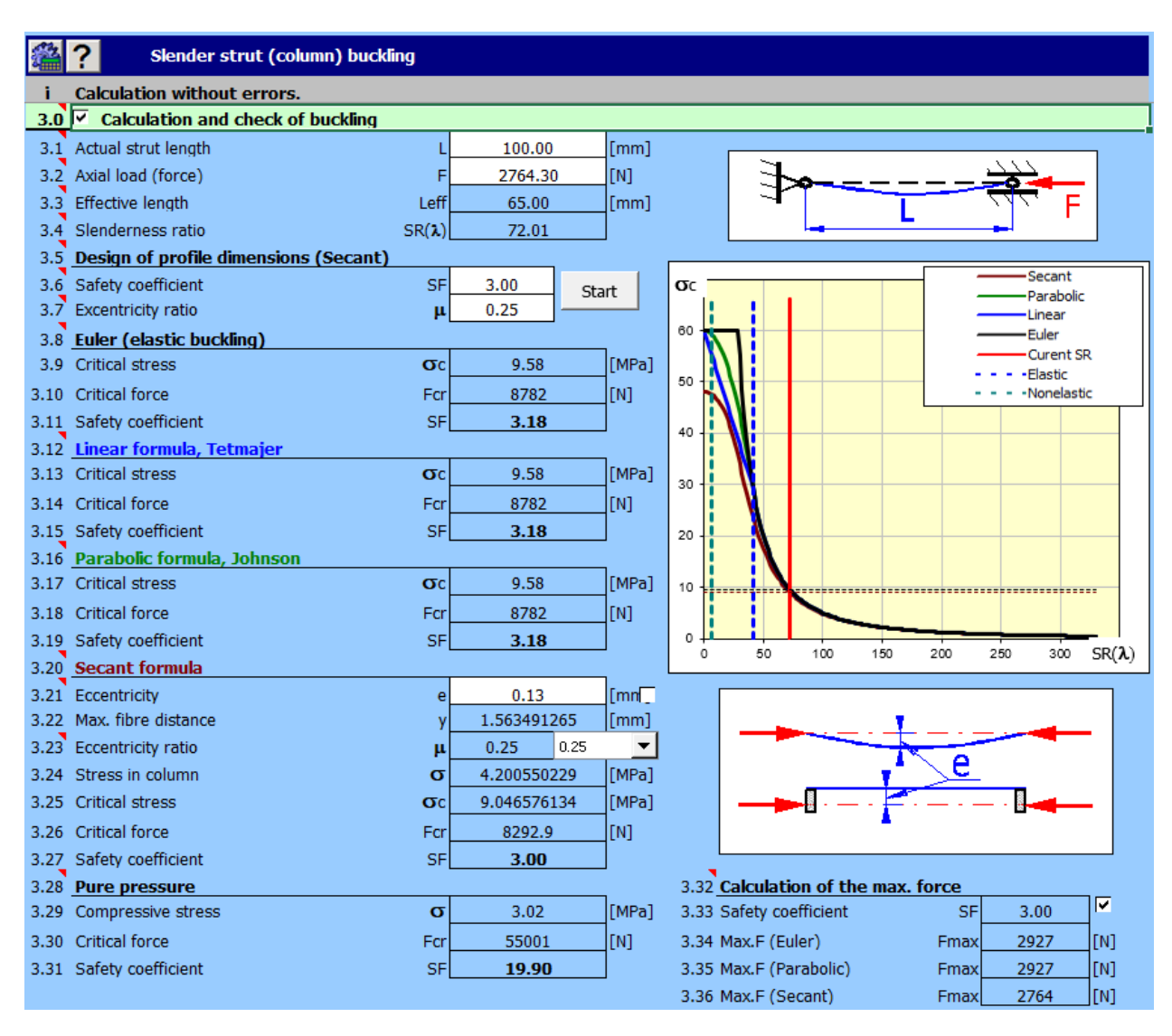


Figure B.5: Buckling Short Edge - FOS Results [MITcalc]

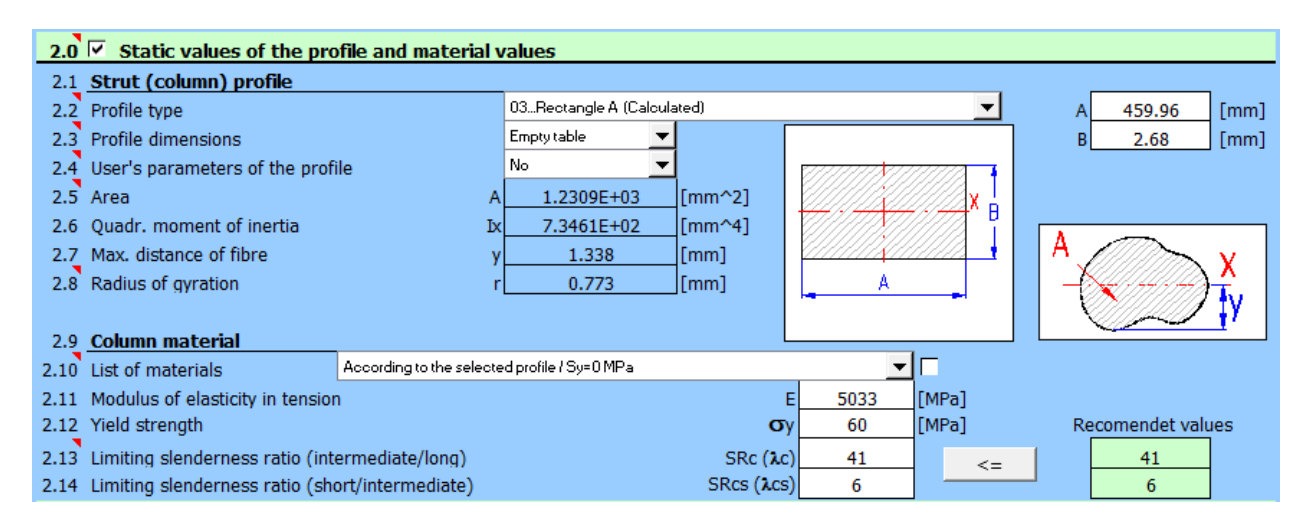


Figure B.6: Buckling Long Edge - Dimensions and Material Properties [MITcalc]

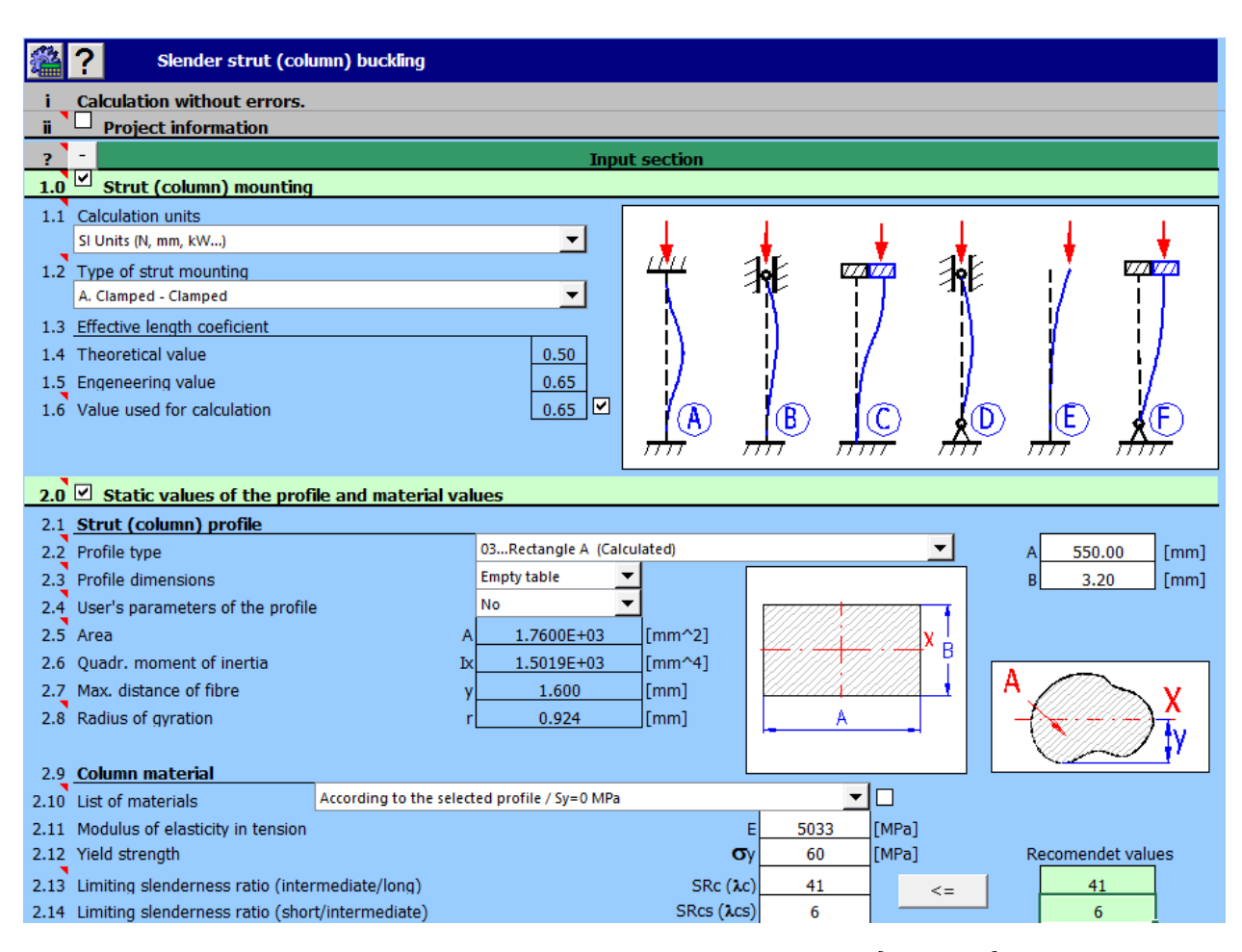


Figure B.7: Buckling Long Edge - Calculations [MITcalc]

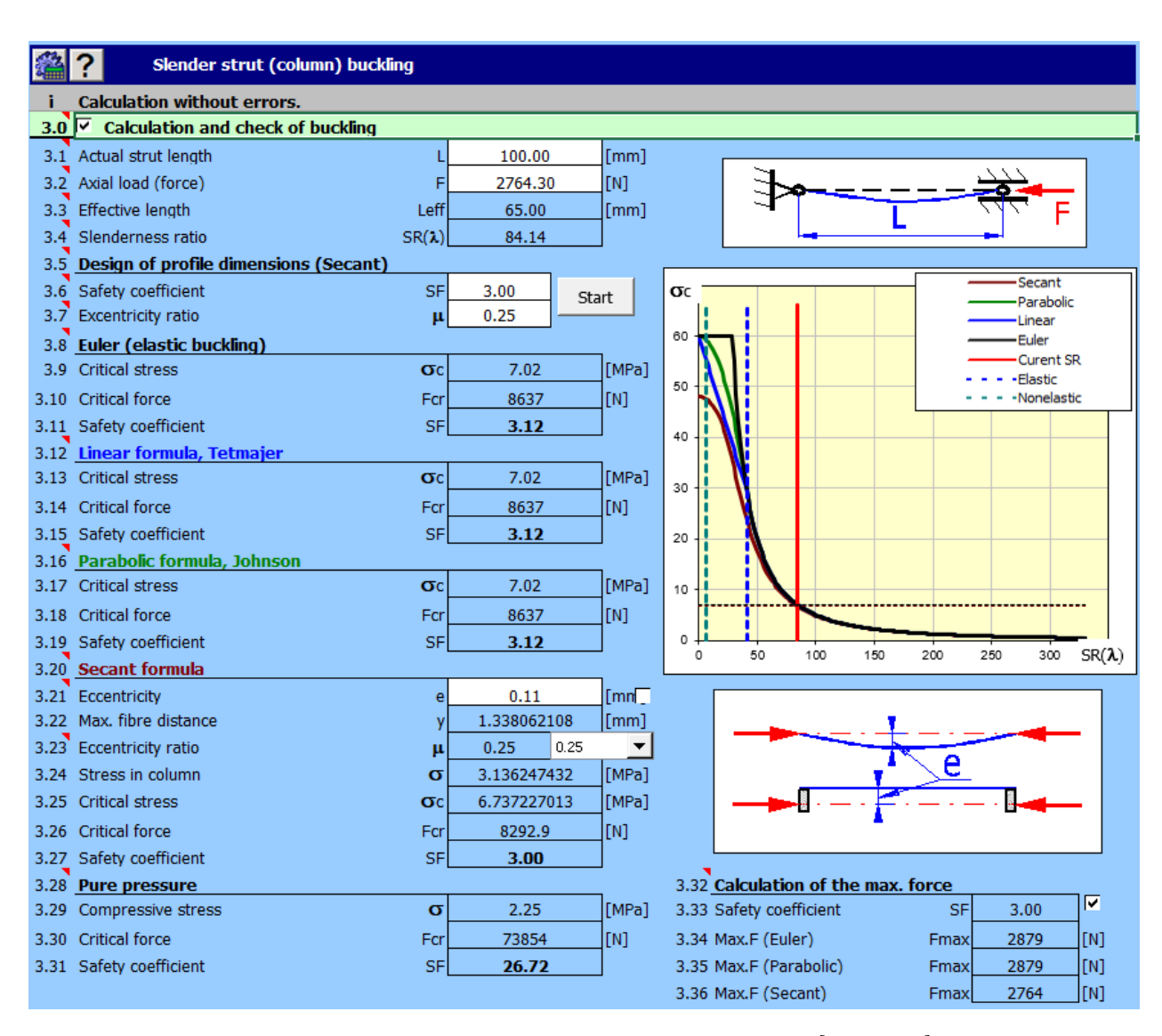


Figure B.8: Buckling Long Edge - FOS Results [MITcalc]

Appendix C

SOLIDWORKS Simulation Results for Deflection and Buckling

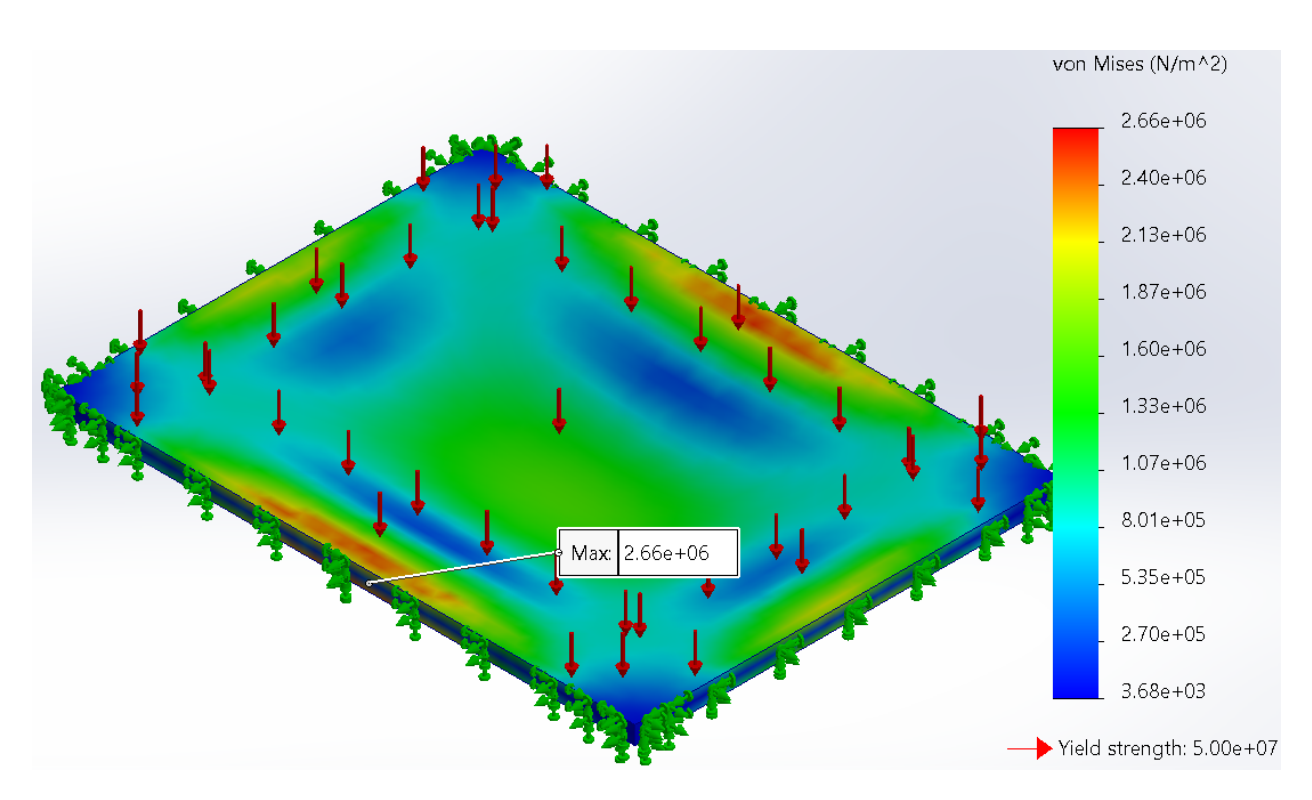


Figure C.1: Cold Plate Von Mises Stress

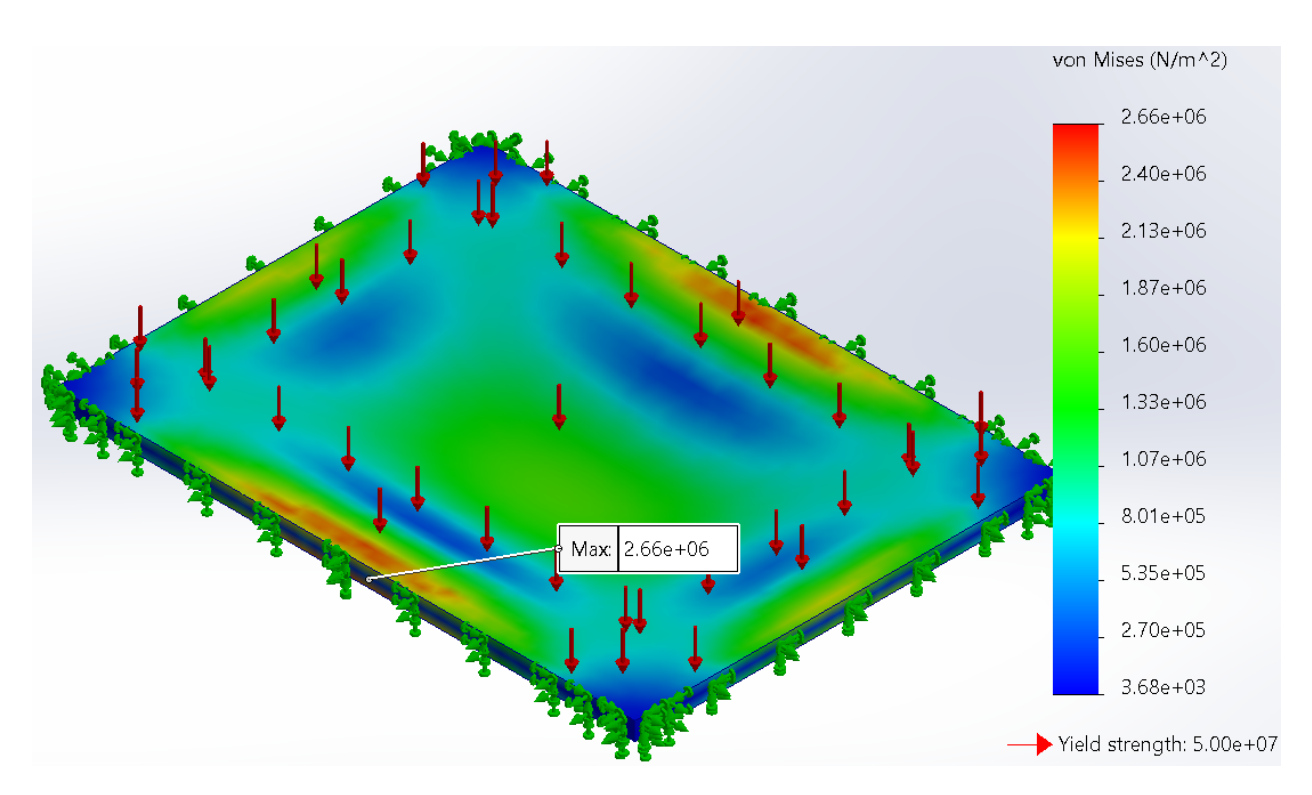


Figure C.2: Brace Plate Von Mises Stress - Four Fixed Edges

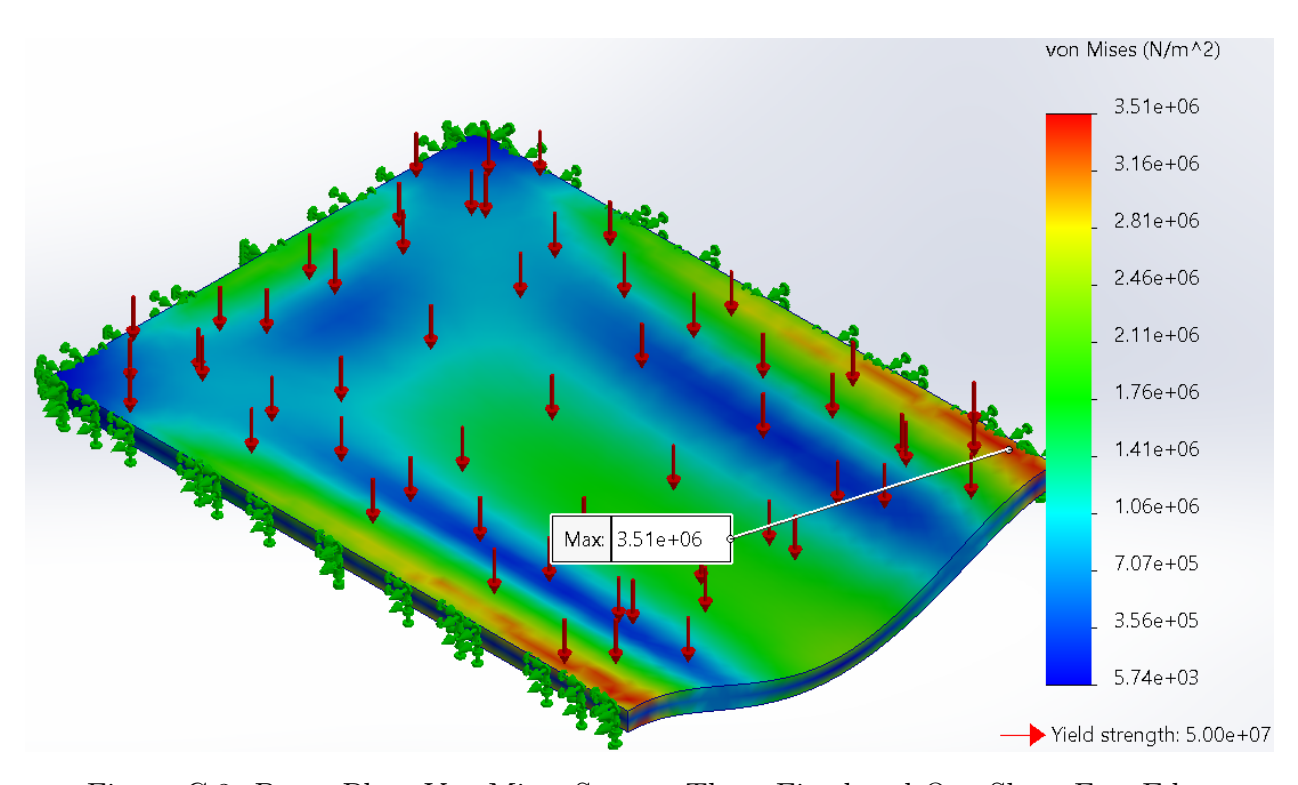


Figure C.3: Brace Plate Von Mises Stress - Three Fixed and One Short Free Edge

Appendix D
 MATLAB Script for Ideal Gas Law

```
%% PV=nRT
clear
clc
close all
fs = 20;
%% Find n
% Design Parameters
P1 = 13789.5; % Airbag Pressure (Pa)
V1 = 0.00240;
                  % Volume of air in airbag based on max height (m^3)
V2 = 0.0012;
                  % Array volume of the air in the inflated airbag (m^3)
R = 8.314;
                  % Gas constant (J/mol*Kelvin)
                  % Ambient Air temperature(Kelvin)
T1 = 294;
T2 = 273.15;
                  % Chill water Temperature (Kelvin)
% Find n
  = P1*V1/(R*T1);
%% Create Plots for P vs. V (const T) and P vs. T (const V)
% Create array space to vary Temperature and Volume
nТ
          = 1000;
T array = linspace(T2,T1,nT);
nV
          = nT;
                                   % must be same dimension as T_array for surf
V_array = linspace(V2,V1,nV);
% P vs. V with constant T
P_T1
     = n*R*T1./V_array;
     = n*R*T2./V array;
P T2
figure()
plot(V array,P T1,V array,P T2)
title('P vs. V', 'FontSize', fs)
xlabel('V [m^{3}]','FontSize',fs)
ylabel('P [Pa]','FontSize',fs)
legend(['T = ', num2str(T1), 'K'], ['T = ', num2str(T2), 'K'], 'FontSize', fs)
% P vs. T with constat V
P V1
      = n*R*T_array./V1;
     = n*R*T_array./V2;
P V2
```

```
figure()
plot(T_array,P_V1,T_array,P_V2)
title('P vs. T', 'FontSize', fs)
xlabel('T [K]','FontSize',fs)
ylabel('P [Pa]','FontSize',fs)
legend(['V = ',num2str(V1),' m^{3}'],['V = ',num2str(V2),' m^{3}'],'FontSize',fs)
% Create surf plot for varying both T and V
P 3D
     = zeros(nT, nV);
for i = 1:nT
   for j = 1:nV
        P 3D(i,j) = n*R.*(T array(j)./(V array(i)));
    end
end
figure()
surf(T_array, V_array, P_3D, 'LineStyle', 'none')
title('P = P(T,V)','FontSize',fs)
xlabel('T [K]','FontSize',fs)
ylabel('V [m^{3}]','FontSize',fs)
zlabel('P [Pa]','FontSize',fs)
```

Appendix E

Air Flow Schematics

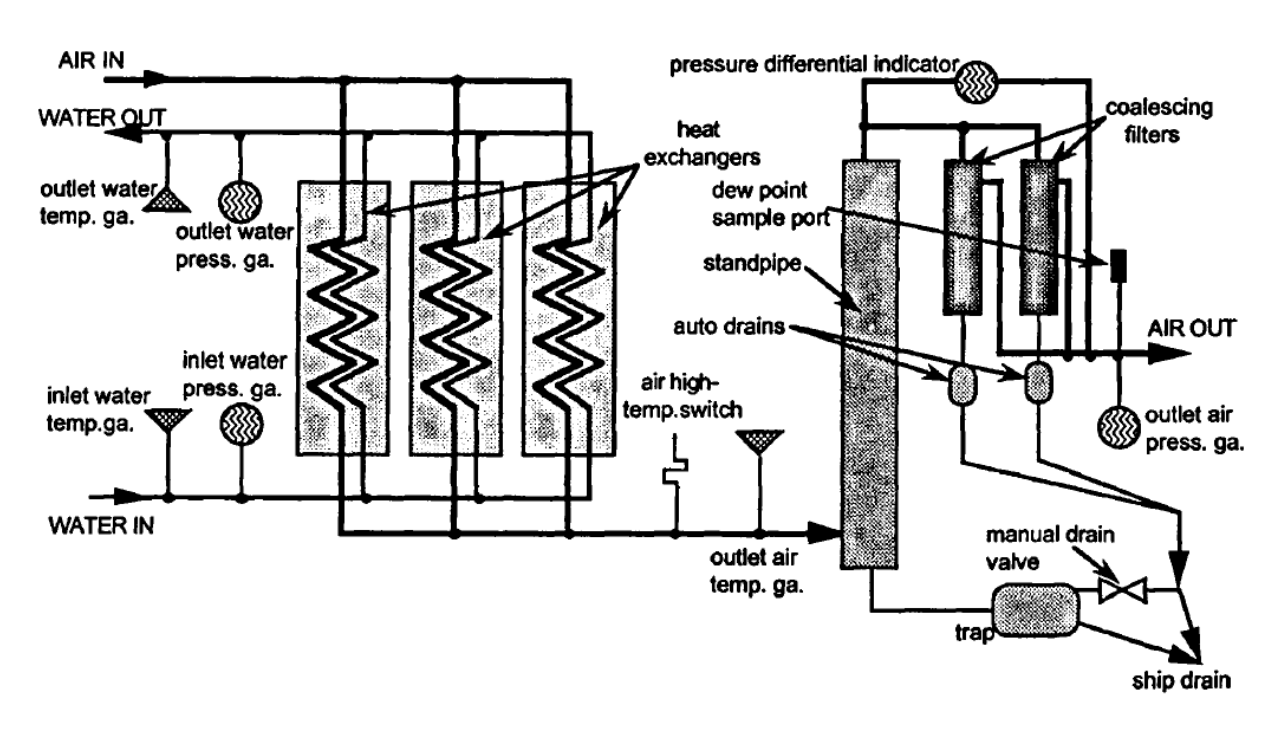


Figure E.1: Condenser-Filter Dehydrator - Flow Schematic Diagram NSTM-551

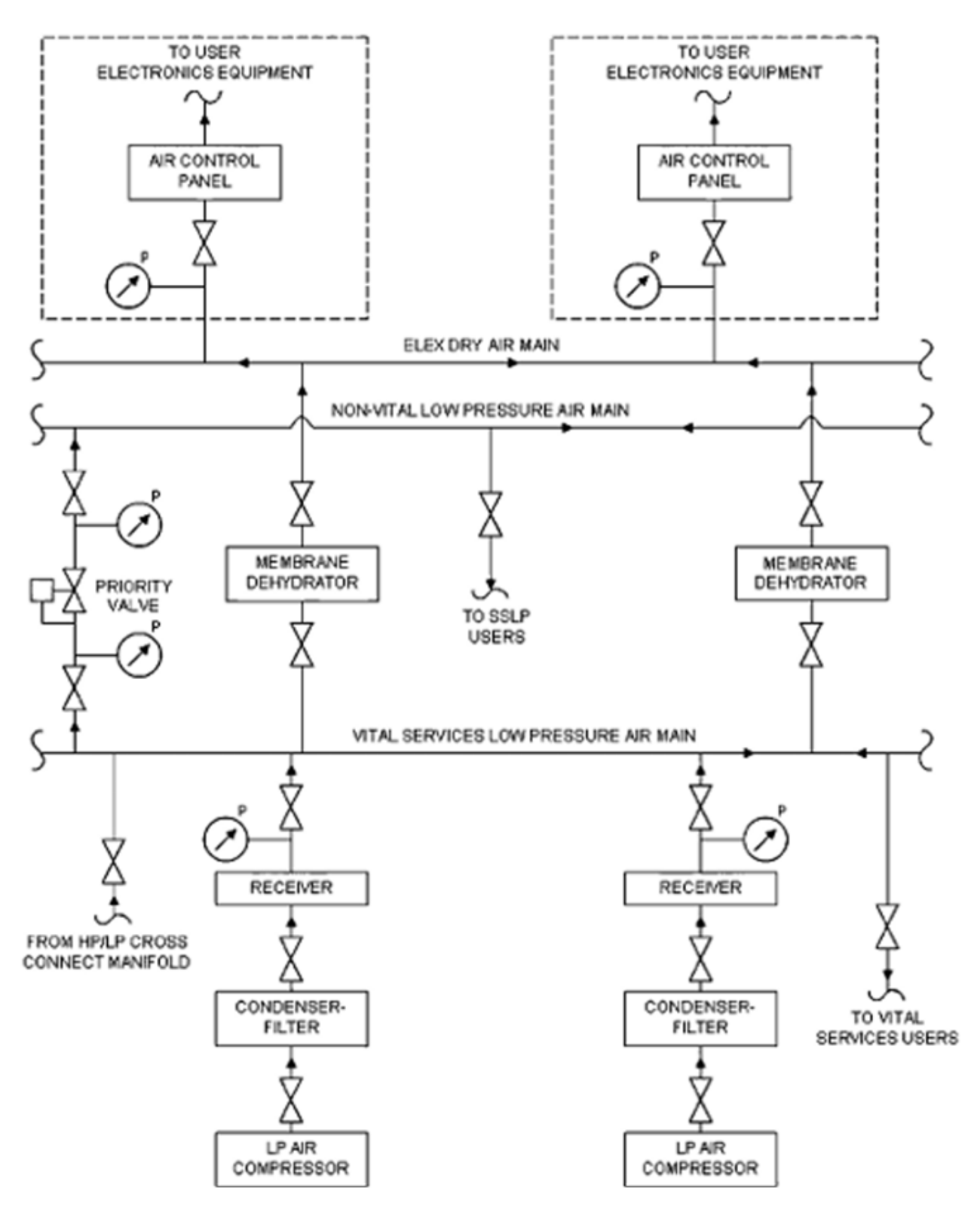


Figure E.2: Typical LP Air System Layout NSTM-551

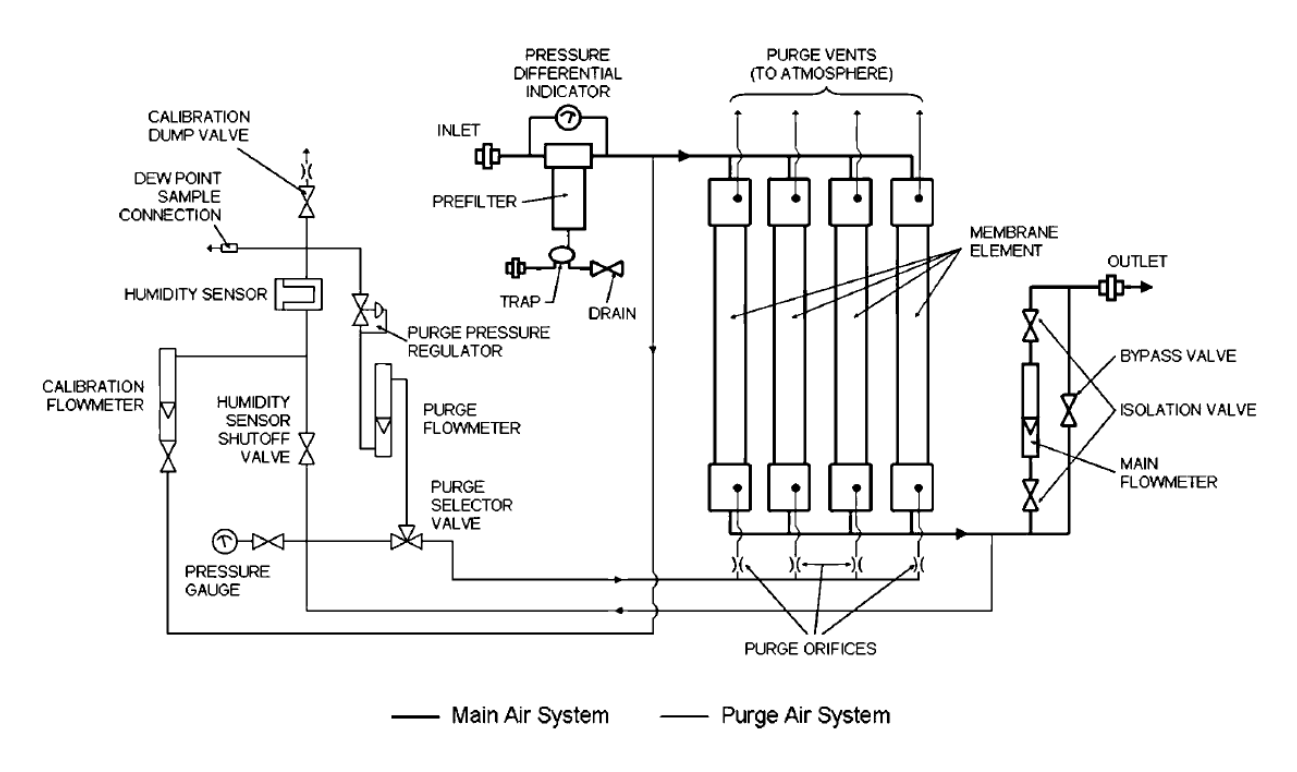


Figure E.3: Membrane Dehydrator - Flow Schematic Diagram NSTM-551

Appendix F

Prototype Material List from TBUILD

TSLOTS QUOTE

Reference Number: #TB005497

Quote Date: **12-18-2023**Project Name: **MockUp**



TSLOTS By Bonnell Aluminum 1201 S. Freeport Industrial Pkwy

Clearfield, UT 84015

Fax: (800)824-2049

Phone: (877)777-5753

Thank you for the opportunity to quote!

Due to the prevailing inflationary conditions for supplies, labor, operating expenditures and billet premiums, prices shown on this quotation are for budgetary purpose only and subject to change without notice.

The lead-time stated is an estimate. Please contact your Customer Account Representative for current lead-times at time of ordering. Please reference the quote number when ordering.

This quotation is subject to Bonnell Aluminum 2021's Terms and Conditions of Sales. For details, please visit below:

https://www.bonnellaluminum.com/pdf/standard-terms-and-conditions.pdf.

Unless otherwise noted, all TSLOTS quotes have a machining tolerance of +/- .030" and a cut to length tolerance of +/- .015".

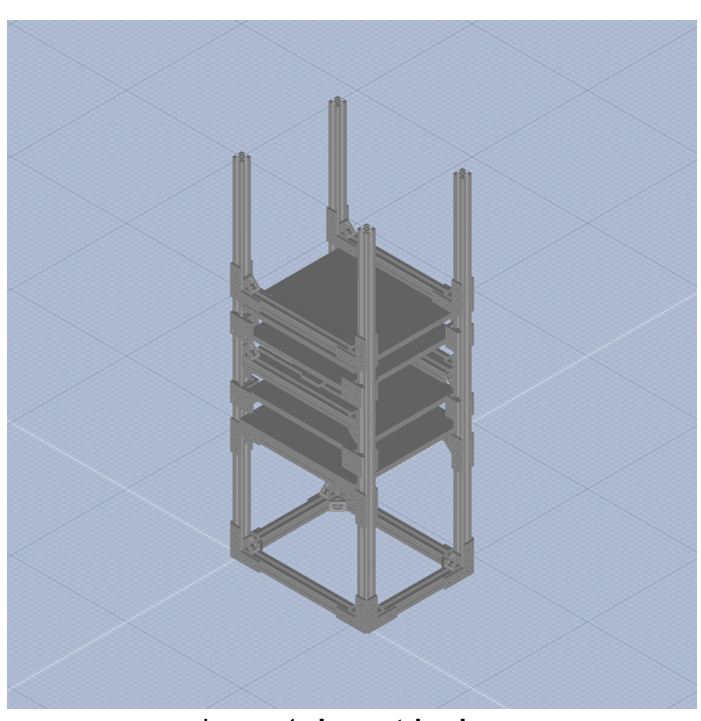


Image 1: Isometric view



Image 2: Front view

Reference Number: #TB005497

Quote Date: **12-18-2023** Project Name: **MockUp**



#	Item #	Description	Size	Qty	Price, \$ / Unit	Ext Price, \$
Extr	usions					
1	650000	1.00" X 1.00" T-slotted Extrusion	36"	4	0.300 / IN	43.20
	660002	Cut To Length TS1010, 1010-QR / 2828		4	2.310 / EA	9.24
2	650000	1.00" X 1.00" T-slotted Extrusion	12"	6	0.300 / IN	21.60
	660002	Cut To Length TS1010, 1010-QR / 2828		6	2.310 / EA	13.86
3	650000	1.00" X 1.00" T-slotted Extrusion	9"	2	0.300 / IN	5.40
	660002	Cut To Length TS1010, 1010-QR / 2828		2	2.310 / EA	4.62
4	650002	1.00" X 2.00" T-slotted Extrusion	12"	2	0.509 / IN	12.22
	660000	Cut To Length-TS1020 / 2856		2	2.310 / EA	4.62
Con	nponents					
5	651171	1/4-20 x 1/2" BHSCS & Economy T- Nut	-	168	0.517 / EA	86.86
6	651717	1/4-20x3/4" FHSCS&DROP IN TNUT	-	8	2.540 / EA	20.32
7	653069	10S 2 Hole Inside Corner Gusset	-	28	5.104 / EA	142.91
8	657055	10 S Short Single Flange Linear Bearing	-	8	57.845 / EA	632.80
9	657059	10 S Short Double Flange Linear Bearing	-	2	60.906 / EA	121.81
10	658213	10S 5 Hole "L" Cut Out Plate	-	24	17.670 / EA	424.08
11	682884	1/2" Clear Polycarbonate	1 SQ FT	1	24.036 / SQ FT	24.04
	660062	Cutting Plastic Panels <= 48" Dimensions: 12 x 11.5		1	12.474 / EA	12.47
	660211	Countersink hole-plastic panels		4	5.580 / EA	22.32
12	682884	1/2" Clear Polycarbonate	1 SQ FT	2	24.036 / SQ FT	48.07
	660062	Cutting Plastic Panels <= 48" Dimensions: 11 x 11		2	12.474 / EA	24.95
13	682884	1/2" Clear Polycarbonate	1 SQ FT	1	24.036 / SQ FT	24.04
	660062	Cutting Plastic Panels <= 48" Dimensions: 11.75 x 11.5		1	12.474 / EA	12.47
	660211	Countersink hole-plastic panels		4	5.580 / EA	22.32

^{*}Price Does Not Include Assembly or Freight Charges

#	Item #	Description	Size	Qty	Price, \$ / Unit	Ext Price, \$
					Total Weight	41 lbs